

**METHODS FOR QUALITY MONITORING IN ULTRASONIC WELDING  
OF CARBON FIBER REINFORCED POLYMER COMPOSITES**

**by**

**Lei Sun**

A dissertation submitted in partial fulfillment  
of the requirements for the degree of  
Doctor of Engineering  
(Manufacturing)  
in the University of Michigan  
2021

Doctoral Committee:

Professor S. Jack Hu, Co-chair

Professor Pingsha Dong, Co-chair

Professor J. Judy Jin

Research Associate Professor Theodor Freiheit

Lei Sun

[sunleium@umich.edu](mailto:sunleium@umich.edu)

ORCID iD: 0000-0002-7439-6023

© Lei Sun

---

All Right Reserved

2021

**DEDICATION**

**To my family**

## ACKNOWLEDGEMENTS

First and foremost, I would like to express my deepest gratitude and respect to my co-advisors, Professor S. Jack Hu and Professor Pingsha Dong. They have inspired my enthusiasm for research, provided me with valuable guidance, and shared their great vision with me. Without their persistent help and unreserved guidance, this dissertation would not have been possible.

I also deeply appreciate Professor Theodor Freiheit for continuously supporting me throughout my doctoral research. I am very fortunate to have a such great advisor, who provided me with regular communications, solved my confusion in time, and gave me advice step by step. His continuous help, profound knowledge, and responsible attitude ensured that I could complete my research efficiently and with high quality.

My sincere gratitude also goes to Professor J. Judy Jin for her constructive suggestions and valuable feedbacks. Her knowledge from different perspectives have greatly inspired me and improved my research quality.

I would like to thank my dear colleagues in Professor Hu's lab for their kind help and friendship. They include but are not limited to: Professor Mihaela Banu, Baicun Wang, Changbai Tan, Jaekwang Shin, Weiling Wen, Tae Hwa Lee, Yang Li, Yinbao Tian, and Ying Luo. I would also like to thank Yang Li, Taehwa Lee, Chenhui Shao, and Grace Guo for providing me research data. Thanks to all my friends who accompanied me during the period I studied at the University of Michigan. Their friendship has made my life full of pleasure and happiness.

Finally, and most importantly, I want to thank my dear parents for always believing in me, encouraging me, and supporting me. Without their endless love and

encouragement, I would not have the courage and confidence to face all the challenges during the Ph.D. study and the difficulties faced during the pandemic.

## TABLE OF CONTENTS

<b>DEDICATION .....</b>	<b>ii</b>
<b>ACKNOWLEDGEMENTS .....</b>	<b>iii</b>
<b>LIST OF TABLES .....</b>	<b>viii</b>
<b>LIST OF FIGURES .....</b>	<b>ix</b>
<b>LIST OF APPENDICES .....</b>	<b>xiii</b>
<b>ABSTRACT.....</b>	<b>xiv</b>
<b>CHAPTER 1 INTRODUCTION .....</b>	<b>1</b>
1.1 Background and Motivation .....	1
1.2 Research Objectives.....	4
1.3 Assumptions of the Work .....	7
1.4 Dissertation Organization .....	7
References.....	9
<b>CHAPTER 2 LITERATURE REVIEW AND STATE-OF-THE-ART.....</b>	<b>13</b>
2.1 Introduction.....	13
2.2 State-of-the-art of Joining Technologies .....	14
2.3 Mechanisms and Characteristics of Ultrasonic Welding.....	15
2.4 Weld Attributes, Joint Performance, and Weld Quality Determination .....	16
2.5 Signal Processing, Feature Selection, and Dimension Reduction .....	19
2.6 Monte Carlo Simulation.....	24
2.7 Weld Quality Monitoring.....	25
2.8 Weld Experiments Setup and Data Acquisition.....	29
2.9 Conclusion .....	35
References.....	36

**CHAPTER 3 FEATURE-BASED WELD QUALITY CLASSIFICATION FOR ULTRASONIC WELDING OF CARBON FIBER REINFORCED POLYMER THROUGH BAYESIAN REGULARIZED NEURAL NETWORK.....45**

3.1 Introduction.....45

3.2 Weld Experiments.....47

    3.2.1 Material Selection .....47

    3.2.2 Experimental Setup.....47

3.3 Weld Attributes, Performance, and Quality.....49

3.4 Feature Extraction, Selection, and Classification .....52

    3.4.1 Signal Pre-processing and Feature Extraction .....52

    3.4.2 Feature Selection.....57

    3.4.3 The BRNN Classification Method.....59

3.5 Case Study and Discussion .....62

    3.5.1 Comparison of Classification Methods.....62

    3.5.2 Comparison of Feature Selection Methods and Influence of Number of Features .....65

    3.5.3 BRNN Classification Sensitivity and Robustness .....68

3.6 Conclusion .....71

References.....73

Appendix.....76

**CHAPTER 4 QUALITY DETECTION AND CLASSIFICATION FOR ULTRASONIC WELDING OF CARBON FIBER COMPOSITES USING TIME-SERIES DATA AND NEURAL NETWORK METHODS.....83**

4.1 Introduction.....83

4.2 Weld Experiments and Weld Quality Determination .....86

    4.2.1 Material Selection and Weld Machine.....86

    4.2.2 Data Collection and Weld Quality Determination.....87

4.3 Deep Learning Classification Methodologies.....89

    4.3.1 Neural Network Structure and Application .....90

4.4 Simulation of Time-Series Signal Data with Multivariate Monte Carlo Simulation.....93

    4.4.1 Multivariate Monte Carlo Simulation.....93

    4.4.2 Process Signals Simulated by Multivariate Monte Carlo Simulation.....94

4.5 Case Study .....103

    4.5.1 Feature-based Model.....103

4.5.2	Time-series-based Model.....	105
4.6	Discussion.....	107
4.6.1	Sensitivity of the Size of Simulated Process Signals.....	107
4.6.2	Classification Accuracy of CNN Model Trained with Simulated Data on Experimental Signals .....	109
4.6.3	Robustness of CNN Models Trained with Simulated Data .....	110
4.7	Conclusion .....	112
	References.....	115
	Appendix.....	120
<b>CHAPTER 5 CONCLUSION AND FUTURE WORK.....</b>		<b>125</b>
5.1	Summary and Conclusion.....	125
5.2	Applicability of the Work .....	127
5.3	Contributions .....	127
5.4	Recommendations for Future Work.....	128

## LIST OF TABLES

Table 2.1	Signal processing methods applied in welding process.....	20
Table 2.2	The strengths and weaknesses of commonly used selection methods in welding process.....	24
Table 2.3	The ranges of different weld parameters.....	32
Table 3.1	Weld quality classification based on weld energy.....	52
Table 3.A.1	Features list extracted from four signal sources.....	76
Table 3.A.2	The physical meanings of significant features.....	76
Table 3.A.3	Fisher’s ratio value of each feature.....	77
Table 3.A.4	Parsimonious feature set size screened by the proposed Fisher’s ratio and clustering overlap analysis method (from a total possible feature set size of 61).....	78
Table 3.A.5	The classification accuracy of parsimonious feature set size screened by the proposed Fisher’s ratio and clustering overlap analysis method (from a total possible feature set size of 61).....	78
Table 3.B.1	The size of good-welds and bad-welds of each channel in dataset1 and dataset2.....	80
Table 4.1	The percentage of error between the experimental and simulated process signal curves.....	101
Table 4.2	Classification accuracy comparison and validation of simulated data classified by SBRNN methodology with the same input dimension....	102
Table 4.3	Training time comparison of SBRNN, TBRNN, and CNN under 560, 1120, 2240, and 3360 simulated sample sizes.....	109
Table 4.C.1	The classification accuracy of feature-based signals obtained by different machine learning and deep learning methodologies.....	124
Table 4.C.2	The classification accuracy of experimental and simulated process signals obtained by different machine learning and deep learning methodologies.....	124

## LIST OF FIGURES

Figure 1.1.	An overview of the tasks and approaches of the dissertation.....	6
Figure 2.1.	Three typical failure modes: (a) interfacial separation, (b) nugget shear, fracture, and (c) nugget pull-out fracture.....	18
Figure 2.2.	Predicted versus experimental dependencies of cohesive parameters: (a) shear strength, (b) shear toughness, and (c) weld area on the welding energy.....	19
Figure 2.3.	The CFRP coupons using in weld experiments.....	30
Figure 2.4.	(a) Ultrasonic composite welding machine; (b) schematic diagram of joining process.....	30
Figure 2.5.	The related experiment apparatus using in welding process: (a) universal testing systems, (b) oven, and (c) SEM.....	31
Figure 2.6.	The main effects of lap-shear strength tests with different weld parameters.....	33
Figure 2.7.	Illustration of weld area which is calculated by <i>ImageJ</i> .....	34
Figure 2.8.	The evolution of microstructure of the cross-section through the weld zone.....	35
Figure 3.1.	(a) Ultrasonic composite welding machine, (b) schematic diagram of joining process.....	48
Figure 3.2.	Association of weld quality to weld process parameters, weld attributes, and joint performance.....	50
Figure 3.3.	Diagram of shear strength and weld area variation with weld energy determined by microstructure analysis.....	51
Figure 3.4.	Comparison of each signal under different weld quality.....	55
Figure 3.5.	Schematic diagram of features extracted from: (a) power signal, (b) energy signal, (c) force signal, and (d) distance signal.....	56
Figure 3.6.	The distributions of feature 6 (the peak value of power signal) extracted from the UCW power signal. The good-weld distribution completely overlaps the under-weld distribution, $R_{61} = 1$ , and has a large overlap with the over-weld distribution, $R_{62} = 0.459$ , implying that it may only be weak in distinguishing abnormal weld classes.....	59

Figure 3.7.	Example neural network structure for the BRNN methodology using the optimal feature data set input size.....	61
Figure 3.8.	Comparison of classification accuracy under different number of features based on (a) Fisher’s ratio, and (b) LDA feature selection method.....	64
Figure 3.9.	Classification accuracy with number of features which selected by Fisher’s ratio and clustering overlap.....	66
Figure 3.10.	The classification results of weld quality under BRNN classification method with different feature selection methods.....	67
Figure 3.11.	Pareto chart of ANOVA analysis of variation of $\pm 5\%$ feature value of 61 features.....	69
Figure 3.12.	Variance contributions of different numbers of features based on the ANOVA test of variation of $\pm 5\%$ feature value (a) to total classification accuracy; and (b) to $\alpha$ error and $\beta$ error.....	70
Figure 3.A.1	The distribution of the Fisher’s ratio extracted from the ultrasonic composite welding process.....	79
Figure 3.B.1	Classification results of each channel from two datasets with and without feature selection.....	81
Figure 3.B.2	Total accuracy of each channel from two datasets with and without feature selection.....	82
Figure 4.1.	(a) The CRFP coupons, and (b) schematic diagram of ultrasonic composite welding joining process.....	87
Figure 4.2.	Weld quality distribution of the relationship regarding with lap-shear strength and weld energy.....	89
Figure 4.3.	Typical structure of CNN algorithm.....	90
Figure 4.4.	A schematic diagram of the TBRNN model.....	91
Figure 4.5.	The schematic diagram of transmission of CNN model.....	93
Figure 4.6.	A schematic diagram of MMC simulation with copulas based on inflection points, (a) is the distribution of experimental process signals, (b) is the simulated process signals.....	96
Figure 4.7.	The enlarged region squared by green dashed line in Figure 4.6, (a) is the distribution of experimental process signals, (b) is the simulated process signals.....	96
Figure 4.8.	The comparison of 90% CI of the experimental and the simulated process signal curves of force signal for under-welds: (a) 400 <i>J</i> , (b) 600 <i>J</i> , and (c) 800 <i>J</i> .....	98
Figure 4.9.	The comparison of 90% CI of the experimental and the simulated process signal curves of power signal for under-welds: (a) 400 <i>J</i> , (b) 600 <i>J</i> , and (c) 800 <i>J</i> .....	99

Figure 4.10. The comparison of 90% CI of the experimental and the simulated process signal curves of force signal for good-welds: (a) 1000 <i>J</i> and (b) 1200-1300 <i>J</i> .....	99
Figure 4.11. The comparison of 90% CI of the experimental and the simulated process signal curves of power signal for good-welds: (a) 1000 <i>J</i> and (b) 1200-1300 <i>J</i> .....	99
Figure 4.12. The comparison of 90% CI of the experimental and the simulated process signal curves of force signal for of over-welds: (a) 1300 <i>J</i> and (b) 1400 <i>J</i> .....	100
Figure 4.13. The comparison of 90% CI of the experimental and the simulated process signal curves of power signal for of over-welds: (a) 1300 <i>J</i> and (b) 1400 <i>J</i> .....	100
Figure 4.14. The confusion matrix of (a) simulated process signals, and (b) simulated features-based signals (Class 1 represents under-welds, Class 2 represents good-welds, and Class 3 represents over-welds).....	103
Figure 4.15. The classification accuracy of SBRNN, TBRNN, SVM, and kNN under experimental and simulated feature-based signals.....	104
Figure 4.16. The classification accuracy of SBRNN, TBRNN, CNN, SVM, and kNN under original and simulated process signals.....	106
Figure 4.17. The sensitivity of classification accuracy with the number of simulated samples under the condition of feature-based signals and process signals.....	108
Figure 4.18 Classification accuracy of a CNN model trained under different sizes of simulated process signals and tested by only experimental process signals or only simulated process signals.....	109
Figure 4.19. Classification accuracy variation with noise variation added on the experimental 112 process signal curves, simulated 112 process signal curves, and simulated 1120 process signal curves.....	111
Figure 4.20. The comparison of experimental process signals and the noisy process signals when amplification factor $n = 1$ .....	112
Figure 4.A.1 The simulation distribution comparison of three MMC simulation approaches.....	121
Figure 4.B.1 Power and force signals comparison of the experimental and the simulated process signal curves listed by under-welds, good-welds, and over-welds (the size of the simulation is 10 times than the size of the experimental signals, (a) represents power signals, (b) represents force signals).....	122

Figure 4.B.2 Distance signals comparisons of the experimental and the simulated process signal curves (the size of the simulation is 10 times than the size of the experimental signals)..... 123

Figure 5.1. The structure of self-diagnosis, self-feedback, and self-control system..... 130

## LIST OF APPENDICES

Appendix 3.A.....	76
Appendix 3.B.....	79
Appendix 4.A.....	120
Appendix 4.B.....	122
Appendix 4.C.....	124

## ABSTRACT

Carbon fiber reinforced composites have been increasingly used in various industrial sectors, especially in the automotive industry. Ultrasonic welding is considered as an effective approach to joining such composites. Reliable weld quality classification and prediction methods are needed to ensure quality and reduce manufacturing costs. However, existing methods have two weaknesses. The first one is that the majority of the existing methods are based on signal feature data extracted from the original experimental time-series data. Feature-based models may not take full advantage of the information contained in the large amounts of time-series data available, even though the models are simple and easy to program. On the other hand, when using experimental time-series data to conduct weld quality monitoring, the data size may be insufficient for training neural network-based methods for quality monitoring or classification. Therefore, a method is needed to augment experimental data while preserving the statistical characteristics of the experimental data.

To find reliable quality monitoring models in various situations, this dissertation proposes two neural network models that are respectively applied to feature-based data and full time-series-based data and compares their performances.

The dissertation first investigates the relationship between weld energy and joint performance in ultrasonic welding of carbon fiber reinforced polymer (CFRP) sheets through weld experiments. The weld quality classes for training quality monitoring algorithms are determined from welded joint lap-shear strength and the microstructure of the weld zone. These pre-defined weld quality classes are the output criteria for weld quality monitoring on feature-based models and time-series-based models. For feature-based weld quality monitoring, a simple and efficient feature selection method is first developed to screen the most significant features for classification from multiple weld

quality classes. A Bayesian regularized neural network (BRNN) is then demonstrated to be more accurate and robust when classifying weld quality classes in ultrasonic composite welding when using feature-based data as the input than the previously proposed methods of support vector machine (SVM), k-nearest neighbors (kNN), and linear discriminant analysis (LDA).

To address the limited size of experimental data, a Multivariate Monte Carlo (MMC) simulation with copulas approach is proposed to reasonably generate large amounts of time-series process signals for ultrasonic composite welding. With both experimental data and a large quantity of simulated data, a deep convolutional neural network (CNN) is applied to weld quality classification. The CNN model is found to be more accurate and robust, not only under small training data set sizes, but also under large training data set sizes when compared with previously researched classification methods applied in ultrasonic welding.

In conclusion, neural network-based models could achieve high accuracy using feature signals and the full time-series process signals.

## CHAPTER 1

### INTRODUCTION

#### 1.1 Background and Motivation

Today, polymeric composite materials such as carbon fiber reinforced polymers (CFRP) are widely used in many engineering products, particularly in transportation systems due to their high strength to weight ratio and other unique properties. The global demand for CFRP material has increased from 33,000 tons in 2010 to 78,500 tons in 2018. Moreover, the forecasted demand in 2022 will reach to 120,500 tons [1, 2]. Since the composites have the properties of lightweight, high temperature resistance, high corrosion resistance, high strength-to-weight ratio, etc., they have become a great choice for reducing structural weights and improving fuel efficiency in various automotive and aerospace applications [3-8]. The automotive industry accounts for more than 70% of the CFRP consumption, with a forecast consumption in 2025 of approximately 220,100 tons. It is foreseeable that CFRP will play an increasingly significant role in the automotive industry.

In manufacturing structures made of CFRP composites, cost-effective joining processes are important. Currently available joining methods include adhesive bonding, mechanical fastening, and fusion-based welding techniques [9-11]. Although the adhesive bonding technique has the advantages of relative low cost, lightweight, and consistent joint quality, these techniques are not considered as being environmentally friendly in addition to the lack of reparability. Mechanical fastening offers the advantages of easy assembly and disassembly, but at an increased cost, added weight, reduced strength, etc. As a result of these considerations, fusion-based joining technique is most attractive for joining CFRP composites for the automotive industry due to its short cycle time and good joint reliability [11, 12]. The main fusion-based

joining techniques for CFRP materials are laser welding, resistance welding, vibration welding, and ultrasonic welding [13, 14]. Ultrasonic welding offers a good process controllability, consumes less energy, and is capable of joining different types of CFRP materials. As a result, ultrasonic welding has become a preferred process for joining CFRP composites [3, 15-17].

Ultrasonic welding is particularly suited for joining thin and highly conductive, dissimilar materials [18, 19]. The associated bonding mechanisms have been well studied by many researchers. Some of the well-established joint formation mechanisms are: 1) chemical bonding involving diffusion at the weld interface within a certain temperature regime; 2) local melting caused bonding; 3) metallurgical adhesion triggered by severe plastic deformation; and 4) mechanical interlocking [20]. However, most of the well-established joint formation mechanisms may not be applicable for ultrasonic welding of CFRP composites [21]. In ultrasonic welding of composite workpieces, the high-frequency oscillation is transmitted to the workpieces to be joined in the perpendicular direction to the ultrasonic horn axis. Frictional heat is generated through the combination of surface and intermolecular friction oscillations at the interface [13]. The polymer melts and then a weld begins to form when the temperature at the interface reaches the melting temperature [13].

As such, ultrasonic welding process is considered as a low heat input process for joining either metals [19, 22, 23] or composite materials [23, 24], thus it avoids some of the negative impacts of excessive heat on the microstructure and properties of a weldment, e.g., metallurgical defects such as the brittle phases or the formation of intermetallic compounds that commonly exist in most other fusion welds [20]. Brittle phases and porosity can be detrimental to fatigue resistance and reduce the strength of the joint. Due to these desirable attributes of ultrasonic welding, it has received increasing research for achieving reliable joint quality in manufacture of CFRP composite structures.

With the increasing demand for CFRP composites, manufacturing cost and quality assurance become more and more important. For example, if a defective weld is

undetected, the resulting cost implications escalate for automotive products [25-27]. Poor weld quality will not only reduce the strength and fatigue resistance of a joint in a specific component, but can have a more global consequence at a structural level, leading to unstable fracture and collapse [28-30]. In spite of its importance, however, the quality of a joint can be difficult to monitor and predict due to complex process dynamics and resulting variations in material properties during weld formation process. Therefore, it is desirable to infer weld quality implicitly through measuring certain weld attributes and resulting joint performance parameters, e.g., joint strengths from lap-shear [30-33].

Traditional weld quality detection methods are based on weld attribute inspections, selected performance testing (e.g., fatigue testing and fracture mechanics evaluation), which can be insufficient for continuous quality monitoring purposes [29, 34-40]. Therefore, intelligent or smart weld quality monitoring and prediction methods have been proposed recently in order to improve quality monitoring reliability and efficiency [41-44]. The idea is to develop a network-like correspondence between the physical weld quality information and the operational data obtained during the welding process, and then perform real-time monitoring and prediction through various forms of process and weld attribute data. Specific approaches that have been applied to weld quality monitoring in ultrasonic welding are analytical regression models, statistical process control, and machine learning algorithms [45-46]. Among these methods, machine learning algorithms are proven to be the most promising process technique of all for weld quality monitoring [45-47].

Since determining the weld quality through mechanical performance testing such as lap-shear strength and fatigue testing through a periodical sampling is destructive, an alternative way is needed to predict weld quality through process parameters, weld attributes, and joint performance. This would require the development of a model to relate welding process parameters, weld attributes, and joint performance to weld quality classifications. These models can help detect abnormal welds or the trend towards the negative aspects of welding during weld quality monitoring. However,

there have been rather limited research efforts to date on the development of effective weld quality classification algorithms for UCW. Few have adopted machine learning techniques to classify or predict different weld quality classes. Additionally, nearly all of the research efforts on weld quality monitoring have been based on limited sample size of laboratory data. With complex relationships among inputs and outputs, the use of a limited number of input parameters can severely affect the effectiveness in training and validating machine learning algorithms.

In summary, there are three major gaps in the state of the research in introducing advanced machine learning algorithms for effectively monitoring and predicting ultrasonic composite welding (UCW) quality: 1) there is a lack of a well-established relationship among process parameters, weld attributes, and joint mechanical performance for UCW. Existing models only use some parts of process parameters and limited weld attributes to related to joint mechanical performance, which may result in the loss of useful information from available data for weld quality monitoring. 2) Input data in existing models are only based on limited weld process experiments. Therefore, the resulting weld quality monitoring algorithms may not be applicable for general applications, particularly for production environment. 3) Nearly all the existing weld quality classification or prediction models are based on a set of pre-defined features extracted from the time-series process signals. However, there exist uncertainties in whether these pre-defined features have been properly defined and extracted from a given set of process signals. Some of the uncertainties includes: 1) Feature definitions can be rather subjective and limited by available process data; 2) Feature extraction requires pre-processing of process signals, which may result in loss of useful signal information. In view of the above critical assessments, this dissertation aims to develop neural network models that are respectively applied to both feature-based data and full time-series-based data so that the deficiencies in existing models discussed earlier can be mitigated for UCW quality monitoring and assurance purposes.

## **1.2 Research Objectives**

The first objective of this research is to develop a more general relationship

between weld quality classes and weld process parameters, weld attributes, and joint performance. With such a relationship, weld quality classes can be applied to train classification and prediction through neural network algorithms. The second objective is to apply neural network-based models to achieve robust and advantageous for weld quality monitoring in UCW under various input data formats. Finally, an efficient and versatile data simulation approach will be developed for generating a large amount of simulated process data that are consistent with experimental welding process signals. These simulated process data can be used for supporting the training of neural network-based models for weld quality monitoring algorithms when sufficient experimental data are limited in scope.

The major research tasks are described as follows:

- (1) *Define the relationship between welding process signals, their characteristics, and weld quality classes through a detailed examination of weld experimental data.* It has been well established that welding process signals contain information about the weld formation process which can be related to final weld geometric attributes, lap-shear strengths, and weld quality classes. This can be accomplished through the development of a set of process signal characteristic features that can be related to weld quality classes as a set of output criteria for training of quality monitoring algorithms.
- (2) *Investigate the performance of limited experimental feature-based data on quality monitoring in UCW and develop an algorithm that can improve its classification accuracy and efficiency.* UCW is a relatively new process to the automotive industry. As such, there is still lack of a detailed understanding of the impact of process parameters on various weld attributes and the resulting joint performance. Therefore, nearly all of the existing quality monitoring methods on UCW are based on a set of pre-defined features that can be extracted from time-series process signals. However, the efficiency of these methods may not be satisfactory. It can be hypothesized that an advanced neural network algorithm trained with feature-based data should perform better, compared to other non-neural network

techniques for weld quality monitoring purpose. Additionally, since different feature sets may affect classification accuracy, it is hypothesized that a new feature selection method that considers multiple weld quality classes to select the most significant features will be simple but efficient.

- (3) *Investigate the feasibility using simulated time-series-based data for training weld quality monitoring algorithm when lacking of a large amount of UCW process data.* The majority of existing research on weld quality monitoring in ultrasonic welding are based on features extracted from limited weld experiments and process data that may be insufficient to support the training and validation of the advanced quality monitoring algorithms. Therefore, it is desirable to develop a methodology for supplement available process signals with simulated process signals for data-driven model development purpose. In so doing, feature-based quality classification models can be replaced by taking advantage of deep neural network classification model by using both actual and simulated time-series process signal data.

The above tasks and their interrelationships are illustrated in Figure 1.1.

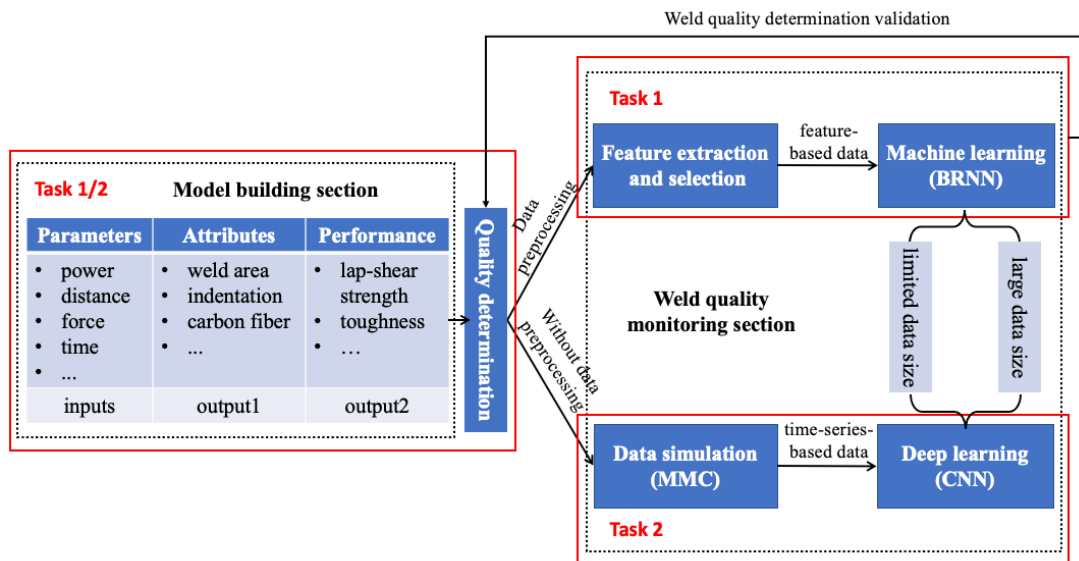


**Figure 1.1. An overview of the tasks and approaches of the dissertation**

### **1.3 Assumptions of the Work**

The input data of all classification and prediction models in the dissertation are based on hundreds of weld experiments described in Chapter 2. However, if there are issues in the materials and the weld experiments, the subsequent weld quality determination, feature extraction and selection, data simulation, quality monitoring, and the conclusion will be invalid. Therefore, the related assumptions of the materials and experiments are:

- (1) Since all of the weldments are produced from the same production batch, there will be no obvious defects and differences between weldments;
- (2) The experimental environment will not have a significant influence on the welding results;
- (3) The procedure of weld experiments is correct;
- (4) The 112 samples collected contained all possible weld quality classes in UCW;

### **1.4 Dissertation Organization**

This dissertation is written in a multi-manuscript format. Chapter 1 serves as an integrated introduction while Chapter 2 provides a state-of-the-art review of representative publications in this overall subject area and provide necessary background information on UCW process descriptions, weld attributes, and weld quality and mechanical performance test procedures. Experimental data generation process is also described. The content of Chapter 3 has already been published in *SME Journal of Manufacturing Systems*. The title of the paper is ‘Feature-based quality classification for ultrasonic welding of carbon fiber reinforced polymer through Bayesian Regularized Neural Network’. The content of Chapter 4 has been finalized and submitted to *SME Journal of Manufacturing Systems*. The title of the paper is ‘Quality Detection and Classification for Ultrasonic Welding of Carbon Fiber Composites using Time-series Data and Neural Network Methods’.

Chapter 3 first investigates the relationship between weld parameters, attributes, and joint performance in ultrasonic welding of injection modeled CFRP material to pre-define weld quality classes. Specifically, the classes are pre-defined by the correlation among weld energy, maximum lap-shear strength, and the microstructure of weld zone. Then the chapter proposes a simple and efficient feature selection method that combines Fisher's ratio and clustering overlap analysis to screen the most significant features for predicting from multiple weld quality classes. Several feature selection and weld quality classification methods are compared. A Bayesian Regularized Neural Network (BRNN) model is found to be more accurate and robust when classifying weld quality in UCW than the previously proposed methods of support vector machine (SVM), k-nearest neighbors (kNN), and linear discriminant analysis (LDA) when using limited size feature-based data as the input.

Chapter 4 also uses the correlation among weld energy levels, maximum lap-shear strength and the percentage of carbon fiber mixed within weld zone to determine weld quality classes. The pre-defined weld quality classes are the output criteria of following deep learning quality monitoring algorithms. Next, the chapter proposes a Multivariate Monte Carlo (MMC) simulation with copulas approach that can generate reasonably large amounts of time-series process signals in UCW. With the large data generated by simulation approach, a deep Convolutional Neural Network (CNN) model is applied to perform weld quality classification. The model is found to be more accurate and robust, not only under small size of input data, but also under large training data set size, when compared with previously researched methods applied in ultrasonic welding. In addition, neural network-based models can obtain higher accuracy with the input of feature-based data and time-series-based data compared with non-neural network techniques.

Chapter 5 summarizes the key findings and major contributions of this research. Further areas of research are also highlighted for taking advantage of the approaches developed in this study.

## References

- [1] Global demand for carbon fiber from 2010 to 2022 (in 1,000 metric tons). Statista. <https://www.statista.com/statistics/380538/projection-demand-for-carbon-fiber-globally/>. (Accessed May 20, 2021).
- [2] Global carbon fiber demand from 2016 to 2025, by market (in metric tons). Statista. (<https://www.statista.com/statistics/689198/worldwide-carbon-fiber-demand-by-market/>). (Accessed May 20, 2021).
- [3] L. Sun, S.J. Hu, T. Freiheit, Feature-based quality classification for ultrasonic welding of carbon fiber reinforced polymer through Bayesian regularized neural network, *Journal of Manufacturing Systems* 58 (2021) 335-347.
- [4] M. Sauer, M. Kuhnel, *Composites Market Report 2019*, Carbon Composite e.V., Ed, 2019.
- [5] K. Salonitis, J. Pandremenos, J. Paralikas, G. Chryssolouris, Multifunctional materials: engineering applications and processing challenges, *Journal of Advanced Manufacturing Technology* 49 (2010) 803-826.
- [6] Y. Lu, Y. Li, N. Li, X. Wu, Reduction of composite deformation based on tool-part thermal expansion matching and stress-free temperature theory, *Journal of Advanced Manufacturing Technology* 88 (2017) 1703-1710.
- [7] M. Golzar, M. Poorzeinolabedin, Prototype fabrication of a composite automobile body based on intergraded structure, *Journal of Advanced Manufacturing Technology* 49 (2010) 1037-1045.
- [8] A.v. Grootel, J. Chang, B.L. Wardle, E. Olivetti, Manufacturing variability drives significant environmental and economic impact: The case of carbon fiber reinforced polymer composites in the aerospace industry, *Journal of Cleaner Production* 261 (2020) 121087.
- [9] What techniques can I use to weld Nylon? TWI. <https://www.twi-global.com/technical-knowledge/faqs/faq-what-techniques-can-i-use-to-weld-nylon>. (Accessed May 20, 2021).
- [10] J. Leone, Plastic joining methods. Science. <https://sciencing.com/plastic-joining-methods-6924074.html>. (Accessed May 20, 2021).
- [11] A. Pramanik, A.K. Basak, Y. Dong, P.K. Sarker, M. Uddin, G. Littlefair, A.R. Dixit, S. Chattopadhyaya, Joining of carbon fibre reinforced polymer (CFRP) composites and aluminium alloys-A review, *Composites Part A: Applied Science and Manufacturing* 101 (2017) 1-29.
- [12] T. Ishikawa, K. Amaoka, Y. Masubuchi, T. Yamamoto, A. Yamanaka, M. Arai, J. Takahashi, Overview of automotive structural composites technology developments in Japan, *Composites Science and Technology* 155 (2018) 221-246.

- [13] A. Yousefpour, M. Hojjati, J.-P. Immarigeon, Fusion bonding/welding of thermoplastic composites, *Journal of Thermoplastic Composite Materials* 17(4) (2016) 303-341.
- [14] A.P.d. Costa, E.C. Botelho, M.L. Costa, N.E. Narita, J.R. Tarpani, A review of welding technologies for thermoplastic composites in aerospace applications, *Journal of Aerospace Technology and Management* 4(3) (2012) 255-265.
- [15] Y.P. Korkolis, J. Li, B. Carlson, E. Chu, Special issue: Forming and joining of lightweight and multimaterial systems, *Journal of Manufacturing Science and Engineering* 137(5) (2015) 050201.
- [16] S.S. Lee, T.H. Kim, S.J. Hu, W.W. Cai, J.A. Abell, J. Li, Analysis of weld formation in multilayer ultrasonic metal welding using high-speed images, *Journal of Manufacturing Science and Engineering* 137(3) (2015) 031016.
- [17] B. Kang, W. Cai, C.-A. Tan, Dynamic response of battery tabs under ultrasonic welding, *Journal of Manufacturing Science and Engineering* 135(5) (2013) 051013.
- [18] H.P.C. Daniels, Ultrasonic welding, *Ultrasonics* 3(4) (1965) 190-196.
- [19] E.A. Neppiras, Ultrasonic welding of metals, *Ultrasonics* 3(3) (1965) 128-135.
- [20] S. Lee, Process and quality characterization for ultrasonic welding for lithium-ion batteries, University of Michigan 2013.
- [21] C. Ageorges, L. Yea, M. Hou, Advances in fusion bonding techniques for joining thermoplastic matrix composites: a review, *Composites* 32(6) (2001) 839-857.
- [22] M.P. Matheny, K.F. Graff, Ultrasonic welding of metals, *Power Ultrasonics* 2015, pp. 259-293.
- [23] S. Krüger, G. Wagner, D. Eifler, Ultrasonic welding of metal/composite joints, *Advanced Engineering Materials* 6(3) (2004) 157-159.
- [24] J. Tsujino, T. Ueoka, K. Hasegawa, Y. Fujita, T. Shiraki, T. Okada, T. Tamura, New methods of ultrasonic welding of metal and plastic materials, *Ultrasonics* 34(2-5) (1996) 177-185.
- [25] Understanding the true cost of weld defects. Miller.  
<https://www.millerwelds.com/resources/article-library/the-real-cost-of-missed-or-defective-welds>. (Accessed May 20, 2021)
- [26] S.N. Tell, A. Murumkar, H.D. Sawant, S.D. Jadhav, V.K. Yakkundi, P.N. Jadhav, Cost of quality for automobile industry: a review, *Equinox* 2018 – 4th International Conference on Engineering Confluence, Mumbai, 2018, pp. 47-53.
- [27] S.N. Tell, V. Majali, U. Bhushi, V.G. Surange, Impact of poor quality cost in automobile industry, *International Journal of Quality Engineering and Technology* 4(1) (2014) 21-41.
- [28] Y. Li, B. Yu, B. Wang, T.H. Lee, M. Banu, Online quality inspection of ultrasonic composite welding by combining artificial intelligence technologies with welding process signatures, *Materials & Design* 194 (2020).

- [29] T. Zhao, C. Broek, G. Palardy, I.F. Villegas, R. Benedictus, Towards robust sequential ultrasonic spot welding of thermoplastic composites: Welding process control strategy for consistent weld quality, *Composites Part A: Applied Science and Manufacturing* 109 (2018) 335-367.
- [30] K. Wang, D. Shriver, Y. Li, M. Banu, S.J. Hu, G. Xiao, J. Arinez, H.-T. Fan, Characterization of weld attributes in ultrasonic welding of short carbon fiber reinforced thermoplastic composites, *Journal of Manufacturing Processes* 29 (2017) 124-132.
- [31] M. Pouranvari, H.R. Asgari, S.M. Mosavizadch, P.H. Marashi, M. Goodarzi, Effect of weld nugget size on overload failure mode of resistance spot welds, *Science and Technology of Welding and Joining* 12(3) (2013) 217-225.
- [32] M. Pouranvari, S.P.H. Marashi, Factors affecting mechanical properties of resistance spot welds, *Materials Science and Technology* 26(9) (2013) 1137-1144.
- [33] J.O. Obielodan, A. Ceylan, L.E. Murr, B.E. Stucker, Multi-material bonding in ultrasonic consolidation, *Rapid Prototyping Journal* 16(3) (2010) 180-188.
- [34] K. Wang, D. Shriver, M. Banu, S.J. Hu, G. Xiao, J. Arinez, H.-T. Fan, Performance prediction for ultrasonic spot welds of short carbon fiber-reinforced composites under shear loading, *Journal of Manufacturing Science and Engineering* 139(11) (2017) 111001.
- [35] S.G. Arul, S.F. Miller, G.H. Kruger, T.-Y. Pan, P.K. Mallick, A.J. Shih, Experimental study of joint performance in spot friction welding of 6111-T4 aluminium alloy, *Science and Technology of Welding and Joining* 13(7) (2008) 629-637.
- [36] B. Jonsson, J. Samuelsson, G.B. Marquis, Development of weld quality criteria based on fatigue performance, *Welding in the World* 55 (2013) 79-88.
- [37] Z. Ma, Y. Zhang, Characterization of multilayer ultrasonic welding based on the online monitoring of sonotrode displacement, *Journal of Manufacturing Processes* 54 (2020) 138-147.
- [38] P. Dong, Quantitative weld quality acceptance criteria: an enabler for structural lightweighting and additive manufacturing, *Welding Journal* 99 (2020) 39-51.
- [39] Y. Yu, P. Wang, X. Pei, P. Dong, H. Fang, Fatigue resistance characterization of frictions stir welds between complex aluminum extrusions: An experimental and finite element study, *International Journal of Fatigue* 141 (2020) 105861.
- [40] J. Zhang, P. Dong, A hybrid polygonal element method for fracture mechanics analysis of resistance spot welds containing porosity, *Engineering Fracture Mechanics* 59(6) (1998) 812-825.
- [41] S.A. David, J. Chen, B.T. Gibson, Z. Feng, Intelligent weld manufacturing: role of integrated computational welding engineering, in: Y.Z. Shanben Chen, Zhili Feng (Ed.), *Transactions on Intelligent Welding Manufacturing*, Springer, Singapore 2018.

- [42] S.C.A. Alfaro, P. Drews, Intelligent systems for welding process automation, *Journal of the Brazilian Society of Mechanical Science and Engineering* 28(1) (2006) 25-29.
- [43] D. Lee, N. Ku, T.-W. Kim, J. Kim, K.-Y. Lee, Y.-S. Son, Development and application of an intelligent welding robot system for shipbuilding, *Robotics and Computer-Integrated Manufacturing* 27(2) (2011) 377-388.
- [44] J. Davis, T. Edgar, J. Porter, J. Bernaden, M. Sarli, Smart manufacturing, manufacturing intelligence and demand-dynamic performance, *Computers & Chemical Engineering* 47 (2012) 145-156.
- [45] W.G. Guo, J.J. Jin, S.J. Hu, Profile monitoring and fault diagnosis via sensor fusion for ultrasonic welding, *Journal of Manufacturing Science and Engineering* 141(8) (2019) 081001.
- [46] W. Guo, J.J. Jin, S.J. Hu, Profile monitoring and fault diagnosis via sensor fusion for ultrasonic welding, 2016 International Manufacturing Science and Engineering Conference, Blacksburg, Virginia, USA, 2016.
- [47] V.I. Fernandez, In situ monitoring of ultrasonic welding of thermoplastic composites through power and displacement data, *Journal of Thermoplastic Composite Materials* 28(1) (2013) 66-85.

## CHAPTER 2

### LITERATURE REVIEW AND STATE-OF-THE-ART

#### 2.1 Introduction

This chapter first reviews the literature related to the proposed research in detail. This includes the state-of-the-art of relevant joining techniques, particularly, the weld formation mechanisms of ultrasonic welding process, and existing criteria in weld quality determination. Various methods of signal processing, feature selection and dimension reduction, and quality monitoring for ultrasonic welding are then discussed. Welding experiments and data acquisition techniques conducted by Wang *et al.* [1] and Li *et al.* [2] are introduced at the end, which serves a starting point of this research. Note that in their investigations [1, 2], the material used was injected molded short carbon fiber reinforced Nylon 6 plastic coupons. The main weld variables and parameters of weld experiments were determined by a two-level full factorial experimental design that found that weld energy levels are the most significant factor in determining weld attributes and joint performance. Under optimal parameter settings, weld attributes such as weld area and microstructure of weld zone were extracted, and joint performance such as maximum lap-shear strength was measured to determine weld quality. The weld quality determination criteria are the output criteria of quality monitoring algorithms in further chapters.

Based on available literature, the existing methods for weld quality monitoring in ultrasonic welding can be categorized into three types: (1) building regression analytical models, (2) constructing statistical process control charts, and (3) monitoring by machine learning algorithms. Given the complex data nature, multiple data sources, large amount of data as input, typically associated with ultrasonic welding process, machine learning algorithms should be a better choice for the process quality

monitoring purpose, compared with the analytical model and control chart. However, to do so, some gaps exist. These include: 1) lack of a sufficient understanding of the relationship among weld parameters, weld attributes, performance; 2) lack of sufficient number of weld experiments that can be used as training data to support deep learning algorithms; 3) lack of research on quality monitoring models that directly take time-series process signals as the input. These gaps must be addressed in order to achieve a reliable weld quality classification for ultrasonic welding process.

The remainder of this chapter is organized as follows: Section 2.2 reviews the state-of-the-art of joining technologies that are adopted in various manufacturing processes for joining CFRP materials. Section 2.3 describes the mechanisms and characteristics of ultrasonic welding. Section 2.4 reviews the typical weld attributes and the performance of weldments extracted in ultrasonic welding process and the commonly used criteria to determine weld quality. Section 2.5 discusses the methods for signal processing, feature selection and dimension reduction for ultrasonic welding. Section 2.6 introduces the Monte Carlo simulation approach using to generate large amounts of time-series process signals. Section 2.7 lists the existing quality monitoring models in ultrasonic welding. Section 2.8 reviews the weld experiments and data collection from the previous research. Finally, section 2.9 summarizes and concludes the chapter.

## **2.2 State-of-the-art of Joining Technologies**

The main joining technologies for CFRP materials in manufacturing are adhesive bonding, mechanical fastening, and fusion welding [3-5]. Each joining technique has specific characteristics. For instance, adhesive bonding joins CFRP materials with a polymer/solvent mixture that bonds the workpieces together after solidification. This technique has the advantages of low cost, lightweight, good fatigue-resistance, and good sealing and insulation performance. However, this technique needs special surface treatment before gluing, and requires high precision during the joining process. Moreover, an adhesive joint is a permanent connection which cannot be disassembled after being formed [3-8]. When precision bonding is not required, mechanical fastening

techniques are preferred. This involves creating a joint with fasteners such as screws or rivets. This technique is more suited for joining stronger plastics without special pretreatment to the surface. Workpieces joined through mechanical fastening can be assembled and disassembled repeatedly, as such, the assembly is easy to repair and replace. Nevertheless, the process adds weight to the workpieces and introduces fatigue due to loading at specific positions [3-5, 9-11]. Finally, fusion welding has the strengths of fast joining speed, high strength, high reliability, lightweight, etc. [3-5]. Due to these advantages, fusion welding accounts for a large proportion of CFRP joints in various industries [12-15]. Typical fusion joining techniques of CFRP materials are laser welding, resistance welding, vibration welding, and ultrasonic welding [3-5]. Among them, ultrasonic welding has better weld parameters control, less energy consumption, and good capability for joining different shapes of CFRP materials, and is considered superior to laser welding, resistance welding, and vibration welding [16-18].

### **2.3 Mechanisms and Characteristics of Ultrasonic Welding**

Ultrasonic welding can be applied to both metals and composites. Started in the mid-1960's [19, 20], ultrasonic metal welding (UMW) is a widely applied technique in industry. In recent decades, industries like automotive, aerospace, marine and electric appliances have extensively applied ultrasonic welding processes due to its simplicity and safety. The application of ultrasonic welding to CFRP composites in automotive industry, however, is relatively new. A physical understanding of the process has not been completely understood yet [21, 22]. Therefore, in this section, previous research on the fundamental mechanisms and characteristics of ultrasonic composite welding (UCW) are reviewed.

Ultrasonic welding is the process that joins the surfaces of two objects by high-frequency vibration wave transmission. Under pressure, the surfaces of the objects rub against each other through vertical vibration, and then form a fusion connection between the molecular layers [19, 20, 23, 24]. The weld system elements are composed of a press, an anvil, an ultrasonic stack, the power supply, and the controller [25, 26]. The press locates two weld objects together under pressure by pneumatic or electric

drive. The anvil provides a place to locate the weld materials. The core of an ultrasonic welding machine is ultrasonic stack, which consists of a converter, an optimal booster, and a horn. The converter transforms a high-frequency electrical signal into mechanical vibration with equivalent frequency. The booster modifies the amplitude of the mechanical vibration. The horn applies the amplified mechanical vibration to the parts to be welded. The power supply and controller generate the high power signals at high frequency and control the horn movement, respectively [26].

Ultrasonic waves act on the material contact surfaces with high-frequency vibrations when applied to thermoplastic materials, producing tens of thousands of high-frequency vibrations per second [27-29]. The workpieces are fixed in the middle of the anvil and the horn, and then the energy of high-frequency acoustic vibration generated by a power supply is transmitted to the horn then to the workpieces. When the vertical vibration reaches a certain amplitude, energy is transmitted to the weld zone. Due to the large acoustic impedance at the weld joint interface, friction between the molecules at the interface will cause viscoelastic heat leading to local heat accumulation. Moreover, poor thermal conductivity of thermoplastic materials concentrates the heat in the weld zone. With increasing temperature, the contact surfaces of two workpieces melt rapidly. Under pressure, they are joined together, however, the pressure will last for a few seconds in order to solidify the materials when the ultrasonic waves cease. The two workpieces have then formed a strong molecular chain in the weld zone [3].

The molecular chain in the weldment should have the same good properties as the workpiece materials after welding process. In summary, the UCW process can be summarized in five steps: 1) horn and workpieces vibrate; 2) viscoelastic heating is generated due to intermolecular friction; 3) heat accumulates at the weld zone and the temperature rises; 4) the polymer melts and the carbon fiber flows into the melt pool; and 5) intermolecular diffusion of polymer chains forms across the interface [29].

#### **2.4 Weld Attributes, Joint Performance, and Weld Quality Determination**

There is an association between weld process parameters, weld attributes, joint performance, and weld quality. From the association of these four elements, weld

quality can be indirectly determined by weld attributes and joint performance, such as lap-shear strength, toughness, weld area, indentation, and microstructure of weld zone, etc.

### **Weld attributes and joint performance analysis**

Analyzing weld parameters is a common approach when researching weld quality. In previous research, parameters like weld time, speed, energy, displacement, etc., are the primary factors captured during the process [1, 28, 30, 31]. In addition, Liu and Chang [32] studied how weld parameters like amplitude and hold time impact joint performance when welding Nylon composites. H. Pouranvari *et al.* [33] modeled the effects of weld parameters on the weld nugget size. Other authors introduced an energy director as an approach to improve weld quality joint strength [32, 34, 35]. Generally speaking, specifying optimal weld parameters will lead to a higher probability of better weld attributes and joint performance.

General characteristics of ultrasonic welding that characterize a weld process fall into two common types, weld attributes and joint performance. Specifically, weld attributes are the external characteristics of weldments such as the thermo-mechanically affected zone, cracks, weld shapes, and so on [33, 36-38]. Joint performance represents the intrinsic properties of the weldments. These properties cannot be acquired by observation such as lap-shear strength, bond density, and toughness, but need to be tested by dedicated apparatus [39, 40]. However, joint performance is a more objective approach for determining weld quality [41-44].

### **Weld quality determination**

Weld quality determination is a core activity that must be completed before classification and prediction training tasks can be undertaken. Classification algorithms must have training criteria to predict different weld quality classes. Some researchers have defined quality through examining the microstructure of the weld zone [45-47]. For example, when using a microstructural analysis of the weld zone, three common failure modes can be observed at different weld energy levels, as shown in Figure 2.1

[45]. They are interfacial separation, nugget shear fracture, and nugget pull-out fracture. Specifically, interfacial separation occurs when weld energy ranges from 200  $J$  to 600  $J$ , which is caused by polymer fracture. This failure mode is characterized by a small weld area and low strength. For nugget shear fracture, which occurs when the weld energy is between 600  $J$  and 1000  $J$ , the polymer ruptures and the carbon fiber simultaneously pulls out from the polymer matrix. Nugget pull-out fracture, which occurs when energy larger than 1000  $J$ , is characterized by pull-out of composite from one workpiece then sticking to the other piece.

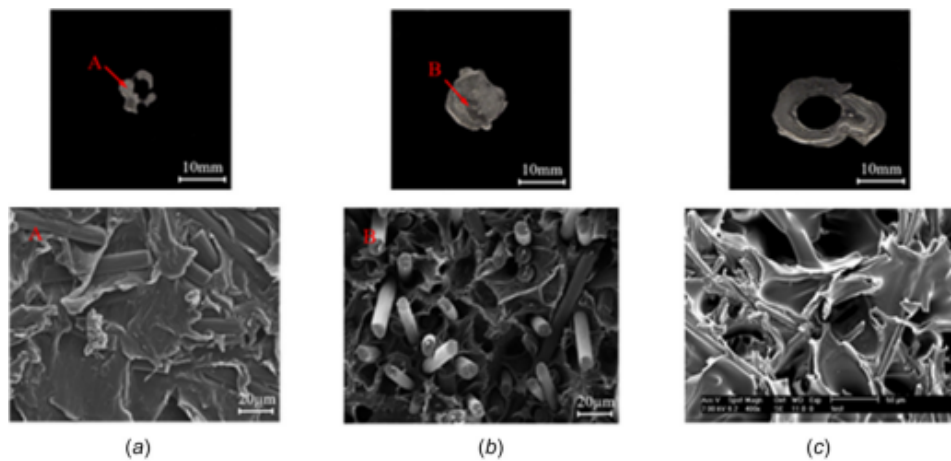


**Figure 2.1. Three typical failure modes: (a) interfacial separation, (b) nugget shear fracture, and (c) nugget pull-out fracture [45]**

Other researchers use analytical models of weld attributes and performance (e.g., weld area, thickness, horn indentation, lap-shear strength, stiffness, etc.) to classify different weld quality types [1, 2, 39, 45, 47-51]. For instance, Wang *et al.* [1, 45] developed an analytical model for shear toughness and maximum lap-shear strength from weld parameters such as weld energy. This model explains the relationship in detail and allows the determination of parameters ranges corresponding to different weld quality, as shown in Figure 2.2. The weld area, lap-shear strength, and toughness can be divided into piecewise functions. Details of the analytical models can be found in [45]. To a certain extent, the weld attributes and joint performance are predictable from these models.

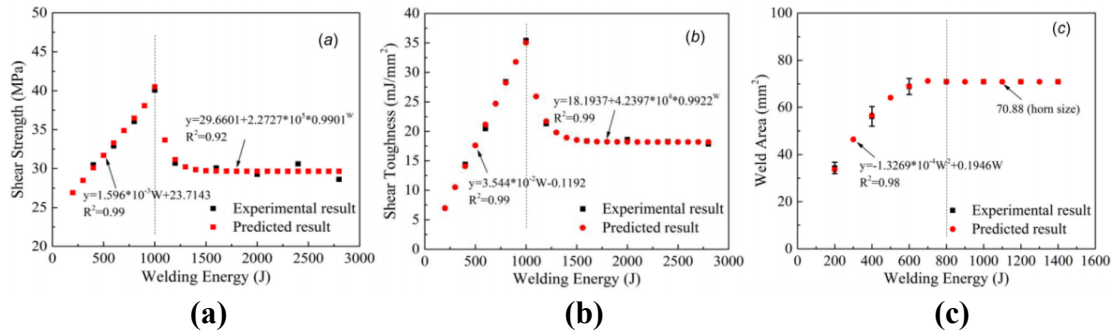


**Figure 2.2. Predicted versus experimental dependencies of cohesive parameters: (a) shear strength, (b) shear toughness, and (c) weld area on the welding energy [45]**

In summary, the mechanisms and characteristics of UCW have been described, and other researchers' work on parameters, weld attributes and joint performance have been summarized. Next, how the data from weld experiments can be processed is reviewed.

## 2.5 Signal Processing, Feature Selection, and Dimension Reduction

The main parameters of the ultrasonic welding process are current, voltage, travel speed, power, force, and displacement, etc. These signals all have potential as inputs into quality prediction algorithms. However, the variety of signals that can be collected does not necessary mean all of them are helpful for quality detection and monitoring during the welding process. Therefore, signals and the processing methods will be first reviewed, then the feature selection and dimension reduction methods will be discussed.

### Signal processing methods

Signals are very important for quality detection and monitoring in welding process. Different signals can be directly obtained from welding process software or be acquired by external sensors. Specifically, in ultrasonic welding, the commonly signals extracted are clamping force [52], clamp displacement [30, 52], power [30, 52], weld energy [1, 45, 53] and temperature [54], etc. However, due to noise in the environment and the welding process, it is difficult to directly adopt these signals for fault detection.

Therefore, signals should be filtered first prior to further feature selection and dimension reduction in order to mitigate the impact of noise.

When acquiring welding process signals, no matter if it is in the laboratory or during a production process, noise cannot be avoided. It usually comes from background and the welding process, which is an obstacle to extracting valuable information [55]. The noise appearing in a welding process is frequently assumed stochastic, with a Gaussian distribution [56, 57]. The probability density function  $p$  of Gaussian noise is shown in Equation (2.1).

$$P_G(z) = \frac{1}{\sigma\sqrt{2\pi}} e^{-\frac{(z-\mu)^2}{2\sigma^2}} \quad (2.1)$$

where  $z$  is the Gaussian random variable,  $\mu$  is the mean value, and  $\sigma$  is the standard deviation [58]. In order to reduce the negative impact of Gaussian noise, Gaussian filters, median filters, and Wiener filter are typically applied to remove the noise, not only for parametric digital signals but also for vision image signals [59]. Literature related to filtering of signals for various welding processes are listed in Table 2.1.

**Table 2.1 Signal processing methods applied in welding process**

Data source (signals)	Processing methods	Weld type	Refs
Arc spectrum, arc sound signal, arc voltage signal, temperature signal	FFT/STFT/Wavelet packet	GMAW, GTAW	[60] [61] [62] [63] [64]
Photodiode, visual sensor, spectrometer, acoustical sensor, pyrometer, plasma sensor	FFT/STFT/Kalman filter/Wavelet packet/High (low)-pass filter	Laser welding	[65] [66] [67] [68] [69]
Arc current signal, arc voltage signal	Moving average	P-MAG	[70]
Ultrasonic signals: power signal, energy signal, force signal	FFT/Wavelet packet/Gabor filter	Ultrasonic welding	[71] [72]

Focusing only on ultrasonic welding, power, energy, displacement, force, and frequency signals have been preprocessed by unique processing methods. For example, Grasso *et al.* [73, 74] and Shao *et al.* [75] applied a statistical process control (SPC) chart to tune the parameters and screen the signals. Another common filter is a wavelet

transform [76-78], where the signal is transformed into the time-frequency domain with a window size varying with the frequency. This filter reduces insignificant frequency parts but keeps the characteristic frequency bands.

Additionally, signal to noise ratio (SNR), mean square error (MSE) or root mean square error (RMSE), and peak signal-to-noise ratio (PSNR) are parameters used for determining the efficiency of filters [56].

(1) In the signal-to-noise ratio (SNR), a higher ratio indicates the background noise is less obvious.

$$SNR = \frac{P_{signal}}{P_{noise}} \quad (2.2)$$

where  $P_{signal}$  is the average power of raw signals, and  $P_{noise}$  is the average power of noise [79, 80].

(2) MSE and RMSE represent the measurement of the degree of difference between an estimator and an estimated amount [81, 82]:

$$MSE = \frac{1}{mn} \sum_0^{m-1} \sum_0^{n-1} \|I(i, j) - K(i, j)\|^2 \quad (2.3)$$

$$RMSE = \sqrt{MSE} \quad (2.4)$$

where  $I$  and  $K$  are the two-dimension categories,  $m$  and  $n$  are the size of  $I$  and  $K$ .

(3) PSNR usually compares the maximum signal and the background noise. The higher the value, the better the quality of the reconstructed signal [83].

$$PSNR = 10 \cdot \log_{10} \left( \frac{MAX_I^2}{MSE} \right) \quad (2.5)$$

where  $MAX_I^2$  is the maximum possible value of the signal, MSE is the mean squared error of the signal.

In general, the aim of signal processing is a preprocessing transformation in preparation for feature extraction. Features represent points or characteristics from multiple continuous data signals that summarize its information, and therefore extraction creates a new dataset [84-86]. Generally, the features to be extracted are

determined by criteria defined by researchers, and may be represented by peak values, inflection points, slopes, areas, etc.

### **Feature selection and dimension reduction methods**

The object of feature selection is to filter irrelevant or redundant features from a raw dataset. This process finds a parsimonious set of features to reduce the problem's dimension and but keep maximum information content. This is useful for decreasing computational effort, controlling quality, and saving time when faced with the large input of ultrasonic welding data [86, 87]. Common approaches used in dimensionality reduction are discussed as follows:

(1) *Correlation analysis*: Correlation analysis is a statistical method that is calculated from the variance and co-variance matrix to evaluate the correlation among features [88]. It helps to quantify the correlation among different variables in order to reduce the redundancy between features. Correlation measures range from -1 to 1, where a negative correlation means the trend of one variable decreases as the trend of the other increases. Conversely, positive correlation indicates both variables trend in the same direction. As the absolute value of correlation measure increases, the stronger their correlation. When the correlation measure equals 0, the two variables are independent. Angam Praveen *et al.* [78] applied correlation analysis to reduce white noise and then select features. Yaser *et al.* [89] studied signal correlation for monitoring tool wear in ultrasonic welding.

(2) *Fisher's ratio*: Fisher's ratio is a measure for the linear discrimination power of two variables representing classes with different means  $\mu_1$  and  $\mu_2$ , and variance  $\sigma_1^2$  and  $\sigma_2^2$  [90].

$$Fisher's\ ratio = \frac{(\mu_1 - \mu_2)^2}{\sigma_1^2 + \sigma_2^2} \quad (2.6)$$

Fisher's ratio can be used for feature selection, as the higher the Fisher's ratio, the lower repeatability of the two features. As such, a higher Fisher's ratio indicates better feature discrimination [90]. Related concepts are F-test (analysis of variance ANOVA) and  $p$ -value. As an application example, each feature

acquired from a welding process has a mean and variance, and each feature is compared to all others by calculating the pairwise Fisher's ratio. If the ratio value is larger than a threshold, the feature will be kept. Otherwise, the features will be removed.

- (3) *Linear discriminant analysis*: Linear discriminant analysis (LDA) selects features by projecting data from a training set on a line using tools from linear combination that minimizes the distribution of projected sample points within the same class, while simultaneously maximizing the distribution of projected points from the other classes. Features are sequentially added to the model, the distance between the different classes is calculated, and a feature is retained when the distance between the classes increases after the projection.

The LDA approach has been used for feature selection in UMW. For example, Nazir and Shao [91] used LDA and the high dimension discriminant analysis - quadratic discriminant analysis - to select features and then classify weld quality. The classification accuracy was respective 97%, 99.5%, or 83.5% when using individual acoustic emission, displacement, or power features as the input. In addition, Guo *et al.* [92] applied LDA and variant discriminant analysis methods based on LDA, such as vectorized LDA, uncorrelated multilinear LDA, and regularized uncorrelated multilinear LDA, to classify five weld quality types in UMW. The overall identification rate of these LDA methods was around 73%.

In summary, the three approaches applied to feature selection and dimension reduction in welding process are listed in Table 2.1.

**Table 2.2 The strengths and weaknesses of commonly used selection methods in welding process**

Methods	Strengths and weaknesses
Correlation thresholds	<p><b>Pros:</b> Applying correlation thresholds works for similar features provide redundant information. And the method is fast and simple to calculate.</p> <p><b>Cons:</b> There is an issue to choose proper threshold, if the threshold is set too low, useful information will be dropped, otherwise, redundant information may be kept; keeping which correlated feature is another significance.</p>
Fisher's ratio	<p><b>Pros:</b> Fisher's ratio is an intuitive, fast and simple measurement for linear or nonlinear discriminating power of variables.</p> <p><b>Cons:</b> It is not robustness for dealing with multidimensional categories; there is an issue to select the proper Fisher's threshold.</p>
LDA	<p><b>Pros:</b> LDA is a supervised dimensionality reduction approach that uses labels to measure the differences of features from each category.</p> <p><b>Cons:</b> The method is not suitable for a non-Gaussian distributed data input and the approach has the limitation in dimensionality reduction when dimension is larger than <math>k-1</math>.</p>

## 2.6 Monte Carlo Simulation

Multivariate Monte Carlo (MMC) simulation is a method using random sampling and statistical distributions first published by Stanislaw Ulam, and used by Von Neumann in computer modelling in the late 1940s [93]. The basic principle of the simulation is an approach which based on the probability model of the existing data, and then estimates the samplings by introducing a random parameter [94]. Usually, there are three commonly types of MMC simulation for generating data: they are 1) normal approximation MMC simulation [95], 2) semi-empirical distribution MMC simulation [96], and 3) empirical distribution MMC simulation with copulas [97]. The difference of them are the assumptions. For example, 1<sup>st</sup> approach uses the normal distribution as the assumption. While the 2<sup>nd</sup> and the 3<sup>rd</sup> approach assume the original data follows semi-empirical and empirical distribution, respectively. In addition, the 3<sup>rd</sup> approach also introduces a copulas factor, which takes joint probability of each data

point into consideration. Since the time-series-based data of ultrasonic welding is dependent with the previous data points, the empirical distribution MMC simulation with copulas is determined as the most proper approach to generate large amounts of data.

In literature review, Papadrakakis *et al.* [98] used MMC simulation method incorporating the importance sampling technique for selecting the most significant samples. Then the author optimized the reliability-based structural of large-scale systems through these samples. With the simulated signals, the optimal design optimization parameters could be determined. In another one, Heslop *et al.* [99] adopted the same simulation approach on time-series paleoclimatic records to simulate the sampling of paleoclimate involving the addition types of noises. The Chapter 4 of the dissertation also used copulas MMC simulation approach to generate large amounts of time-series process signals of UCW to train the deep convolutional neural network algorithm. The comparison and selection of three commonly MMC simulation approaches is described of the Appendix 4.A in Chapter 4.

## **2.7 Weld Quality Monitoring**

Beyond of feature selection and dimension reduction, classification is also very important to quality detection and monitoring [60, 61]. Appropriate classification algorithms can detect various weld classes effectively. The criteria used to measure the accuracy of classification methods are  $\alpha$  error and  $\beta$  error. In previous research, support vector machine (SVM) [91, 100], k-nearest neighbors (kNN) [91], and artificial neural network (ANN)-based models [49, 101, 102] have been used for fault detection and prediction, not just in ultrasonic welding [72], but in other welding process such as arc welding [60, 64, 103], friction stir welding [104], and laser welding [65, 66].

### **Support vector machine**

A SVM is a generalized linear classifier that searches for a maximum-margin hyperplane within the raw data. The algorithm seeks to identify a decision boundary that maximizes the distance between the nearest units of different classes [105, 106].

The SVM algorithm is robustness against overfitting when dealing with high-dimensional classification. However, kernel mechanisms must be included to solve nonlinear classification problems [107]. Because the approach is memory intensive [108], selecting proper kernels is tricky. Also, sometimes the method does not scale well to large datasets. Therefore, an SVM algorithm should generally be selected when the sample size is small. A mathematical explanation of the algorithm will be discussed in Chapter 3.

Previous use of SVM in welding includes Zhang *et al.* [60], who proposed SVM cross-validation for weld type detection in arc welding [60, 64, 103], and Chen *et al.* [103] who formulated an SVM-based fuzzy rules system for laser welding [65]. In addition, Wang *et al.* [72] combined SVM and backpropagation-ANN (B-ANN) to screen features and classify joint strength in resistance ultrasonic welding system. In general, SVM and SVM-based selection or classification approaches commonly appear as methods for quality monitoring in welding techniques. Nevertheless, the approach has limitations when applied to multi-dimensional or large volumes of input data.

### **K-nearest neighbors**

The idea of the kNN algorithm is to calculate the distance of an observation to its k-nearest neighbors in the testing data set. When the majority of these k-nearest neighbors belong to a given class, the new sample is classified as that class. The disadvantage of this algorithm is it must calculate the distance to all samples before ranking the distances to establish the k-nearest neighbors. This requires a large computational overhead to obtain classification results when the size of the sample set is very large.

Nazir and Shao [91] compared kNN with LDA for weld quality monitoring in UMW based on various features. With sensor fusion, kNN could obtain an identification accuracy around 99%.

### **Artificial neural networks**

An ANN is an operational model that was created in 1990s to exploit the architecture of the human brain to perform tasks. The algorithm consists of inputs, outputs and a large amount of interconnected cells or ‘neurons’ [109, 110]. As the number of neurons increase, the more complicated the model will be. Each neuron layer correlates its input and output with an activation function or propagation function. Usually *sigmoid* and *ReLU* are selected as the activation functions. Weight functions act on each path from the previous layer to the next layer, denoting the importance of each connection.

At the input,  $\mathbf{z}^{(0)} = \mathbf{x}$ , and output,  $\mathbf{z}^{(L)} = \mathbf{a}^{(L)}$ , layers. Activation functions in hidden layers is denoted by a  $\sigma$  function. In the hidden layers, weight function multiplies the output side of the previous hidden layer to the input side of the hidden layer. The transmission function has a form like:

$$\mathbf{a}^{(l)} = \mathbf{W}^{(l)} \mathbf{z}^{(l-1)} \quad (2.7)$$

$$\mathbf{z}^{(l)} = \sigma(\mathbf{a}^{(l)}) \quad (2.8)$$

where the hidden layer  $l$  ranges from 1 to  $L$ . When a bias term is introduced, the form changes to:

$$\mathbf{a}^{(l)} = \mathbf{W}^{(l)} \mathbf{z}^{(l-1)} + \text{bias} \quad (2.9)$$

The other detailed parameters with input and neurons are listed as:

$$a_{nj}^{(l)} = \text{value of } a_j^{(l)} \text{ with input } \mathbf{x}_n \quad (2.10)$$

$$z_{nj}^{(l)} = \text{value of } z_j^{(l)} \text{ with input } \mathbf{x}_n \quad (2.11)$$

where subscript  $n$  indicates the dimension of input, subscript  $j$  indicates the neuron number. Considering hidden layer  $l$ ,  $a_{nj}^{(l)}$  is a function of weight function  $w_{ji}^{(l)}$  for each neuron  $i$ , the chain rule could be represented as:

$$\frac{\partial R_n(\boldsymbol{\theta})}{\partial w_{ji}^{(l)}} = \frac{\partial R_n(\boldsymbol{\theta})}{\partial a_{nj}^{(l)}} \frac{\partial a_{nj}^{(l)}}{\partial w_{ji}^{(l)}} \quad (2.12)$$

where  $R_n(\boldsymbol{\theta}) = (y_n - f(\mathbf{x}_n))^2$  represents as the loss function. Two terms are defined as:

$$\delta_{nj}^{(l)} := \frac{\partial R_n(\boldsymbol{\theta})}{\partial a_{nj}^{(l)}} \quad (2.13)$$

$$z_{ni}^{(l-1)} := \frac{\partial a_{nj}^{(l)}}{\partial w_{ji}^{(l)}} \quad (2.14)$$

$\delta_{nj}^{(l)}$  works as the criterion to move back toward input layer.

When propagating to next layer, the chain is derivative of the form:

$$\delta_{nj}^{(l)} = \sum_m \frac{\partial R_n(\boldsymbol{\theta})}{\partial a_{nm}^{(l+1)}} \frac{\partial a_{nm}^{(l+1)}}{\partial a_{nj}^{(l)}} \quad (2.15)$$

where  $m$  indexes the nodes in layer  $l+1$ .

Then:

$$\frac{\partial a_{nm}^{(l+1)}}{\partial a_{nj}^{(l)}} = \frac{\partial \sum_r w_{mr}^{(l+1)} z_{nr}^{(l)}}{\partial a_{nj}^{(l)}} = \frac{\partial \sum_r w_{mr}^{(l+1)} \sigma(a_{nr}^{(l)})}{\partial a_{nj}^{(l)}} = w_{mj}^{(l+1)} \sigma'(a_{nj}^{(l)}) \quad (2.16)$$

In summary, the propagation principle with loss function could be represented as:

$$\delta_{nj}^{(l)} = \sum_m \delta_{nm}^{(l+1)} w_{mj}^{(l+1)} \sigma'(a_{nj}^{(l)}) \quad (2.17)$$

then the correlation with layer  $l$  and  $l+1$  are connected.

When determining the weight and bias of the neural network models, the network is trained using optimization techniques. A learning rate is used to define the size of the corrective steps at each iteration, driving the program towards its optimal result [111]. A high learning rate will shorten the training time, but decreases accuracy [112, 113].

ANN-based models are the most applied approach used for fault detection and prediction, not only in ultrasonic welding system, but also for other types of welding processes. For example, perception ANN had been used for classifying weld flaws by analyzing parametric digital signals in arc welding [64, 68, 69, 71] and vision digital signals acquired from radiographic images in welding process [114]. In friction stir welding, supervised learning ANN was used for sensor-based monitoring and control [104]. Neural network-based deep learning algorithms like convolutional neural

network (CNN) [115, 116], generative adversarial network (GAN) [116], and deep neural network (DNN) [117] have been used to detect and classify quality through image signals in arc welding [116] and laser welding [117]. For example, Li *et al.* [49] applied a backpropagation ANN to predict weld quality under each of three surface contact conditions, with a gap, polished, and as-received. The overall identification error rate was around 3% for with a gap, 6% for polished, and 40% for as-received. In addition, Lee *et al.* [118] used a neural network algorithm to classify weld quality in resistance spot welding, with about 88.8% of the total number of sample's lap-shear strength successfully inferred for the welding type. In general, ANN and deep learning neural network algorithms can deal with large amounts of input data and uncertain or non-linear relationships between inputs and outputs.

## **2.8 Weld Experiments Setup and Data Acquisition**

This section introduces the UCW experiments that provided the data for this thesis in detail, including the material, the weld machine and related apparatus, as conducted by [2] and [1].

### **Material selection**

The material used in this research is injection molded CFRP Nylon 6 plastic sheets. It is a semi-crystalline material [1] consisting of two parts, the carbon fiber reinforcement and the matrix. The reinforcement is what determines the rigidity and strength of the material, while the matrix is a doped polymer resin. The material has a matrix consisting of polyamide 6 reinforced with 30% weight fraction of fibers. The dimension of the workpieces to be welded are 138 *mm* (length)\*38 *mm* (width)\*3 *mm* (depth). The contact area of two workpieces is 38 *mm*×38 *mm*. In addition, the mean diameter and the length of the fibers are 8  $\mu\text{m}$  and 250  $\mu\text{m}$ , respectively [2]. The CFRP samples are described in Figure 2.3.

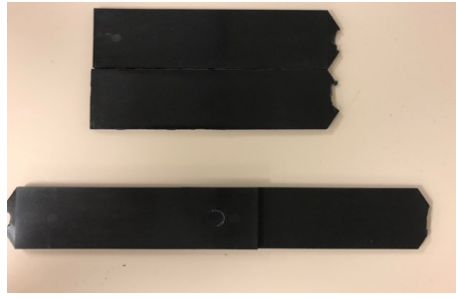


**Figure 2.3.** The CFRP coupons using in weld experiments

**Weld machine and related apparatus**

The CFRP coupons were joined using an *iQ Servo Ultrasonic Welding Machine* [119], which has an ultrasonic generator generating a 20 kHz vibration, and a tool head with a horn diameter of 9.5 mm. The weld machine and the schematic diagram of joining process are illustrated in Figure 2.4. In addition, other apparatus used in the experiments include an oven [120], a universal tensile testing system [121], and a scanning electron microscope [122]. They are shown in Figure 2.5.

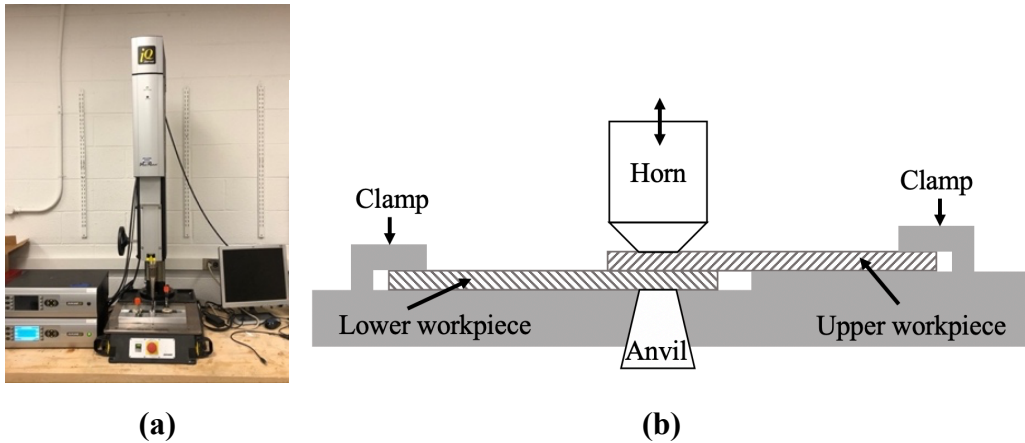


**Figure 2.4.** (a) Ultrasonic composite welding machine, (b) schematic diagram of joining process

- (1) *Oven*: An oven was used for baking the test coupons to remove the moisture. The reasons of removing the moisture are that it would weaken the joining strength and reduce the weld effect. The oven type is *Thermo Scientific Lindberg/Blue M 1100°C Box Furnace BF51700 Series* [120]. The baking temperature was preset at around

70°C for dehumidifying of CFRP material. The weldments need to be baked at the preset temperature for at least 1 day (around 24 hours), and then it takes around 1 day (around 24 hours) to cool down before welding.

- (2) *Universal testing systems*: A lap-shear strength tester was used to test the loading capacity of welded coupons. The tester is a *3345 Series Universal Testing Systems* with *force transducer model 2519-107* up to 5000 N and 1123 mm vertical test space. The related processing software is *Bluehill Universal* [121].
- (3) *Scanning electron microscope*: A scanning electron microscope (SEM) was used for visualizing the microstructure of the welded workpiece. SEM equipment such as 1) *Thermo Fisher Quanta 3D SEM/FIB*, 2) *Thermo Fisher Nova 200 Nanolab SEM/FIB*, and 3) *Thermo Fisher Helios 650 Nanolab SEM/FIB* were used to capture the microstructure of weld zone. In addition, the weld area was calculated by software *ImageJ* [122]. The contact surfaces of two workpieces after being separated and the weld zone were scanned and analyzed with *ImageJ*, where the weld area was differentiated by setting binary pixels.

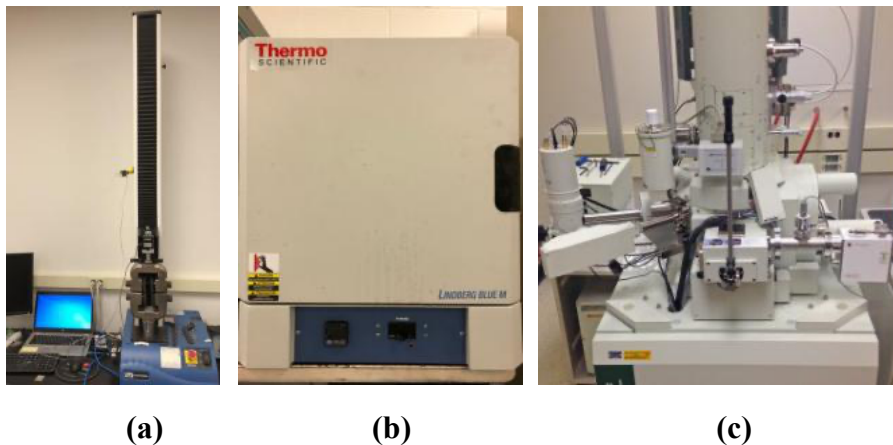


**Figure 2.5. The related experiment apparatus using in welding process: (a) universal testing systems, (b) oven, and (c) SEM**

### Data acquisition

Detailed welding process steps are described in Chapter 3. In addition, according to the weld experiments conducted by [2] and [1], a two-level full factorial experimental design was performed to extract which parameters have the most significant influence on weld attributes and joint performance [1]. The parameters that have the most significant influence on weld results are weld energy, trigger force, plunge speed, holding time and amplitude. The ranges of these parameters are listed in Table 2.3. The minimum, median, and maximum value were selected as the variables for weld experiments. Under each experiment, the rest of the parameters were kept at fixed values. Three replicate tests were performed under the same parameter settings, and the welded samples were tested on a tensile machine with a constant displacement speed of  $2 \text{ mm/min}$ . The main effect of the lap-shear test was the average strength value of these weld parameters are shown in Figure 2.6. As can be seen in the figure, the maximum lap-shear load-weld energy relationship has the largest slope among all the parameters, which indicates the weld energy has the most significant influence on the maximum lap-shear load. Therefore, the weld energy was selected as the key parameter of the welding process. The best setting for the other process parameter variables was also determined. Based on the weld experiments, the optimal process parameter settings extracted from experimental design was a trigger force of  $200 \text{ N}$  ( $45 \text{ lb}$ ), a weld speed of  $0.3 \text{ mm/s}$  ( $0.0118 \text{ in/s}$ ), a holding time of  $6 \text{ s}$ , and a vibration amplitude of  $\pm 33 \text{ }\mu\text{m}$  (95% of the peak value). Under these optimal welding process parameter settings, weld coupons were fabricated at weld energy levels of  $200 \text{ J}$ ,  $400 \text{ J}$ ,  $600 \text{ J}$ ,  $800 \text{ J}$ ,  $1000 \text{ J}$ ,  $1200 \text{ J}$ ,  $1400 \text{ J}$ , and  $1600 \text{ J}$  [1].

**Table 2.3 The ranges of different weld parameters**

<b>Weld Parameters</b>	<b>Ranges</b>
Trigger force	100 ~ 200 <i>N</i>
Weld energy	200 ~ 600 <i>J</i>
Plunge speed	0.1 ~ 0.3 <i>mm/s</i>
Holding time	2 ~ 6 <i>s</i>
Amplitude	85% ~ 95%

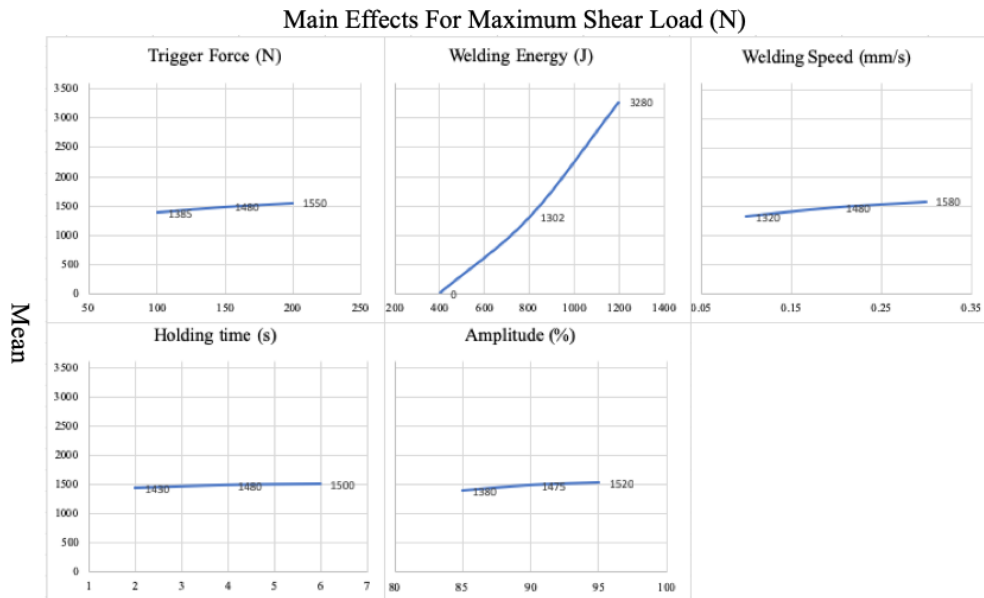


**Figure 2.6. The main effects of lap-shear strength tests with different weld parameters**

### **Weld attributes and joint performance extraction**

When completing data acquisition from weld experiments, weld attributes such as the microstructure and weld area, and weld performance such as the maximum lap-shear strength of each weldment were tested and measured in order to determine weld quality classes.

The lap-shear strength test is used to test the strength of the workpieces after the joining process. There is a threshold of weld parameter that determines the maximum lap-shear strength. When the weld energy level is too low, the weld may be hard to form. In contrast, when the energy level is higher than the threshold, the microstructure of weld zone may be disrupted due to the overheating, which makes the maximum lap-shear strength value decrease.

The weld area is another indicator that represents the weld effects. Area was captured and calculated by software *ImageJ*. The weld area of a sample is shown in Figure 2.7. Usually, the relationship of weld energy and weld area is to first increase then converge to a constant value. This is because the weld area depends on the size of horn. When the energy level is less than the threshold, the weld area will be less than

the area of the horn. When the weld energy exceeds a threshold, the weld area will reach the horn cross sectional area and thereafter be constant.



**Figure 2.7.** Illustration of weld area which is calculated by *ImageJ*

Another significant indicator is microstructure of the weld zone. The evolution of the microstructure of a cross-section is shown in Figure 2.8. Between the yellow lines is the weld zone. The green and red ovals surround where the flow of carbon fiber and the generation of pores occurred during the welding process, respectively. As can be seen, when weld energy is lower than  $800 J$ , there is a lower volume fraction of carbon fiber in the weld zone. However, large pores are generated in the polymer matrix due to the overheating when weld energy is larger than  $1200 J$  [45]. Therefore,  $800 J$  and  $1200 J$  can be considered approximately as the lower and upper weld energy boundary of good-welds. The detailed weld quality determination criteria are described both in Chapter 3 and Chapter 4.

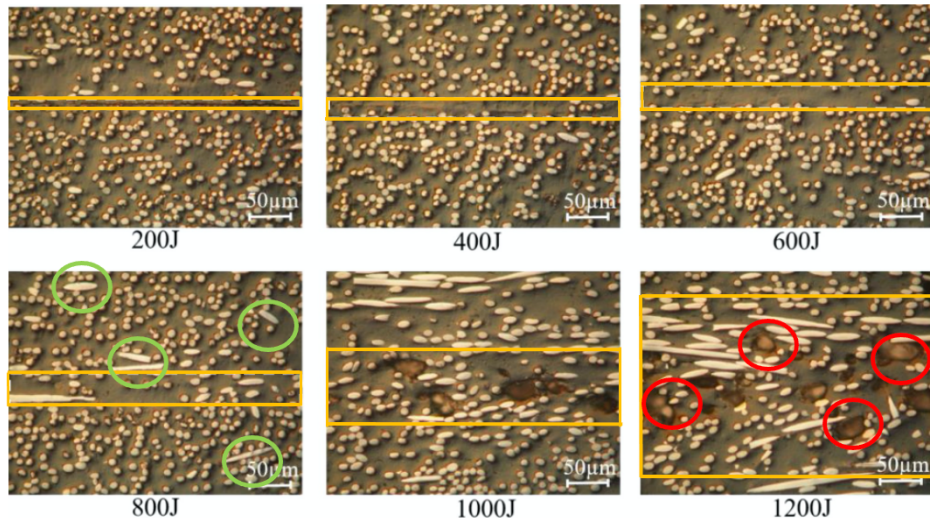


**Figure 2.8. The evolution of microstructure of the cross-section through the weld zone [45]**

## 2.9 Conclusion

Although there is some research on weld quality monitoring in ultrasonic welding, such as: 1) There is a lack of comprehensive understanding of correlation among weld parameters, attributes, joint performance, and weld quality in UCW. Most of the existing weld quality determination criteria are based on regression analytical models which may have some limitations when weld parameters are changed. 2) Weld experiment data set size may be insufficient to train and validate weld quality monitoring algorithms in ultrasonic welding. Even when quality monitoring algorithms obtained from laboratory weld experiments are accurate, they do not necessarily reproduce similar good results in the production environment. 3) Nearly all the existing quality monitoring models use feature-based data as their input. Feature-based data is simple and efficient for quality monitoring when there is small training data set size. However, when using large amounts of data as the input, some uncertainties arise for feature-based model, namely it is hard to define the features manually, it is hard to extract and select the features properly, and feature-based signals need more preprocessing and may lose some information, while time-series experimental process signals are easy to acquire and process. These are the gaps that will be addressed in this dissertation.

## References

- [1] K. Wang, D. Shriver, Y. Li, M. Banu, S.J. Hu, G. Xiao, J. Arinez, H.-T. Fan, Characterization of weld attributes in ultrasonic welding of short carbon fiber reinforced thermoplastic composites, *Journal of Manufacturing Processes* 29 (2017) 124-132.
- [2] Y. Li, J. Arinez, Z. Liu, T.H. Lee, H.-T. Fan, G. Xiao, M. Banu, S.J. Hu, Ultrasonic welding of carbon fiber reinforced composite with variable blank holding force, *Journal of Manufacturing Science and Engineering* 140(9) (2018) 091011.
- [3] A. Yousefpour, M. Hojjati, J.-P. Immarigeon, Fusion bonding/welding of thermoplastic composites, *Journal of Thermoplastic Composite Materials* 17(4) (2016) 303-341.
- [4] V.K. Stokes, Joining methods for plastics and plastic composites: an overview, *Polymer Engineering and Science* 29(19) (1989) 1310-1324.
- [5] J. Leone, Plastic joining methods. Science. <https://sciencing.com/plastic-joining-methods-6924074.html>. (Accessed May 20, 2021).
- [6] R.D. Adams, J. Comyn, Joining using adhesives, *Assembly Automation* 20(2) (2000) 109-117.
- [7] F.L. Palmieri, M.A. Belcher, C.J. Wohl, K.Y. Blohowiak, J.W. Connell, Laser ablation surface preparation for adhesive bonding of carbon fiber reinforced epoxy composites, *International Journal of Adhesion and Adhesives* 68 (2016) 95-101.
- [8] J.-H. Lu, J.P. Youngblood, Adhesive bonding of carbon fiber reinforced composite using UV-curing epoxy resin, *Composites Part B: Engineering* 82(1) (2015) 221-225.
- [9] N. Chowdhury, W.K. Chiu, J. Wang, P. Chang, Static and fatigue testing thin riveted, bonded and hybrid carbon fiber double lap joints used in aircraft structures, *Composites Structure* 121 (2015) 315-323.
- [10] W.E. Elsayed, U.A. Ebead, K.W. Neale, Studies on mechanically fastened FRP-strengthening systems, *ACI Structural Journal* 106(1) (2007) 49-59.
- [11] P.P. Camanho, M. Lambert, A design methodology for mechanically fastened joints in laminated composite materials, *Composites Science and Technology* 66(15) (2006) 3004-3020.
- [12] T. Suzuki, J. Takahashi, Prediction of energy intensity of carbon fiber reinforced plastics for mass-produced passenger cars, Conference: 9th Japan International SAMPE Symposium, Tokyo, Japan, 2005.
- [13] F. Rezaei, R. Yunus, N.A. Ibrahim, E.S. Mahdi, Development of short-carbon-fiber-reinforced polypropylene composite for car bonnet, *Polymer-Plastics Technology and Engineering* 47(4) (2008) 351-357.

- [14] K. Friedrich, A.A. Almajid, Manufacturing aspects of advanced polymer composites for automotive applications, *Applied Composites Materials* 20 (2012) 107-128.
- [15] M. Holmes, Carbon fibre reinforced plastics market continues growth path, *Reinforced Plastics* 57(6) (2013) 24-29.
- [16] Y.P. Korkolis, J. Li, B. Carlson, E. Chu, Special issue: Forming and joining of lightweight and multimaterial systems, *Journal of Manufacturing Science and Engineering* 137(5) (2015) 050201.
- [17] S.S. Lee, T.H. Kim, S.J. Hu, W.W. Cai, J.A. Abell, J. Li, Analysis of weld formation in multilayer ultrasonic metal welding using high-speed images, *Journal of Manufacturing Science and Engineering* 137(3) (2015) 031016.
- [18] B. Kang, W. Cai, C.-A. Tan, Dynamic response of battery tabs under ultrasonic welding, *Journal of Manufacturing Science and Engineering* 135(5) (2013) 051013.
- [19] E.A. Neppiras, Ultrasonic welding of metals, *Ultrasonics* 3(3) (1965) 128-135.
- [20] B. Lewis, K. Arthur, K. Claus, Ultrasonic welding, Cavitron Ultrasonics Inc, United States, 1959.
- [21] H. Potente, Ultrasonic welding-principle & theory, *Materials & Design* 5(5) (1984) 228-234.
- [22] Z. Mao, B.C. Goswami, Studies on the process of ultrasonic bonding of nonwovens: part 1 - theoretical analysis, *Journal of Engineered Fibers and Fabrics* 10(2) (2001).
- [23] H.P.C. Daniels, Ultrasonic welding, *Ultrasonics* 3(4) (1965) 190-196.
- [24] M.P. Matheny, K.F. Graff, Ultrasonic welding of metals, *Power Ultrasonics* 2015, pp. 259-293.
- [25] H. Gochermann, Apparatus for welding components together with the use of ultrasound, Telefunken Sendertechnik GmbH, United States, 1981.
- [26] Components. Ultrasonic welding.  
[https://en.wikipedia.org/wiki/Ultrasonic\\_welding](https://en.wikipedia.org/wiki/Ultrasonic_welding). (Accessed May 20, 2021).
- [27] S. Krüger, G. Wagner, D. Eifler, Ultrasonic welding of metal/composite joints, *Advanced Engineering Materials* 6(3) (2004) 157-159.
- [28] F. Balle, G. Wagner, D. Eifler, Ultrasonic metal welding of aluminium sheets to carbon fibre reinforced thermoplastic composites, *Advanced Engineering Materials* 11(1-2) (2009) 35-39.
- [29] A. Benatar, T.G. Gutowski, Ultrasonic welding of PEEK graphite APC-2 composites, *Polymer Engineering and Science* 29(23) (1989) 1705-1989.
- [30] V.I. Fernandez, In situ monitoring of ultrasonic welding of thermoplastic composites through power and displacement data, *Journal of Thermoplastic Composite Materials* 28(1) (2013) 66-85.

- [31] I.F. Villegas, L. Moser, A. Yousefpour, P. Mitschang, H.E. Bersee, Process and performance evaluation of ultrasonic, induction and resistance welding of advanced thermoplastic composites, *Journal of Thermoplastic Composite Materials* 26(8) (2012) 1007-1024.
- [32] S.-J. Liu, I.-T. Chang, Optimization the weld strength of ultrasonically welded nylon composites, *Journal of Composites Materials* 36(5) (2002) 611-624.
- [33] M. Pouranvari, H.R. Asgari, S.M. Mosavizadch, P.H. Marashi, M. Goodarzi, Effect of weld nugget size on overload failure mode of resistance spot welds, *Science and Technology of Welding and Joining* 12(3) (2013) 217-225.
- [34] G. Ramarathnam, T.H. North, R.T. Woodhams, Ultrasonic welding using tie-layer materials, part II: factors affecting the lap-shear strength of ultrasonic welds, *Polymer Engineering and Science* 32(9) (1992) 612-619.
- [35] I.F. Villegas, Strength development versus process data in ultrasonic welding of thermoplastic composites with flat energy directors, *Composites Part A: Applied Science and Manufacturing* 65 (2014) 27-37.
- [36] M. Pouranvari, S.P.H. Marashi, Factors affecting mechanical properties of resistance spot welds, *Materials Science and Technology* 26(9) (2013) 1137-1144.
- [37] H. Eisazadeh, M. Hamedi, A. Halvae, New parametric study of nugget size in resistance spot welding process using finite element method, *Materials & Design* 31(1) (2010) 149-157.
- [38] P. Marashi, M. Pouranvari, S.M.H. Sanaee, A. Abedi, S.H. Abootalebi, M. Goodarzi, Relationship between failure behaviour and weld fusion zone attributes of austenitic stainless steel resistance spot welds, *Materials Science and Technology* 24(12) (2013) 1506-1512.
- [39] S.S. Lee, T.H. Kim, S.J. Hu, W.W. Cai, J.A. Abell, J. Li, Characterization of joint quality in ultrasonic welding of battery tabs, *Journal of Manufacturing Science and Engineering*. 135(2) (2013) 021004.
- [40] S.S. Lee, C. Shao, T.H. Kim, S.J. Hu, E. Kannatey-Asibu, W.W. Cai, J.P. Spicer, J.A. Abell, Characterization of ultrasonic metal welding by correlating online sensor signals with weld attributes, *Journal of Manufacturing Science and Engineering* 136(5) (2014) 051019.
- [41] F. Keller, D.W. Smith, Correlation of the strength and structure of spot welds in aluminum alloys, *Welding Journal* 23 (1944).
- [42] R.C. McMaster, F.C. Lindrall, The interpretation of radiographs of spot welds in alclad 24S-T and 75S-T aluminum alloys, *Welding Journal* 25 (1946) 707-723.
- [43] J. Heuschkel, The expression of spot-weld properties, *Welding Journal* 59 (1952).
- [44] J.S. Jr., J. Baker, Spot weldability of high-strength sheet steels, *Welding Journal* 59 (1980).

- [45] K. Wang, D. Shriver, M. Banu, S.J. Hu, G. Xiao, J. Arinez, H.-T. Fan, Performance prediction for ultrasonic spot welds of short carbon fiber-reinforced composites under shear loading, *Journal of Manufacturing Science and Engineering* 139(11) (2017) 111001.
- [46] T. Zhao, C. Broek, G. Palardy, I.F. Villegas, R. Benedictus, Towards robust sequential ultrasonic spot welding of thermoplastic composites: Welding process control strategy for consistent weld quality, *Composites Part A: Applied Science and Manufacturing* 109 (2018) 335-367.
- [47] Y. Li, Z. Liu, J. Shen, T.H. Lee, M. Banu, S.J. Hu, Weld quality prediction in ultrasonic welding of carbon fiber composite based on an ultrasonic wave transmission model, *Journal of Manufacturing Science and Engineering* 141(8) (2019) 081010.
- [48] Y. Li, T.H. Lee, C. Wang, K. Wang, C. Tan, M. Banu, S.J. Hu, An artificial neural network model for predicting joint performance in ultrasonic welding of composites, 7th CIRP Conference on Assembly Technologies and Systems, Elsevier BV, 2018, pp. 85-88.
- [49] Y. Li, B. Yu, B. Wang, T.H. Lee, M. Banu, Online quality inspection of ultrasonic composite welding by combining artificial intelligence technologies with welding process signatures, *Materials & Design* 194 (2020).
- [50] S.K. Bhudolia, G. Gohel, K.F. Leong, A. Islam, Advances in ultrasonic welding of thermoplastic composites: A review, *Materials & Design* 13(6) (2020) 1284.
- [51] S.K. Bhudolia, G. Gohel, K.F. Leong, J. Robert J. Barsotti, Investigation on ultrasonic welding attributes of novel carbon/Elium® composites, *Materials & Design* 13(5) (2020) 1117.
- [52] W. Guo, C. Shao, T.H. Kim, S.J. Hu, J.J. Jin, J.P. Spicer, H. Wang, Online process monitoring with near-zero misdetection for ultrasonic welding of lithium-ion batteries: An integration of univariate and multivariate methods, *Journal of Manufacturing Systems* 38 (2016) 141-150.
- [53] K. Wang, Y. Li, M. Banu, J. Li, W. Guo, H. Khan, Effect of interfacial preheating on welded joints during ultrasonic composite welding, *Journal of Materials Processing Technology* 246 (2017) 116-122.
- [54] Z. Zhang, K. Wang, J. Li, Q. Yu, W. Cai, Investigation of interfacial layer for ultrasonic spot welded aluminium to copper joints, *Scientific Reports*, 2017.
- [55] A. Damongeot, G. André, Noise from ultrasonic welding machines: risks and prevention, *Applied Acoustics* 25(1) (1988) 49-66.
- [56] S. Kaur, Noise types and various removal techniques, *International Journal of Advanced Research in Electronics and Communication Engineering* 4(2) (2015).
- [57] D. Slepian, The one-sided barrier problem for Gaussian noise, *The Bell System Technical Journal* 41(2) (1962) 463-501.

- [58] Gaussian noise. Gaussian noise. [https://en.wikipedia.org/wiki/Gaussian\\_noise](https://en.wikipedia.org/wiki/Gaussian_noise). (Accessed May 20, 2021).
- [59] I. MicroImages, Smoothing and noise removal filters, TNTgis - Advanced Software for Geospatial Analysis, 2014.
- [60] Z. Zhang, H. Chen, Y. Xu, J. Zhong, N. Lv, S. Chen, Multisensor-based real-time quality monitoring by means of feature extraction, selection and modeling for Al alloy in arc welding, *Mechanical Systems and Signal Processing* 60-61 (2015) 151-165.
- [61] Z. Zhang, X. Chen, H. Chen, J. Zhong, S. Chen, Online welding quality monitoring based on feature extraction of arc voltage signal, *The International Journal of Advanced Manufacturing Technology* 70(9-12) (2014) 1661-1671.
- [62] J.F. Wang, H.D. Yu, Y.Z. Qian, R.Z. Yang, S.B. Chen, Feature extraction in welding penetration monitoring with arc sound signals, *Proceedings of the Institution of Mechanical Engineers, Part B: Journal of Engineering Manufacture* 225(9) (2011) 1683-1691.
- [63] E. Warinsiriruk, F. Mahfudianto, Design the feature extraction for real time inspection of welding quality, *The 2018 Technology Innovation Management and Engineering Science International Conference*, Bangkok, Thailand, 2018.
- [64] R. Du, Y. Xu, Z. Hou, J. Shu, S. Chen, Strong noise image processing for vision-based seam tracking in robotic gas metal arc welding, *The International Journal of Advanced Manufacturing Technology* 101(5-8) (2018) 2135-2149.
- [65] D. You, X. Gao, S. Katayama, Multisensor fusion system for monitoring high-power disk laser welding using support vector machine, *IEEE Transactions on Industrial Informatics* 10(2) (2014) 1285-1295.
- [66] D.Y. You, X.D. Gao, S. Katayama, Review of laser welding monitoring, *Science and Technology of Welding and Joining* 19(3) (2013) 181-201.
- [67] X. Lu, D. Gu, Y. Wang, Y. Qu, C. Qin, F. Huang, Feature extraction of welding seam image based on laser vision, *IEEE Sensors Journal* 18(11) (2018) 4715-4724.
- [68] F. Zou, Z. Zheng, K. Zhao, H. Sun, Robot tracking system research basing on optical sensors, *Sensors and Smart Structures Technologies for Civil, Mechanical, and Aerospace Systems 2019*, Denver, Colorado, 2019.
- [69] H. Sun, T. Ma, Z. Zheng, M. Wu, Robot welding seam tracking system research basing on image identify, *Sensors and Smart Structures Technologies for Civil, Mechanical, and Aerospace Systems 2019*, Denver, Colorado, 2019.
- [70] Z. Ye, H. Chen, F. Gu, S. Chen, Feature extraction from arc signal for height tracking system of P-MAG welding, *Robotic Welding, Intelligence and Automation 2015*, pp. 95-107.
- [71] L. Mohanasundari, P. Sivakumar, N. Chitra, Feature extraction through chaotic metrics for weld flaw classification, *International Journal of Innovative Technology and Exploring Engineering* 8(4S) (2019).

- [72] X. Wang, S. Guan, L. Hua, B. Wang, X. He, Classification of spot-welded joint strength using ultrasonic signal time-frequency features and PSO-SVM method, *Ultrasonics* 91 (2019) 161-169.
- [73] M. Grasso, B.M. Colosimo, M. Pacella, Profile monitoring via sensor fusion: the use of PCA methods for multi-channel data, *International Journal of Production Research* 52(20) (2014) 6110-6135.
- [74] M. Grasso, P. Albertelli, B.M. Colosimo, An adaptive SPC approach for multi-sensor fusion and monitoring of time-varying processes, *Procedia CIRP* 12 (2013) 61-66.
- [75] C. Shao, K. Paynabar, T.H. Kim, J.J. Jin, S.J. Hu, J.P. Spicer, H. Wang, J. A. Abell, Feature selection for manufacturing process monitoring using cross-validation, *Journal of Manufacturing Systems* 32(4) (2013) 550-555.
- [76] G. Simone, F.C. Morabito, R. Polikar, P. Ramuhalli, L. Udpa, S. Udpa, Feature extraction techniques for ultrasonic signal classification, *International Journal of Applied Electromagnetics and Mechanics* 15 (2001) 291-294.
- [77] R. Polikar, L. Udpa, S.S. Udpa, T. Taylor, Frequency invariant classification of ultrasonic weld inspection signals, *IEEE Transactions on Ultrasonics, Ferroelectrics, and Frequency Control* 45(3) (1998) 614-625.
- [78] A. Praveen, K. Vijayarekha, S.T. Abraham, B. Venkatraman, Signal quality enhancement using higher order wavelets for ultrasonic TOFD signals from austenitic stainless steel welds, *Ultrasonics* 53(7) (2013) 1288-1292.
- [79] L.J. Cronbach, G.C. Gleser, The signal/noise ratio in the comparison of reliability coefficients *Educational and Psychological Measurement* 24(3) (1964).
- [80] F.D. Kahn, The signal: noise ratio of a suggested spectral analyzer, *Astrophysical Journal* 129 (1959) 518-521.
- [81] C.W. Helstrom, Minimum mean-squared error of estimates in quantum statistics, *Physics Letters A* 25(2) (1967) 101-102.
- [82] R.F. Gunst, R.L. Mason, Biased estimation in regression: an evaluation using mean squared error, *Journal of the American Statistical Association* 72(359) (1976) 616-628.
- [83] R. Steele, Peak signal-to-noise ratio formulas for multistage delta modulation with RC-shaped Gaussian input signals, *Bell Labs Technical Journal* 61(3) (1982) 347-362.
- [84] I. Guyon, A. Elisseeff, *An introduction to feature extraction*, Springer, Berlin, Heidelberg, 2016.
- [85] M.S.H. Nizam, A.R.M. Zamzuri, S. Marizan, S.A. Zaki, Vision based identification and classification of weld defects in welding environments: a review, *Indian Journal of Science and Technology* 9(20) (2016).
- [86] J. Tang, S. Alelyani, H. Liu, *Feature selection for classification: a review*, *Data Classification*, CRC Press 2014, pp. 37-64.

- [87] X. Yao, X.D. Wang, Y.X. Zhang, W. Quan, Summary of feature selection algorithms, *Control and Decision* 27(2) (2012) 161-166.
- [88] M. Ezekiel, *Methods of correlation analysis*, 1930.
- [89] Y. Zerehsaz, C. Shao, J. Jin, Tool wear monitoring in ultrasonic welding using high-order decomposition, *Journal of Intelligent Manufacturing* 30(2) (2019) 657-669.
- [90] F.R.S. R.A. Fisher Sc.D., The use of multiple measurements in taxonomic problems, *Annals of Human Genetics* 7(2) (1936) 179-188.
- [91] Q. Nazir, C. Shao, Online tool condition monitoring for ultrasonic metal welding via sensor fusion and machine learning, *Journal of Manufacturing Processes* 62 (2021) 806-816.
- [92] W.G. Guo, J.J. Jin, S.J. Hu, Profile monitoring and fault diagnosis via sensor fusion for ultrasonic welding, *Journal of Manufacturing Science and Engineering* 141(8) (2019) 081001.
- [93] N. Metropolis, The beginning of the Monte Carlo method, *Los Alamos Science* (1987) 125-130.
- [94] C.Z. Mooney, *Monte Carlo simulation*, Sage, Newbury Park, CA, 1997.
- [95] R.M. Neal, *Monte Carlo implementation of Gaussian process models for Bayesian regression and classification*, Department of Statistics, University of Toronto, Department of Statistics, University of Toronto, 1997.
- [96] E. Sangiorgi, M.R. Pinto, A semi-empirical model of surface scattering for Monte Carlo simulation of silicon n-MOSFETs, *IEEE Transactions on Electron Devices* 39(2) (1992) 356-361.
- [97] C. Pan, C. Wang, Z. Zhao, J. Wang, Z. Bie, A copula function based Monte Carlo simulation method of multivariate wind speed and PV power spatio-temporal series, *Energy Procedia* 159 (2019) 213-218.
- [98] M. Papadrakakis, N.D. Lagaros, Reliability-based structural optimization using neural networks and Monte Carlo simulation, *Computer Methods in Applied Mechanics and Engineering* 191(32) (2002) 3491-3507.
- [99] D. Heslop, M.J. Dekkers, Spectral analysis of unevenly spaced climatic time series using CLEAN: signal recovery and derivation of significance levels using a Monte Carlo simulation, *Physics of the Earth and Planetary Interiors* 130(1-2) (2002) 103-116.
- [100] L. Liu, H. Chen, S. Chen, *Online monitoring of variable polarity TIG welding penetration state based on fusion of welding characteristic parameters and SVM*, Springer, Singapore, 2018.
- [101] Ó. Martín, M. López, F. Martín, Artificial neural networks for quality control by ultrasonic testing in resistance spot welding, *Journal of Materials Processing Technology* 183(2-3) (2007) 226-233.
- [102] W. Cai, J. Wang, P. Jiang, L. Cao, G. Mi, Q. Zhou, Application of sensing techniques and artificial intelligence-based methods to laser welding real-time

monitoring: A critical review of recent literature, *Journal of Manufacturing Systems* 57 (2020) 1-18.

[103] S.B. Chen, N. Lv, Research evolution on intelligentized technologies for arc welding process, *Journal of Manufacturing Processes* 16(1) (2014) 109-122.

[104] D. Mishra, R.B. Roy, S. Dutta, S.K. Pal, D. Chakravarty, A review on sensor based monitoring and control of friction stir welding process and a roadmap to Industry 4.0, *Journal of Manufacturing Processes* 36 (2018) 373-397.

[105] T. Hastie, R. Tibshirani, J. Friedman, *The elements of statistical learning: data mining, inference, and prediction*, Springer. pp., New York, 2009.

[106] C. Cortes, V. Vapnik, Support-Vector Networks, *Machine Learning* 20(3) (1995) 273-297.

[107] W.H. Press, S.A. Teukolsky, W.T. Vetterling, B.P. Flannery, *Support vector machines*, Cambridge University Press 2007.

[108] L. Iftode, J.P. Singh, Shared virtual memory-progress and challenges, *Proceedings of the IEEE* 87(3) (1999) 498-507.

[109] J. Zurada, *Introduction to artificial neural systems*, West Publishing Co., St. Paul, MN, USA, 1992.

[110] J.M. A.K. Jain, K.M. Mohiuddin, Artificial neural networks- a tutorial, *Computer* 29(3) (1996) 31-44.

[111] K.P. Murphy, *Machine learning: a probabilistic perspective*, The MIT Press, London, England, 2012.

[112] H.B. Kim, S.H. Jung, T.G. Kim, K.H. Park, Fast learning method for back-propagation neural network, *Neurocomputing* 11(1) (1996) 101-106.

[113] N.O. Attoh-Okine, Analysis of learning rate and momentum term in backpropagation neural network algorithm, *Advances in Engineering Software* 30(4) (1999) 291-302.

[114] N. Nacereddine, A.B. Goumeidane, D. Ziou, Unsupervised weld defect classification in radiographic images using multivariate generalized Gaussian mixture model with exact computation of mean and shape parameters, *Computers in Industry* 108 (2019) 132-149.

[115] P. Sassi, P. Tripicchio, C.A. Avizzano, A smart monitoring system for automatic welding defect detection, *IEEE Transactions on Industrial Electronics* 66(12) (2019) 9641-9650.

[116] Y. Feng, Z. Chen, D. Wang, J. Chen, Z. Feng, DeepWelding: a deep learning enhanced approach to GTAW using multi-source sensing images, *IEEE Transactions on Industrial Informatics* (2019) 1-1.

[117] J. Günther, P.M. Pilarski, G. Helfrich, H. Shen, K. Diepold, First steps towards an intelligent laser welding architecture using deep neural networks and reinforcement learning, *Procedia Technology* 15 (2014) 474-483.

- [118] S.R. Lee, Y.J. Choo, T.Y. Lee, M.H. Kim, S.K. Choi, A quality assurance technique for resistance spot welding using a neuro-fuzzy algorithm, *Journal of Manufacturing Systems* 20(5) (2001) 320-328.
- [119] iQ Servo Ultrasonic Welding. Dukane. <https://www.dukane.com/plastic-welding-products/iq-servo-ultrasonic-welding-2/>. (Accessed May 20, 2021).
- [120] Lindberg/Blue M™ Moldatherm™ Box Furnaces. ThermoFisher Scientific. <https://www.thermofisher.com/order/catalog/product/BF51794C#/BF51794C>. (Accessed May 20, 2021).
- [121] Universal testing systems. Instron. <https://www.instron.us/en-us/products/testing-systems/universal-testing-systems/electromechanical/3300/3340-single-column>. (Accessed May 20, 2021).
- [122] ImageJ. ImageJ. <https://imagej.nih.gov/ij/>. (Accessed May 20, 2021).

**CHAPTER 3**

**FEATURE-BASED WELD QUALITY CLASSIFICATION FOR  
ULTRASONIC WELDING OF CARBON FIBER REINFORCED POLYMER  
THROUGH BAYESIAN REGULARIZED NEURAL NETWORK**

**3.1 Introduction**

Carbon fiber reinforced polymers (CFRP) composite materials are widely used in many industries due to their properties of lightweight, high temperature and corrosion resistance, and high strength-to-weight ratio. In the automotive industry, these materials are excellent for reducing vehicle weight and improving fuel economy and durability. Since different manufacturing processes have important influences on the properties of CFRP, it is important to select the best joining process for CFRP in automotive assemblies. Among the commonly available joining techniques, such as adhesive bonding, mechanical fastening, and fusion-based joining [1-3], fusion-based joining is attractive for its lightweight, high strength, low cost, and fast processing time [3, 4]. The main fusion-based joining techniques for CFRP include laser welding, resistance welding, and ultrasonic welding [5, 6]. Ultrasonic welding has good control of the weld parameters, consumes less energy, and can join different CFRP material types, thus is considered superior to other welding processes by the automotive industry [7].

Ultrasonic welding has been commonly used to join sheet metals in automotive industry, especially for joining lithium-ion batteries [8, 9]. Researchers had developed quality detection and online monitoring algorithms using input signals such as force, sound, power, frequency, etc., for ultrasonic metal welding (UMW). The core of this research was to extract and select the most appropriate and parsimonious set of features that will lead to better monitoring and classification results. For example, Shao *et al.* [10] developed a manufacturing process monitoring algorithm using cross-validation to

select the optimal number of features by partitioning feature subsets. The criterion for selecting features was to minimize false positive ( $\alpha$  or Type I) and false negative ( $\beta$  or Type II) errors acquired for different numbers of features. The  $\beta$  error was intentionally set to be close 0%, but the  $\alpha$  error is still quite high. Chen *et al.* [11] classified weld defects by using a multi-class support vector machine (SVM) to select optimal features and reported a total accuracy >95%. Wang *et al.* [12] adopted a particle swarm optimization SVM algorithm, preprocessing signals by extracting both time and frequency domain features to realize the classification, again reporting an accuracy of ~95%.

Studies of ultrasonic composite welding (UCW) processes include Li *et al.* [13] and Wang *et al.* [14], who built regression models to predict outcomes such as weld area, lap-shear strength, and toughness based on process parameters that were then used to categorize weld quality from acceptable performance ranges. In another work, Li *et al.* [15] applied the backpropagation Artificial Neural Network (ANN) method to predict weld quality under each of three surface contact conditions, as-received, polished, and with a gap. The overall identification error rate for under-, normal-, or over-weld classifications was around 40% for as-received, 6% for polished, and 3% for with a gap. The results indicate the ANN algorithm works well when there are preprocessing before welding process. In addition, both Cai *et al.* [16] and Lee *et al.* [17] used neural network-based algorithm to deal with weld quality in laser welding and resistance spot welding, respectively. For the latter, 88.8% of the total number of samples lap-shear strength were successfully inferred within a standard variation of 1% when dealing with spot welding. In summary, it gives us a hint that the neural network-based model could better solve the weld quality classification issues in different weld types.

The application of ultrasonic welding in CFRP materials is relatively new to the automotive industry. As such, a number of challenges exist, such as a lack of understanding of the impact of welding process parameters on the weld attributes and joint performance, variation in weld signals under the same nominal welding conditions,

and the difficulty in classifying or predicting weld quality. This chapter addresses some of the challenges facing ultrasonic joining of CFRP materials by defining criteria for classifying weld quality. It proposes a simple but efficient feature selection method that considers multiple weld quality types and demonstrates that effective weld quality classification can be achieved from neural network models using features extracted from process signals. This work will help manufacturers improve their weld quality in CFRP assemblies.

The remainder of this chapter is organized as follows: Section 3.2 describes the material and experimental setup. Section 3.3 proposes a weld quality classification method. Section 3.4 presents methods for signal processing, feature selection, and classification. Section 3.5 discusses the process for determining a parsimonious feature set and compares classification results using Bayesian regularized neural network (BRNN) methodology to other common classification methodologies. Additionally, an analysis of variance (ANOVA) is performed to illustrate the robustness of BRNN methodology. Section 3.6 concludes the chapter. In addition, a supplementary validation of BRNN on UMW is presented in the Appendix.

## **3.2 Weld Experiments**

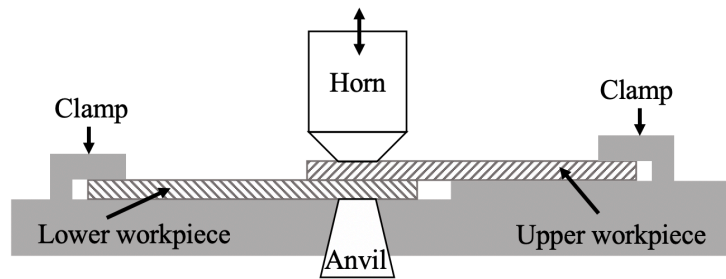
This section introduces a description of the UCW experiment, including the material and the weld machine and related apparatus, as conducted by [13] and [18].

### **3.2.1 Material Selection**

The CFRP sheet used in this work was a semi-crystalline material that consisted of a 30% weight fraction short carbon fiber reinforcement, with an injection molded matrix of doped polyamide 6 polymer resin [18]. The mean diameter and length of the fibers were  $8\ \mu\text{m}$  and  $250\ \mu\text{m}$ , respectively [13]. The welds coupons were of  $138\ \text{mm}$  (length) by  $38\ \text{mm}$  (width) by  $3\ \text{mm}$  (thickness). The contact area of two workpieces was  $38\ \text{mm}$  (length) by  $38\ \text{mm}$  (width).

### **3.2.2 Experimental Setup**

The CFRP weld coupons were joined using an *iQ Servo Ultrasonic Welding machine* [19], which had a servo system, a control system, an ultrasonic generator generating a 20 kHz vibration, a transducer, a tool head with a horn diameter of 9.5 mm, and a mechanical clamping device. The welding machine and the schematic diagram of joining process are illustrated in Figure 3.1. In addition, other equipment used in the experiments include an oven [20], a universal tensile testing system [21], and scanning electron microscope [22].



(a)

(b)

**Figure 3.1. (a) Ultrasonic composite welding machine, (b) schematic diagram of joining process**

The welding process steps are described as follows:

- (1) Sheet coupons are baked in an oven at 70 °C for 24 hours to reduce moisture.
- (2) Coupons are located and clamped on the anvil of the welding machine.
- (3) The welding process is initiated with the horn moving down and contacting the sheet coupons. The joining process is controlled by *iQ Explorer II* software with the specified parameter settings.
- (4) When the weld head reaches a trigger clamping force, a high-frequency, low-amplitude vibration is applied to the workpiece until a predetermined weld energy has been applied.
- (5) After the vibration phase, the clamping force is maintained for several seconds

while the weldment cools down.

- (6) The welding process signals are automatically saved by the *iQ Explorer II* software, where they are available as raw data for further processing and feature extraction.

The welding process parameters were determined using a two-level factorial experiment by Wang *et al.* [18]. The weld process parameters examined were weld energy, trigger force, amplitude, holding time, and plunge speed, and the responses were weld attributes and joint performance. This study determined that weld energy has the largest influence on weld area and maximum lap-shear strength. Therefore, weld energy was selected as the variable of interest for the weld quality model. The best settings for the other process parameter variables were also determined. Based on the weld experiments, the optimal process parameter settings extracted from experimental design was a trigger force of 200 *N* (45 *lb*), a weld speed of 0.3 *mm/s* (0.0118 *in/s*), a holding time of 6 *s*, and a vibration amplitude of  $\pm 33 \mu\text{m}$  (95% of the peak value). Under these optimal welding process parameter settings, weld coupons were fabricated at eight weld energy levels, 200 *J*, 400 *J*, 600 *J*, 800 *J*, 1000 *J*, 1200 *J*, 1400 *J* and 1600 *J* [18].

### **3.3 Weld Attributes, Performance, and Quality**

There is an association between welding process parameters, weld attributes, joint performance, and weld quality. Weld quality is defined here as the degree to which a weldment meets its technical requirements. In a weldment, weld attributes are its external characteristics and weld performance is its intrinsic properties. Based on the correlation of the above four groups of variables, the weld quality can be indirectly determined by weld attributes and joint performance, such as weld area, microstructure of weld zone, and maximum lap-shear strength. This relationship is shown in Figure 3.2. The quality classification standards are the output criteria for classifying weld quality in section 3.5. In addition, weld energy or weld parameters derived from this association can be used to facilitate prediction of weld quality.

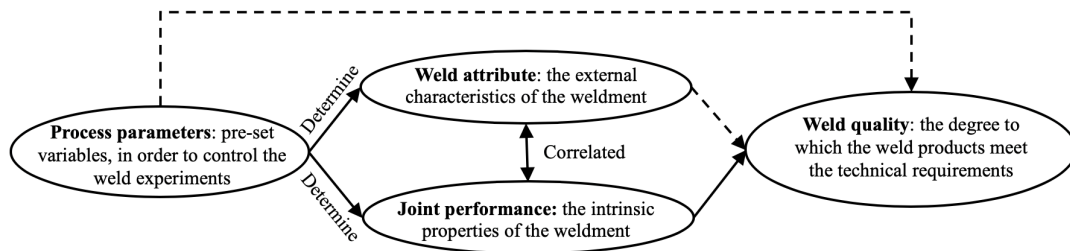


**Figure 3.2. Association of weld quality to weld process parameters, weld attributes, and joint performance**

Weld quality can be quantified from attributes such as weld area and performance characteristics like lap-shear strength. The relationship of weld strength and weld area to weld energy is shown in Figure 3.3. By specifying the required weld strength, three regions of weld quality can be identified, an under-weld (region I), a good-weld (region II), and an over-weld (region III). The figure shows, as weld energy increases there is an asymptotic increase in weld area, and an increase then a decrease in lap-shear strength. The point that corresponds to the maximum shear strength should be included in any definition of a ‘good-weld’ region. However, placement of the boundaries of regions II and III must be determined. Wang *et al.* [18] observed in a study of the evolution of the microstructure in the weld zone that there is less carbon fiber flowing in the weld layer when the weld energy was  $<400 J$ . When the energy reaches 600 to 800  $J$ , the volume fraction of carbon fiber in the weld zone begins to increase. As more weld energy is imposed, a larger volume of polymer matrix is melted, and a larger amount of carbon fiber flows into the weld zone. Therefore, a conservative lower bound for a good-weld is 800  $J$  since increases in the volume flow of carbon fiber will increase the strength of the weldment. This corresponds to a tensile shear strength of 36.5  $MPa$  and a stabilization of the weld area at  $\sim 71 mm^2$ , where the weld quality is deemed acceptable. When the weld energy is higher than 1200  $J$ , there is a corresponding lap-shear strength that falls below the required strength of 31.2  $MPa$ . After this point it was observed that porosity increases in the weld zone due to the polymer overheating, which has a negative impact on weld quality. There is a rapid decrease in lap-shear tensile

strength with increased porosity. Therefore, 1200 J is a good upper bound separating a good-weld from an over-weld.

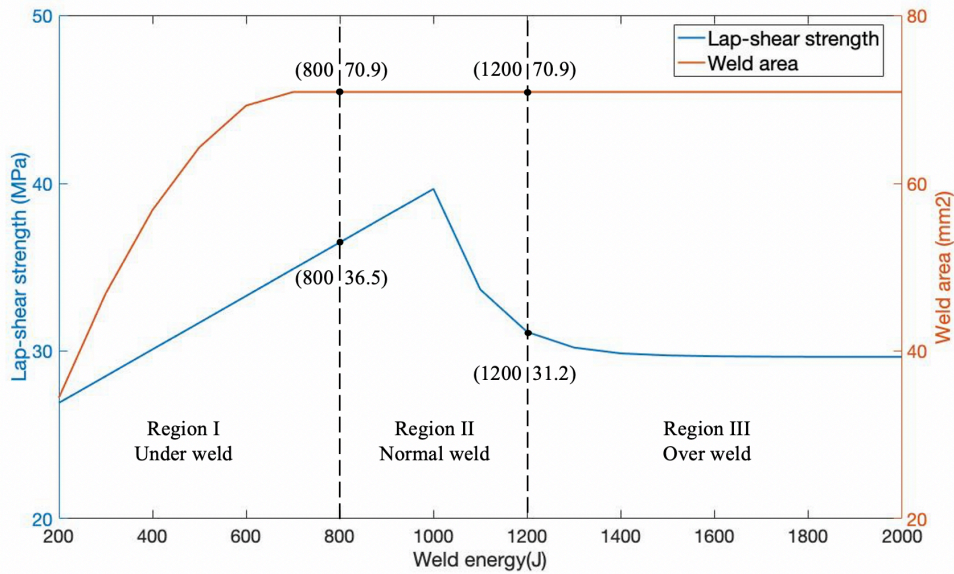


**Figure 3.3. Diagram of shear strength and weld area variation with weld energy determined by microstructure analysis**

The weld quality and the corresponding failure modes observed from microscopic inspection of lap-shear test coupons are summarized in Table 3.1. From a total of 116 weldment samples collected from the experiments, their quality was classified according to the quality classification standards. From this data set, four samples were removed as the outliers when checked for its consistency with the process parameters distributions. Of the remaining 112 samples, 15 were classified as under-welds (13%) and 9 were classified as over-welds (8%), with the balance classified as good-welds (79%).

**Table 3.1 Weld quality classification based on weld energy**

<i>Region</i>	<i>Weld energy</i>	<i>Weld quality and microstructure characteristic</i>	<i>Failure modes</i>	<i>Observed weld performance range</i>	
				<i>shear str.</i>	<i>weld area</i>
I	<800 <i>J</i>	Under-weld. Low carbon fiber flow into the weld zone. No pores generated.	Interfacial separation	0 - 36.5 <i>MPa</i>	0 - 70.9 <i>mm</i> <sup>2</sup>
II	800 - 1200 <i>J</i>	Good-weld. Carbon fiber flows in the weld zone. No to fewer pores generated.	Nugget shear fracture	36.5 - 39.7 -31.2 <i>MPa</i>	70.9 <i>mm</i> <sup>2</sup>
III	>1200 <i>J</i>	Over-weld. Larger volume fraction of carbon fiber in the weld zone. Larger number of pores generated.	Nugget pull-out fracture	31.2 - 29.6 <i>MPa</i>	70.9 <i>mm</i> <sup>2</sup>

In summary, weld energy is a good predictor of weld quality when the other process parameters are optimally selected. The energy can be used to roughly classify welds into three quality regions: under-weld (weld energy <800 *J*), good-weld (weld energy between 800 to 1200 *J*), and over-weld (weld energy >1200 *J*). However, additional confidence in predicting a weld’s quality classification is desired, especially close to these boundaries.

### 3.4 Feature Extraction, Selection, and Classification

A procedure for signal pre-processing and feature extraction was developed, where selected features are used as inputs to the classification algorithm. The feature selection method combines Fisher’s ratio with a clustering overlap analysis to find a parsimonious feature set. This feature set is then used to classify the quality using neural network trained using a Bayesian regularization algorithm. The proposed method is compared to other classification techniques in section 3.5.

#### 3.4.1 Signal Pre-processing and Feature Extraction

Signal noise was reduced with a moving average filter. This filter was sufficient since the noise of welding process had a small amplitude compared to the experimental process signal data. The moving average filter had a window size of 25 and was applied to the power, clamping force (force), and displacement (distance) signals. In addition,

a cumulative energy signal was obtained by numerically integrating the power signal. The three-step signal pre-processing procedure used to extract features is described as follows.

- (1) *Signal start trigger*: At the beginning of the process, there may be background noise not related to the process signals. Therefore, the beginning of the process signals should be identified by setting a threshold trigger. The trigger should be set for when the signal rises about the statistical variance of the noise. The threshold of the start point was defined by Equation (3.1), where  $\mu_N$  and  $\sigma_N$  represent the mean value and the standard deviation of the signal. The equation measures the probability that the noise signal was located in the range of the real signal. Additionally, a 99.99% confidence interval was chosen for the noise band. Therefore, the start point was defined as the first point after filtering that was larger than the threshold value. The moving average filter was applied to the signal after the start point to reduce the impact of noise.

$$\text{thd}(s) = \mu_N + z \times \sigma_N \quad (3.1)$$

- (2) *Feature extraction*. Using the UCW experimental data for illustration, the process signals are plotted in Figure 3.4 by the weld quality and signal types. The signal start time is standardized to zero. In this example, Figures 3.4(a)-3.4(d) represent power, energy, force, and distance signals during the joining process, while each figure is denoted with a number 1 to 3 that represents the under-, good-, and over-weld qualities. For example, Figure 3.4(b2) is the energy signal for a good-weld. In a visual examination of the figures, one can notice a similarity in the signals under the same weld quality classification, and differences in signals between welds of difference quality classifications.

- i. For the power signal, the weld time of a good-weld ranges from 1.5-2 s. The condition where the weld time is shorter or longer than 1.5-2 s corresponds to those classed as under- or over-weld class, respectively. In addition, nearly all of the power signals of a good-weld have a similar pattern, with a clear trough-crest pattern after its peak point.

- ii. For the energy signal, the lower the weld energy, the smoother the energy signal and the larger its slope. In addition, the energy signals of good-welds largely overlap. The curves of the two other weld quality classes, however, are more scattered.
- iii. For the force signal, the average peak force of a good-weld is around 120 *lb*, while the average peak force of the two other weld classes is less than 100 *lb*. Additionally, the smaller the weld energy, the more concentrated the force signal.
- iv. For the distance signal, relative to the distance value, the difference among the distance signals of different weld quality classes is very small, and it is impossible to visually distinguish the difference among three weld quality classes.

In general, this visual inspection indicates there are distinctive characteristics in the signal curves that can be used as candidate features for quality classification. Distinguishing features that can be extracted in this example include signal value and its time at start points, inflection points, end points, slopes between these points, area under the curves, etc.

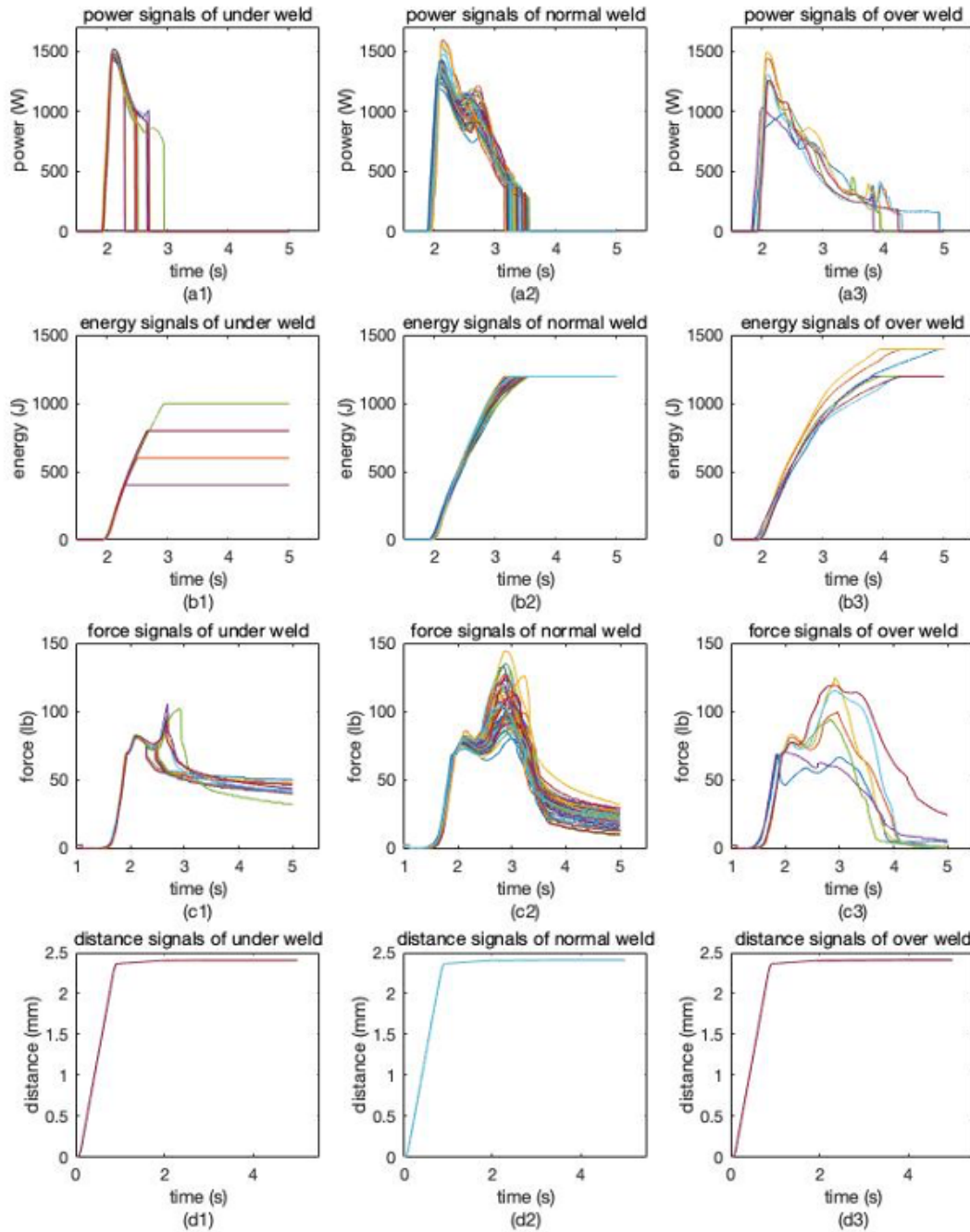
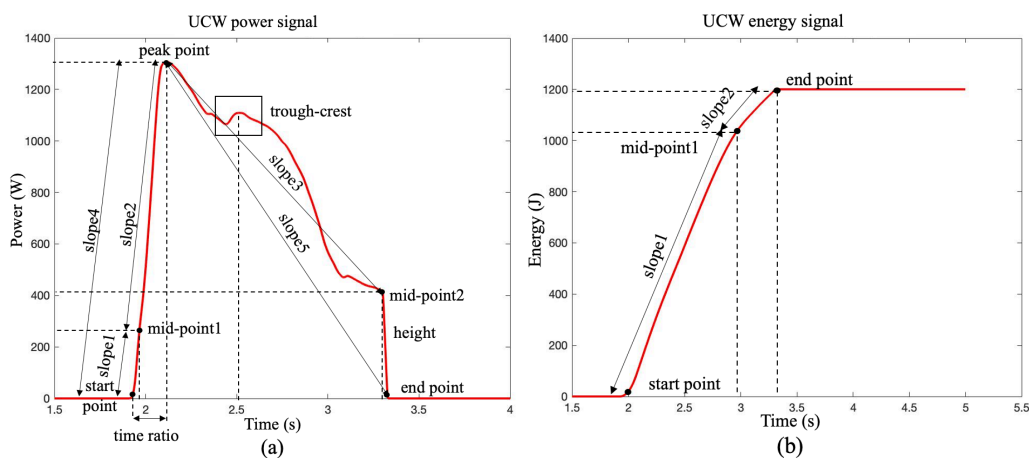


**Figure 3.4. Comparison of each signal under different weld quality**

- (3) *Extracting inflection points.* Inflection points for the signals can be extracted from the first and the second derivatives of the filtered signal curves. Since the signals fluctuate continuously during the weld process, there are numerous local maxima and minimum. Therefore, to ensure the consistency of extracted features under different weld quality classes, it is necessary to pre-define a range for the feature and set a threshold within the range to find derivative zero-crossing points in order

to identify the magnitude and time of the signal's inflection points. For example, when extracting the local minimum of the clamping force at a time of  $\sim 2$ , the time is examined over the range of 1.5-2.5, and the time and force value at which the first zero-crossing point of the first derivative occurs is selected as the inflection point. The position of the zero-crossing point is used to determine the value of the local minimum on the smoothed signals. When multiple zero-crossing points of the first derivative are observed within a range, the second-order derivative is used to distinguish the local maxima or local minimum, or to refine the range for finding the first zero-crossing point.

From the power, energy, force, and distance process parameter signals, a total of 61 features were extracted from the CFRP welding coupon samples. A schematic of the features extracted from these four signals are shown in Figure 3.5, and the corresponding feature identification names are provided in Table 3.A.1 of the Appendix 3.A. Additionally, several features have physical meanings of welding process. They are shown in Table 3.A.2 of the Appendix 3.A. Specially, some significant features have the physical meanings such as the peak values corresponds to the maximum value of each signal, the slopes represent the increasing rate of signals, and some inflection points' times correspond to the moment when the horn touches some special position, etc.



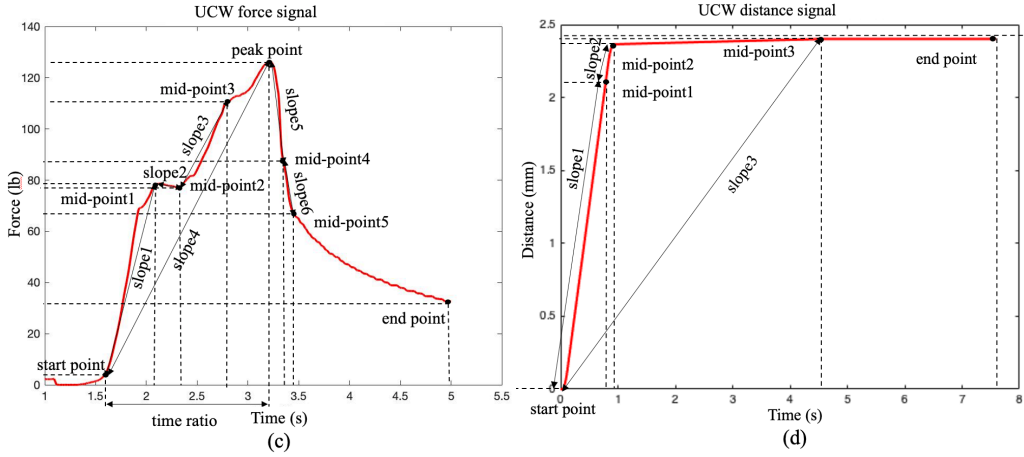


**Figure 3.5. Schematic diagram of features extracted from: (a) power signal, (b) energy signal, (c) force signal, and (d) distance signal**

### 3.4.2 Feature Selection

Many features as defined in Section 3.4.1 can be extracted from the welding process signals. However, when classifying weld quality, some features have redundant information while others have low information quality. Therefore, dimensionality reduction should be employed to select the features that contain the most information. Fisher's ratio [23] is one statistical method used to quantify the degree to which a pair of distributions overlap [10, 24, 25]. Although, Fisher's ratio can generally distinguish between two quality classes, it has weaker performance when trying to distinguish between multiple classes [26]. Thus, a feature selection method that combines Fisher's ratio with a new clustering overlap analysis is proposed to create a parsimonious feature set  $S$ . The clustering overlap analysis is more effective for differentiating between multiple quality classes.

Fisher's ratio, Equation (3.2), compares feature values from the desired quality class with feature values from all other non-desirable quality classes.

$$F_i = \frac{(\bar{x}_1 - \bar{x}_2)^2}{s_1^2 + s_2^2}, i = 1, \dots, n \quad (3.2)$$

Variables  $\bar{x}_1$  and  $s_1^2$  are the sample mean and variance of the feature value from the aggregated non-desirable quality class distributions, e.g., the under and over-welds. Variables  $\bar{x}_2$  and  $s_2^2$  are the sample mean and variance of the aggregated desirable

quality class, e.g., the good-welds. Here  $i$  represents the  $i$ th-feature drawn from a feature set of size  $n$ . The Fisher's ratio value and the distribution of the Fisher's ratio extracted from the UCW process is presented in Table 3.A.3 and Figure 3.A.1 of the Appendix 3.A, respectively. A threshold that each feature's Fisher's ratio must exceed should be defined to determine which features to keep in the parsimonious feature set  $S_F$ . Several values of Fisher's ratio threshold will be explored for the UCW process as discussed in section 3.5.

The clustering overlap analysis differentiates multiple quality classes and is inspired by a statistical  $z$ -test. The idea is to calculate the overlap of the  $6\sigma$ -confidence interval of each feature value distribution of the non-desirable quality with the desirable quality distribution. These ratios are then averaged and compared to a threshold proportion,  $\phi$ , as detailed in Equation (3.3), where  $R_{ij}$  represents the proportion of the feature value's distribution that overlaps non-desirable weld quality classes. Ratios less than the threshold proportion imply there is information present that distinguishes the feature from the desirable quality class, otherwise, the feature is assumed to be non-distinguishing, as illustrated in Figure 3.6. Where under-weld, good-weld and over-weld features are represented by the circle, square and triangle marker, respectively. A threshold for a feature overlap ratio should be defined to determine which features to keep in the parsimonious overlap feature set  $S_O$ . Several overlap ratio threshold values will be explored for the UCW process as discussed in section 3.5.

$$R_{ij} = \frac{\max(\min(\bar{x}_{ij}+3s_{ij}, \bar{x}_{in}+3s_{in}) - \max(\bar{x}_{ij}-3s_{ij}, \bar{x}_{in}-3s_{in}), 0)}{6s_{ij}}, i = 1, \dots, m_1, j = 1, \dots, m_2 \quad (3.3a)$$

$$P_i = \frac{\sum_{j=1}^{m_2} R_{ij}}{m_2}, i = 1, \dots, m_1, j = 1, \dots, m_2 \quad (3.3b)$$

$$\forall i, \text{ if } P_i < \phi, \text{ enter feature into feature set } S_O \quad (3.3c)$$

where  $\bar{x}_{ij}$  and  $s_{ij}$  are the sample mean and standard deviation of the  $i$ th extracted feature of the  $j$ th abnormal quality classes, e.g., the under and over-welds,  $\bar{x}_{in}$  and  $s_{in}$  are the sample mean and standard deviation of  $i$ th extracted feature of the aggregated set of the feature that are the acceptable weld quality classes, e.g., in this example the good-weld class, and where  $i = 1, \dots, m_1$ ,  $m_1$  is the number of the extracted features,

and  $j = 1, \dots, m_2$ ,  $m_2$  is the number of abnormal weld classes exclusive of the acceptable weld classes. In our welding coupon data set,  $m_1 = 61$  and  $m_2 = 2$ , before the parsimonious feature set is selected. For fixed feature  $i$ ,  $\sum R_{ij}$  is averaged by dividing by the number of abnormal weld classes  $m_2$ , as shown in Equation (3.3b). Finally,  $P_i$  is compared to a pre-defined threshold value  $\phi$  to determine if the features should be included in the parsimonious feature set  $S_O$ . The final parsimonious feature set is the union of the Fisher's ratio and overlap ratio parsimonious sets,  $S = S_F \cup S_O$ .

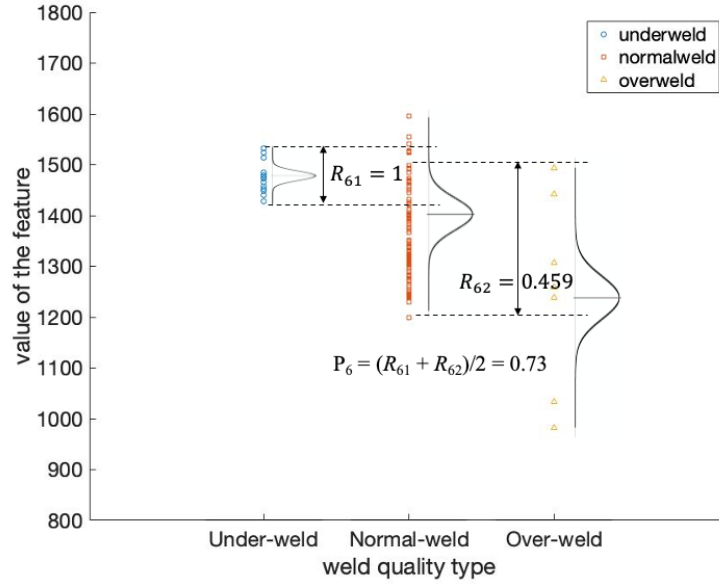


**Figure 3.6. The distributions of feature 6 (the peak value of power signal) extracted from the UCW power signal. The good-weld distribution completely overlaps the under-weld distribution,  $R_{61} = 1$ , and has a large overlap with the over-weld distribution,  $R_{62} = 0.459$ , implying that it may only be weak in distinguishing abnormal weld classes**

### 3.4.3 The BRNN Classification Method

A traditional artificial neural network is trained to determine the nodal weight and bias parameters using a maximum likelihood estimation (MLE) as the error minimization objective. However, this training model is prone to overfitting [27, 28]. Training the network using Bayesian regularization with backpropagation, first proposed by Mackay in 1992 [29], can reduce this overfitting. Bayesian Regularized

Neural Networks (BRNN) are trained by setting a prior probability distribution for the model parameters in advance, usually from a normal distribution, then updating the prior probability distribution to the posterior probability distribution using the Bayesian formula. The weight and bias parameters are determined from a combination of the maximum posterior probabilities by minimizing the mean squared error (MSE) of the nodal weights.

The Bayesian regularized objective function for the training algorithm has the form:

$$MSE = \operatorname{argmin}_{\mathbf{w}} = \sum_{i=1}^m [y_i - f(x_i, \mathbf{w})]^2 \quad (3.4)$$

where  $x_i$  and  $y_i$  are the respective input and output of the  $i$ th class,  $\mathbf{w}$  is a vector of the nodal weight parameters. The posterior probability distribution of network weights is calculated from the Bayesian framework:

$$P(\mathbf{w}|\mathbf{D}, \boldsymbol{\mu}, \boldsymbol{\sigma}) = \frac{f(\mathbf{w}|\boldsymbol{\mu})f(\mathbf{D}|\mathbf{w}, \boldsymbol{\sigma})}{f(\mathbf{D}|\boldsymbol{\mu}, \boldsymbol{\sigma})} \quad (3.5)$$

where  $\mathbf{D}$  is training dataset, which composed of  $x_i$ ,  $\boldsymbol{\mu}$  and  $\boldsymbol{\sigma}$  are the parameters of normal distribution function,  $f(\mathbf{w}|\boldsymbol{\mu})$  is the prior probability which indicates the probability of weights,  $f(\mathbf{D}|\mathbf{w}, \boldsymbol{\sigma})$  is the likelihood function of probability of the data occurring given the weights, while  $f(\mathbf{D}|\boldsymbol{\mu}, \boldsymbol{\sigma})$  is the normalization factor ensuring the total probability is 1 [30].

The structure of the neural network model used to predict the quality classes consists of an input layer, an output layer, and hidden layers. The neural network was constructed and solved using the MATLAB neural network modeling package [31]. In our UCW example, the input layer was sized to the number of parsimonious features determined in section 3.4.2. Note that different feature selection methods will lead to different input layer sizes. The output layer is sized to the number of quality classes determined in section 3.3. Using neural network structuring rule-of-thumbs to reduce overfitting [32, 33], only one hidden layer was used to satisfy the criterion of the number of hidden layers being less than 10% of the size of the input layer. The

number of neurons in the fully connected hidden layer was set to 2/3 of the input layer size, rounding up to the nearest integer.

An example of a neural network structure is presented in Figure 3.7. This example uses the optimal feature set size of 25 as the input, and thus the hidden layer has a fully-connected network of 15 neurons. Each neuron used a *sigmoid* transfer function. A *softmax* transfer function connects to the three quality classes of the output layer. The *softmax* function maps the output of the fully connected hidden layer to an interval (0, 1) for each output class that sums to one for all output classes. This *softmax* transformation is interpreted as the probability of classification for each output class. The weight parameters of each neuron of the hidden layer, with their embedded Bayesian framework, are initially assumed to conform to the normal distribution, and then updated through Bayes formula as the network is trained using cross-entropy as the error objective function. The final classification of the trained network is the class associated with the output node that corresponds to the highest output probability.

During the fitting process, 70% of the input data was randomly assigned as the training and validation datasets, while the remaining 30% was reserved as the testing dataset. In order to determine a measure of the classification accuracy, the network was trained multiple times with randomly assigned input data and the average classification accuracy was recorded. The network training process was stopped when any of these conditions were met: the maximum number of iterations reached 1000, the MSE performance was less than 0.001, or the performance gradient fell below  $10^{-7}$ .

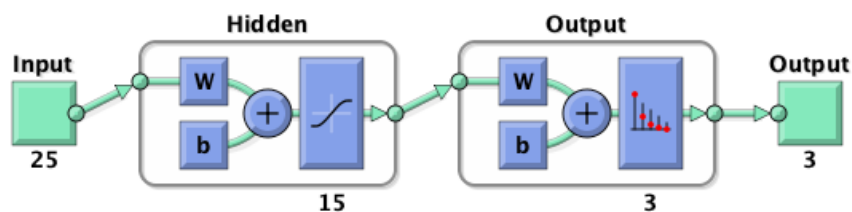


**Figure 3.7. Example neural network structure for the BRNN methodology using the optimal feature data set input size [31]**

### 3.5 Case Study and Discussion

Several UCW scenarios using different numbers of features were evaluated using the BRNN model to classify weld quality. The results were compared to the support vector machine (SVM) and k-nearest neighbor (kNN) classification methods. Different feature selection methods were explored with the UCW dataset to find the best method and feature set size that maximizes classification accuracy. For these scenarios, 56 parsimonious feature sets were selected using eight Fisher's ratio thresholds ranging from 0.01 to 2.0 and seven clustering overlap ratios ranging from  $\phi = 0.408$  to 0.816, taken from  $z$ -scores of  $6\sigma$  for a normal distribution confidence interval of  $0.6\sigma$  to  $1.2\sigma$ . The parsimonious feature set size and the corresponding classification accuracy using the combined screening method is given in Table 3.A.4 and Table 3.A.5 of the Appendix 3.A. Finally, an analysis of variation (ANOVA) was conducted to verify the robustness of the BRNN methodology.

#### 3.5.1 Comparison of Classification Methods

A comparison of the BRNN, SVM, and kNN weld quality classification methods for UCW was conducted on several dimensionally reduced feature sets obtained from Fisher's ratio screening and the linear discriminant analysis (LDA) technique, methods previously adopted by others for screening features in ultrasonic welding.

SVM is a classifier commonly used when the data size is small and linearly separable. Its principle is to determine a hyperplane that maximizes the distance of data in the same class from that hyperplane. When the data classes are not linearly separable, a kernel function  $K(\mathbf{s}, \mathbf{x})$  and a support vector,  $\mathbf{s}$ , are adopted to transform the problem to a higher dimension when determining the hyperplane. The support vector is formed from the closest samples on either side of the hyperplane calculated by a Lagrangian function. The kernel method maps the feature vector  $\mathbf{x}$ , to the output classification vector  $\mathbf{y}$ , using weight parameter matrix  $\mathbf{W}$ , and bias  $b$ . The SVM model is shown in Equation (3.6).

$$\mathbf{y} = \mathbf{W}^T K(\mathbf{s}, \mathbf{x}) + b \quad (3.6)$$

With two classes, the weight parameter matrix and bias are trained to associate values of  $y$  greater than or equal to 0 as one class, and  $y < 0$  are classified as the second class. When there are more than 3 classes, the model is built by partitioning the data using one class as a group and the remaining classes are aggregated as the second group. Then the aggregated group is then sequentially partitioned to build additional models until all classes have been accounted for.

In our weld classification example, a polynomial function with order three was used as the kernel function. When training the SVM for its weights and bias, the input was the size of the feature set and the output size was the three predefined weld quality classes. Five-fold cross-validation was used to determine the SVM model accuracy. This cross-validation partitioned the input data into five groups, training the SVM five times using each group in turn as a testing sample and the remaining four groups as the training samples. The final classification accuracy is taken as the average of the five-fold classification results.

Different from the SVM algorithm, kNN does not build a model to classify the inputs nor require training. The idea of this algorithm is to calculate the distance of a new sample to its  $k$ -nearest neighbors in the testing data set. When the majority of these  $k$ -nearest neighbors belong to a given class, the new sample is classified as that class. The disadvantage of this algorithm is it must calculate the distance to all samples before ranking the distances to establish the  $k$ -nearest neighbors. This requires a large computational overhead to obtain classification results when the size of the sample set is very large. In this work, a 2nd-order Minkowski distance was adopted for the kNN algorithm. The best number of neighbors was determined to be ten after some experimentation, as it avoided a tie when counting the neighbor classes, and achieved the highest classification accuracy.

LDA is a feature selection method that selects its features by projecting data from a training set on a line using tools from linear algebra that minimizes the distribution of projected sample points from the same class while simultaneously maximizing the distribution of projected points from the other classes. As features are sequentially

added to the model, the distance between the different classes is calculated, and a feature is retained when the distance between the classes increases after the projection.

The classification accuracy was compared by first selecting the number of features so that the feature set is spanned, namely 15, 30, 45, and the full feature set of 61 features. This allows the initial trend of variation of classification accuracy to be observed with the number of features. The classification accuracy was calculated using the BRNN, backpropagation-artificial neural networks (B-ANN), SVM, and kNN models. The results are plotted in Figure 3.8, where Figure 3.8(a) shows a comparison of the accuracy for feature sets selected using Fisher’s ratio, while Figure 3.8(b) shows a comparison using the LDA dimension reduction method. As can be seen, the average accuracy of BRNN and B-ANN, including the 95% binomial confidence interval, are both much better than SVM and kNN for weld quality classification in UCW. The confidence bounds are derived by using different randomizations of the training sample set. In all cases, BRNN is slightly better than B-ANN, with the average total accuracy of BRNN above 98% over all feature set sizes. There is also a local maximum with a feature set size of  $\sim 30$ . We conclude that neural network-based methods such as BRNN or B-ANN methods are preferred for feature-based weld quality classification in UCW. The impact of the number of features, their selection methods, and its interaction will be discussed in detail in the next section.

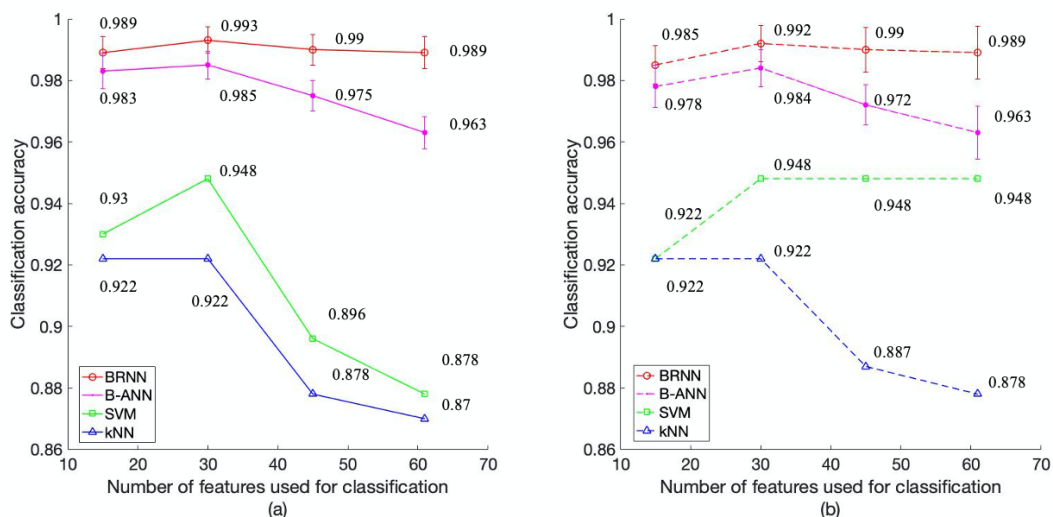


**Figure 3.8. Comparison of classification accuracy under different number of features based on (a) Fisher’s ratio, and (b) LDA feature selection method**

### **3.5.2 Comparison of Feature Selection Methods and Influence of Number of Features**

Although training a neural network using the BRNN methodology has higher accuracy than SVM and kNN, the number of features and different subsets of features still has an influence on classification accuracy. It is not efficient to retain all of the extracted features, nor develop neural network models to screen as many features as possible. Consequently, a comparison of feature selection methods and influence of number of features was performed to evaluate their tradeoff with classification accuracy, and describe which candidate features are significant.

The classification accuracy using 56 parsimonious feature sets determined using the proposed feature selection methodology and the BRNN classification model are plotted in Figure 3.9. The lighter the line color displayed in the figure, the more accurate the classification. This contour plot also shows there is an optimal number of selected features, as shown in the red circle. Classification accuracy decreases when there are too many or too few features. This is consistent with the observations in the previous section. The analysis shows that a clustering overlap threshold of around 0.54-0.68 ( $z$ -score of  $0.8\sigma - 1.0\sigma$ ) presents an accuracy peak that is indicative of being generally more informative than other sets selecting smaller and larger thresholds. Further, when the Fisher’s ratio threshold is between 0.2-0.5, a further improvement to classification accuracy is obtained. A maximum classification accuracy was found when the clustering overlap ratio was 0.612 ( $0.9\sigma$   $z$ -score) and a Fisher’s ratio equal of 0.2, corresponding to an optimal number of features of 25. This region will be further explored under BRNN classification method by varying the number of features from 15 to 36 and comparing different feature selection methods to determine the most significant subset of features for classifying weld quality in UCW.

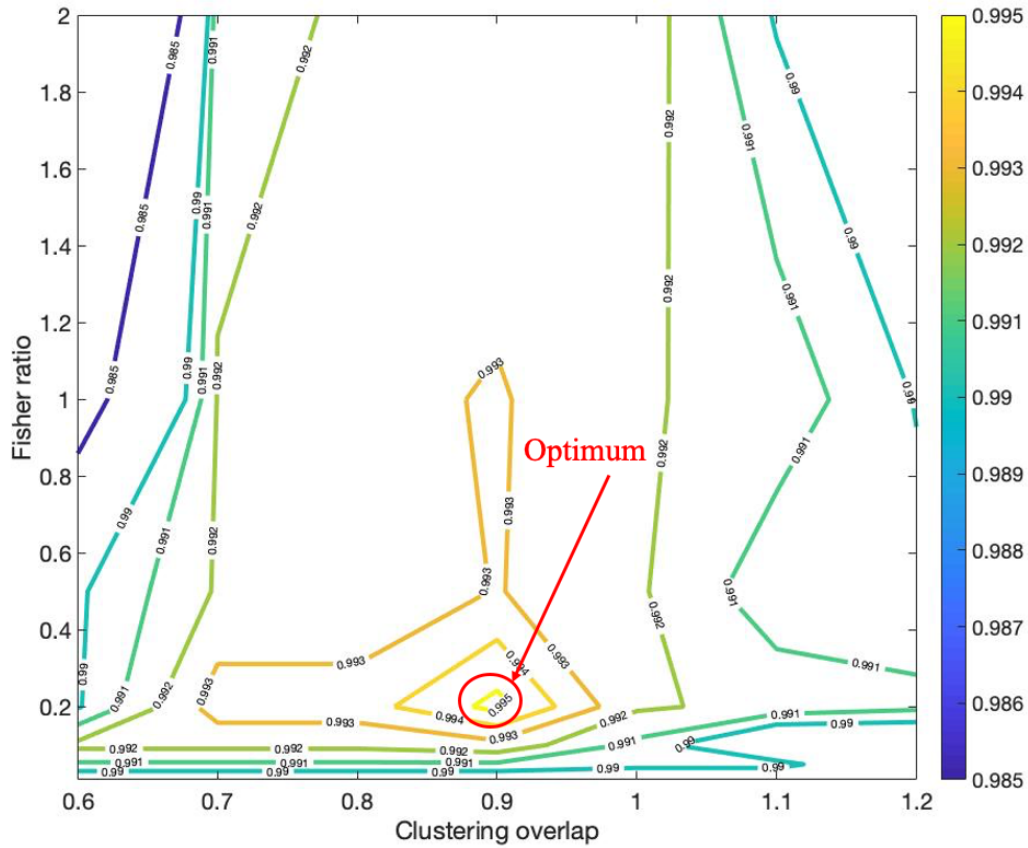


**Figure 3.9. Classification accuracy with number of features which selected by Fisher's ratio and clustering overlap**

As shown in Figure 3.8, only the BRNN classification method will be used to demonstrate the difference in feature selection methods, as its classification accuracy is better than the SVM and kNN classification methods. A comparison of BRNN with three feature selection methods is plotted in Figure 3.10 over a range close to the optimal feature set size. The different bar colors represent the different feature selection methods. As can be seen, the accuracy of all three feature selection methods first increases then decreases over the feature size range of 15 to 36 with an optimal feature size of 25. This implies as feature set size increases up to 25, more information can be obtained from the significant features, while as set size increases past 25, insignificant or redundant features are being retained that start adding to noise and are not conducive to weld quality classification.

The 95% binomial confidence interval of the BRNN classification accuracy for all feature selection methods is about 0.0022-0.0032. The average classification accuracy

of the proposed feature selection method is better than those of the other feature selection methods when the number of features is smaller than 25. The confidence bands of the proposed feature selection method also have less coincidence with the other feature selection methods. When the number of features is larger than 25, the classification accuracy of the three feature selection methods is approximately the same as the confidence bands have a great degree of coincidence. This is because a feature set selected by the proposed Fisher’s ratio and clustering overlap method with fewer than 25 features is more unique than the other feature selection methods. In contrast, when the feature set is greater than 25, the feature set selected is almost the same regardless of the method.

The difference of classification accuracy between the feature selection methods is small, at about 0.001. Considering the large overlap of the error bars in this range, one can conclude that the proposed feature selection method will achieve an equivalent classification accuracy when the number of features is larger than 25. Consequently, the proposed feature selection method not only considers multiple weld classes, but also achieves a classification accuracy equivalent to or better than the other feature selection methods when using the BRNN model.

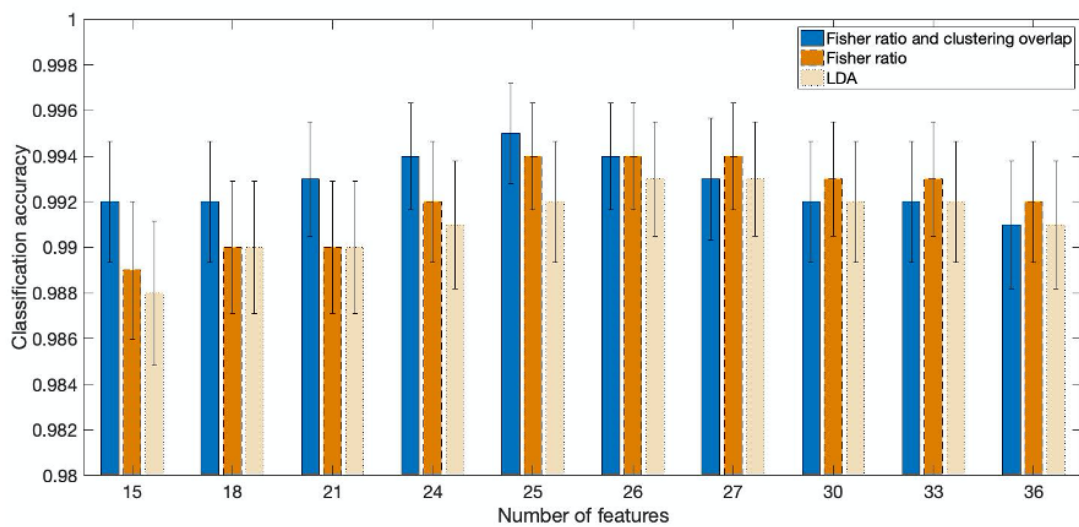


**Figure 3.10. The classification results of weld quality under BRNN classification method with different feature selection methods**

Note that the BRNN classification accuracy reached a maximum when the number of features is between 24 and 27, which is consistent with Figure 3.8, whose maximum accuracy at 25 features was equal to 99.5% with a confidence interval of 0.22%. Examining the 25 extracted features, eleven are from the power signal, five are from the energy signal, and seven are from the force signal, while the last two are from the distance signal. These features represent eight feature signal magnitudes, seven corresponding times, and seven slopes. Most features were acquired from the power and force signals, which is reasonable since that the energy signal is the integral of the power signal. Since the deviation of the distance signal under different weld quality classification methods is very small, few of its features were found to distinguish weld quality. Nevertheless, there is some information in the distance signals so a few significant features were retained.

Features which correspond to the time, magnitude, and slope for the start and peak points of the power signal have the greatest contribution to classifying the weld quality. The trough-crest pattern after the peak power was also observed to be an indicator differentiating under-welds and good-welds, likely from when power is transmitted to the lower workpiece. Energy signal features selected represent its start, inflection, and end points. Force signal features selected are related to its peak point time and inflection points after the peak point. The peak of the force signal can be associated to the point where full clamping of the workpiece is achieved, while the inflection points reflect the points in the process when the workpieces melt and force is transferred from the upper to the lower workpiece. In summary, for quality detection and classification in UCW, features corresponding to the start and peak points and trough-crest pattern of power signals, inflection points in force signals, and related slopes to these points in the power and force signals appear to be of most significance.

### **3.5.3 BRNN Classification Sensitivity and Robustness**

An analysis of variance (ANOVA) was conducted on the BRNN classification method to check its sensitivity and verify its robustness. First, a BRNN model for the full set of 61 extracted features was trained using the UCW dataset. Then each feature's

nominal value was increased and decreased by 5% and input into the BRNN algorithm to classify the weld quality. The variance of the predicted classification accuracy was studied relative to the variance of the features. A Pareto chart of sensitivity is shown in Figure 3.11 by plotting the ratio of the contribution to variance of each feature to the total variance. As can be seen, system error, represented by 'Error/Other' bar, is very large. Inflection point feature values extracted from the distance signals (e.g., features 53, 55, 56, and 60), contribute the most variance to the classification accuracy model, and thus are less desirable for distinguishing among different weld quality classifications. The proposed feature selection method had excluded these features, thus supporting its validity as a feature screening method.

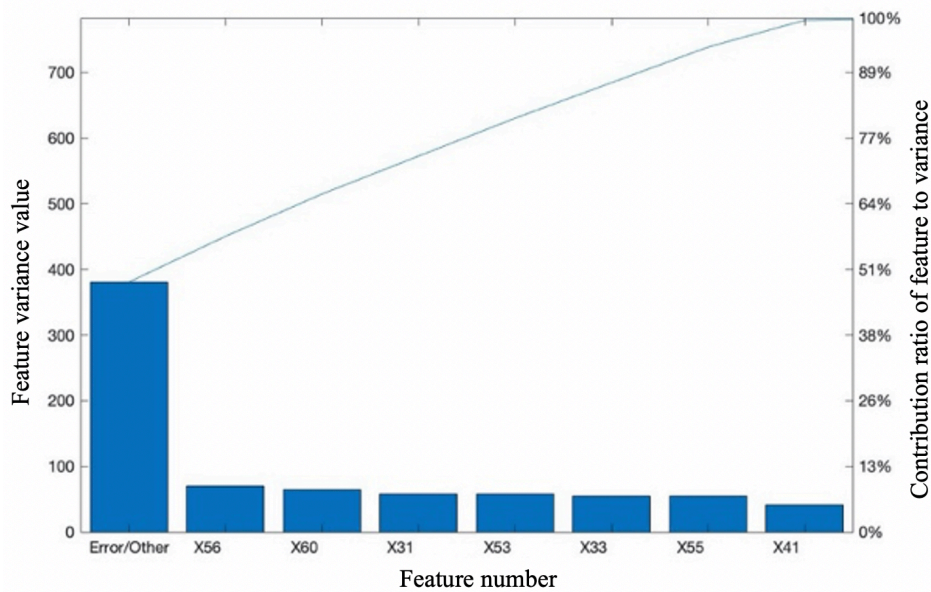


**Figure 3.11. Pareto chart of ANOVA analysis of variation of  $\pm 5\%$  feature value of 61 features**

Additional ANOVA tests were conducted using the data sets generated around the optimal number of features, 23-27, to further verify the reduced sensitivity of the proposed feature selection method. Inputs were again varied by  $\pm 5\%$  of the feature's nominal value. In this case, the structure of the number of hidden layer neurons in the BRNN was changed according to the dimension of inputs. The ANOVA results are

shown in Figure 3.12. Figure 3.12(a) shows the variance contribution to the total classification accuracy, where the bars represent the system errors for the classification accuracy. No features were observed to contribute significantly to classification accuracy variance. The contribution to variance is minimum when the feature size is 25, which matches with the optimal feature set size for classification accuracy show in Figure 3.10. This indicates that all selected features under optimal feature set size made a significant contribution to weld quality classification regardless of their variance. In addition, Figure 3.12(b) represents the variance contribution of  $\alpha$  and  $\beta$  errors. As in Figure 3.12(a), only system error has a significant contribution to variance. Note that the contribution to  $\alpha$  error variance gradually increases as the number of features increases, while the contribution to  $\beta$  error variance decreases as the number of features increases. The aggregate contribution to variance, i.e., the sum of two error contributions to variance, is again minimum when the feature set size is 25.

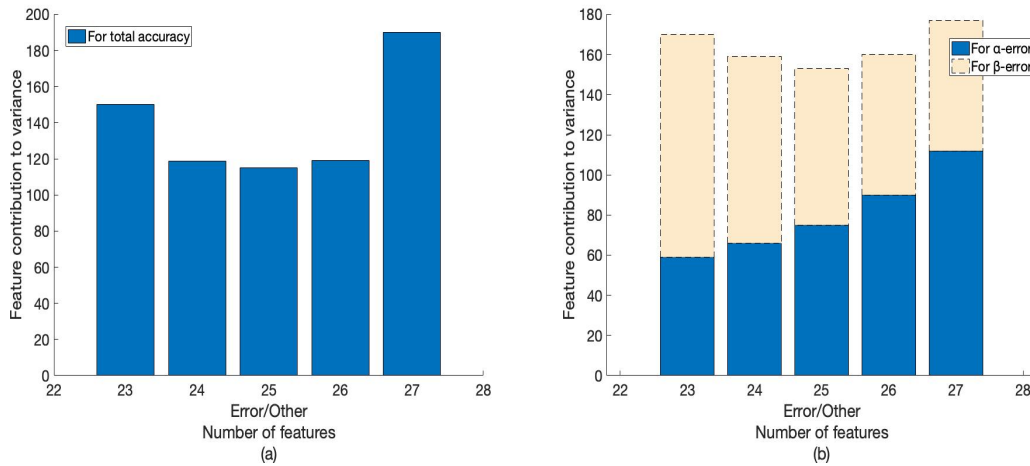


**Figure 3.12. Variance contributions of different numbers of features based on the ANOVA test of variation of  $\pm 5\%$  feature value (a) to total classification accuracy, and (b) to  $\alpha$  error and  $\beta$  error**

In summary, the ANOVA test shows the proposed feature selection method with correctly selected threshold values, when combined with the BRNN classification method, is insensitive and robust to variance in the input feature values, reinforcing the importance of good feature selection.

### 3.6 Conclusion

In this chapter, a method for weld quality classification for ultrasonic welding of CFRP was presented by analyzing the relationship between welding process parameters, weld attributes, and joint performance. Three weld quality classes were used as the output criteria to train classification algorithms based on features extracted and selected from welding process signals. To improve the classification results, a feature selection methodology that combines Fisher's ratio with a new clustering overlap analysis was proposed. Several feature selection methods were compared. A neural network classification model trained with Bayesian regularization and backpropagation was shown to have superior performance. An ANOVA test of the BRNN classification model verifies the robustness of this method. In the Appendix 3.B, one additional case study on UMW was investigated, since the samples from UCW is not sufficient. The results of UMW signals had some improvements compared with the previous classification methods. Therefore, the processes of above-mentioned feature selection method and BRNN classification method have a good effect on distinguishing the weld quality on both UCW and UMW. We summarize the following conclusions for the proposed weld quality classification with BRNN methodology on UCW of CFRP:

- (1) A classification process based on features provides good classification accuracy when data size is small.
- (2) A new clustering overlap method goes beyond distinguishing between normal and abnormal classifications to differentiate between multiple quality classes.
- (3) The proposed feature selection method using Fisher's ratio and the new clustering overlap can achieve at least equivalent to or better results than those selected by LDA or Fisher's ratio alone.
- (4) ANN methods, especially BRNN, are superior with higher classification accuracy and more robust than the traditional methods of SVM and kNN under the same feature selection methods.

- (5) Features such as the start and peak points and the trough-crest pattern in the power signals, inflection point features from the force signals, and the relative slopes of these points were found to be the most significant features for weld quality classification in UCW.

## References

- [1] What techniques can I use to weld Nylon? TWI. <https://www.twi-global.com/technical-knowledge/faqs/faq-what-techniques-can-i-use-to-weld-nylon>. (Accessed May 20, 2021).
- [2] J. Leone, Plastic joining methods. Science. <https://sciencing.com/plastic-joining-methods-6924074.html>. (Accessed May 20, 2021).
- [3] A. Pramanik, A.K. Basak, Y. Dong, P.K. Sarker, M. Uddin, G. Littlefair, A.R. Dixit, S. Chattopadhyaya, Joining of carbon fibre reinforced polymer (CFRP) composites and aluminium alloys-A review, *Composites Part A: Applied Science and Manufacturing* 101 (2017) 1-29.
- [4] T. Ishikawa, K. Amaoka, Y. Masubuchi, T. Yamamoto, A. Yamanaka, M. Arai, J. Takahashi, Overview of automotive structural composites technology developments in Japan, *Composites Science and Technology* 155 (2018) 221-246.
- [5] A. Yousefpour, M. Hojjati, J.-P. Immarigeon, Fusion bonding/welding of thermoplastic composites, *Journal of Thermoplastic Composite Materials* 17(4) (2016) 303-341.
- [6] A.P.d. Costa, E.C. Botelho, M.L. Costa, N.E. Narita, J.R. Tarpani, A review of welding technologies for thermoplastic composites in aerospace applications, *Journal of Aerospace Technology and Management* 4(3) (2012) 255-265.
- [7] H.P.C. Daniels, Ultrasonic welding, *Ultrasonics* 3(4) (1965) 190-196.
- [8] L. Nong, C. Shao, T.H. Kim, S.J. Hu, Improving process robustness in ultrasonic metal welding of lithium-ion batteries, *Journal of Manufacturing Systems* 48 (2018) 45-54.
- [9] W. Guo, C. Shao, T.H. Kim, S.J. Hu, J.J. Jin, J.P. Spicer, H. Wang, Online process monitoring with near-zero misdetection for ultrasonic welding of lithium-ion batteries: An integration of univariate and multivariate methods, *Journal of Manufacturing Systems* 38 (2016) 141-150.
- [10] C. Shao, K. Paynabar, T.H. Kim, J.J. Jin, S.J. Hu, J.P. Spicer, H. Wang, J. A. Abell, Feature selection for manufacturing process monitoring using cross-validation, *Journal of Manufacturing Systems* 32(4) (2013) 550-555.
- [11] Y. Chen, H.-W. Ma, G.-M. Zhang, A support vector machine approach for classification of welding defects from ultrasonic signals, *Nondestructive Testing and Evaluation* 29(3) (2014).
- [12] X. Wang, S. Guan, L. Hua, B. Wang, X. He, Classification of spot-welded joint strength using ultrasonic signal time-frequency features and PSO-SVM method, *Ultrasonics* 91 (2019) 161-169.
- [13] Y. Li, J. Arinez, Z. Liu, T.H. Lee, H.-T. Fan, G. Xiao, M. Banu, S.J. Hu, Ultrasonic welding of carbon fiber reinforced composite with variable blank holding force, *Journal of Manufacturing Science and Engineering* 140(9) (2018) 091011.

- [14] K. Wang, D. Shriver, M. Banu, S.J. Hu, G. Xiao, J. Arinez, H.-T. Fan, Performance prediction for ultrasonic spot welds of short carbon fiber-reinforced composites under shear loading, *Journal of Manufacturing Science and Engineering* 139(11) (2017) 111001.
- [15] Y. Li, B. Yu, B. Wang, T.H. Lee, M. Banu, Online quality inspection of ultrasonic composite welding by combining artificial intelligence technologies with welding process signatures, *Materials & Design* 194 (2020).
- [16] W. Cai, J. Wang, P. Jiang, L. Cao, G. Mi, Q. Zhou, Application of sensing techniques and artificial intelligence-based methods to laser welding real-time monitoring: A critical review of recent literature, *Journal of Manufacturing Systems* 57 (2020) 1-18.
- [17] S.R. Lee, Y.J. Choo, T.Y. Lee, M.H. Kim, S.K. Choi, A quality assurance technique for resistance spot welding using a neuro-fuzzy algorithm, *Journal of Manufacturing Systems* 20(5) (2001) 320-328.
- [18] K. Wang, D. Shriver, Y. Li, M. Banu, S.J. Hu, G. Xiao, J. Arinez, H.-T. Fan, Characterization of weld attributes in ultrasonic welding of short carbon fiber reinforced thermoplastic composites, *Journal of Manufacturing Processes* 29 (2017) 124-132.
- [19] iQ Servo Ultrasonic Welding. Dukane. <https://www.dukane.com/plastic-welding-products/iq-servo-ultrasonic-welding-2/>. (Accessed May 20, 2021).
- [20] Lindberg/Blue M™ Moldatherm™ Box Furnaces. ThermoFisher Scientific. <https://www.thermofisher.com/order/catalog/product/BF51794C#/BF51794C>. (Accessed May 20, 2021).
- [21] Universal testing systems. Instron. <https://www.instron.us/en-us/products/testing-systems/universal-testing-systems/electromechanical/3300/3340-single-column>. (Accessed May 20, 2021).
- [22] ImageJ. ImageJ. <https://imagej.nih.gov/ij/>. (Accessed May 20, 2021).
- [23] F.R.S. R.A. Fisher Sc.D., The use of multiple measurements in taxonomic problems, *Annals of Human Genetics* 7(2) (1936) 179-188.
- [24] B. Wang, S.J. Hu, L. Sun, T. Freiheit, Intelligent welding system technologies: State-of-the-art review and perspectives, *Journal of Manufacturing Systems* 56 (2020) 373-391.
- [25] C. Shao, T.H. Kim, S.J. Hu, J.J. Jin, J.A. Abell, J.P. Spicer, Tool wear monitoring for ultrasonic metal welding of lithium-Ion batteries, *Journal of Manufacturing Science and Engineering* 138(5) (2016) 051005.
- [26] S. Prasad, L.M. Bruce, Limitations of principal components analysis for hyperspectral target recognition, *IEEE Geoscience and Remote Sensing Letters* 5(4) (2008) 625-629.

- [27] A.P. Piotrowsk, J.J. Napiorkowski, Optimizing neural networks for river flow forecasting – Evolutionary Computation methods versus the Levenberg–Marquardt approach, *Journal of Hydrology* 407(1-4) (2011) 12-27.
- [28] A.P. Piotrowsk, J.J. Napiorkowski, A comparison of methods to avoid overfitting in neural networks training in the case of catchment runoff modelling, *Journal of Hydrology* 476 (2013) 97-111.
- [29] D. MacKay, Bayesian interpolation, *Neural Computation* 4(3) (1992) 415-447.
- [30] E. Sariiev, G. Germano, Bayesian regularized artificial neural networks for the estimation of the probability of default, *Quantitative Finance* 20(2) (2020) 311-328.
- [31] Deep Learning Toolbox. MathWorks.  
<https://www.mathworks.com/products/deep-learning>. (Accessed May 20, 2021).
- [32] J. Heaton, Optimal size of the hidden layer, Heaton Research, Inc.2008.
- [33] S.W. Smith, The scientist and engineer's guide to digital signal processing, second edition ed., California Technical Publishing, United States of America, 1999.

## Appendix

### Appendix 3.A

**Table 3.A.1 Features list extracted from four signal sources**

	Features' names and numbers					
<b>Power</b>	<b>1</b>	<b>2</b>	<b>3</b>	<b>4</b>	<b>5</b>	<b>6</b>
	Stime_p	Svalue_p	Mtime1_p	Mvalue1_p	Ptime_p	Pvalue_p
	<b>7</b>	<b>8</b>	<b>9</b>	<b>10</b>	<b>11</b>	<b>12</b>
	TC_p	TCtime_p	TCvalue_p	Mtime2_p	Mvalue2_p	Slope1_p
	<b>13</b>	<b>14</b>	<b>15</b>	<b>16</b>	<b>17</b>	
	Slope2_p	Slope3_p	Slope4_p	Slope5_p	Height_p	
<b>Energy</b>	<b>18</b>	<b>19</b>	<b>20</b>	<b>21</b>	<b>22</b>	<b>23</b>
	Stime_e	Svalue_e	Mtime1_e	Mvalue1_e	Etime_e	Evalue_e
	<b>24</b>	<b>25</b>				
	Slope1_e	Slope2_e				
<b>Force</b>	<b>26</b>	<b>27</b>	<b>28</b>	<b>29</b>	<b>30</b>	<b>31</b>
	Stime_f	Svalue_f	Mtime1_f	Mvalue1_f	Mtime2_f	Mvalue2_f
	<b>32</b>	<b>33</b>	<b>34</b>	<b>35</b>	<b>36</b>	<b>37</b>
	Mtime3_f	Mvalue3_f	Ptime_f	Pvalue_f	Mtime4_f	Mvalue4_f
	<b>38</b>	<b>39</b>	<b>40</b>	<b>41</b>	<b>42</b>	<b>43</b>
	Mtime5_f	Evalue_f	Slope1_f	Slope2_f	Slope3_f	Slope4_f
	<b>44</b>	<b>45</b>	<b>46</b>	<b>47</b>		
	Slope5_f	Slope6_f	Tratio_f	Area_f		
<b>Distance</b>	<b>48</b>	<b>49</b>	<b>50</b>	<b>51</b>	<b>52</b>	<b>53</b>
	Stime_d	Svalue_d	Mtime1_d	Mvalue1_d	Mtime2_d	Mvalue2_d
	<b>54</b>	<b>55</b>	<b>56</b>	<b>57</b>	<b>58</b>	<b>59</b>
	Mtime3_d	Mvalue3_d	Evalue_d	Slope1_d	Slope2_d	Slope3_d
	<b>60</b>	<b>61</b>				
	Area_d	Wtime				

**Table 3.A.2 The physical meanings of significant features**

Source	Feature No.	Feature Name	Description
<b>Power</b>	<b>1</b>	Stime_p	The time when welding process begins
	<b>5</b>	Ptime_p	The time when power signal reaches to the maximum value
	<b>7</b>	Peak2_p	The indicator whether the power is transmitted to the lower
	<b>8</b>	P2time_p	The time when the power is transmitted to the lower
	<b>10</b>	Mtime2_p	The time when joining process stops
	<b>15</b>	Slope4_p	The increasing rate of power signal

	<b>16</b>	Slope5_p	The decreasing rate power signal
	<b>17</b>	Height_p	The power difference when joining process and welding
<b>Energy</b>	<b>18</b>	Stime_e	The time when energy begins to impose on the workpiece
	<b>20</b>	Mtime1_e	The time for the workpiece to solidify from the liquid state
	<b>22</b>	Etime_e	The time when joining process stops
<b>Force</b>	<b>26</b>	Stime_f	The time when force begins to be applied
	<b>30</b>	Mtime2_f	The time when workpieces are liquefied
	<b>34</b>	Ptime_f	The time when workpieces are solidified from liquid state
	<b>38</b>	Mtime5_f	The time when force stops to be applied
	<b>43</b>	Slope4_f	The increasing rate of force signal
<b>Distance</b>	<b>48</b>	Stime_d	The time when horn begins to move down
	<b>52</b>	Mtime2_d	The time when horn begins to contact with upper workpiece
	<b>54</b>	Mtime3_d	The time when horn moves down to the maximum position of the workpiece

**Table 3.A.3 Fisher's ratio value of each feature**

<b>Feature 9</b>	<b>Feature 16</b>	<b>Feature 7</b>	<b>Feature 8</b>	<b>Feature 34</b>	<b>Feature 13</b>	<b>Feature 23</b>
2.387	2.150	1.750	1.689	1.645	1.622	1.001
<b>Feature 35</b>	<b>Feature 36</b>	<b>Feature 42</b>	<b>Feature 19</b>	<b>Feature 2</b>	<b>Feature 47</b>	<b>Feature 12</b>
0.937	0.846	0.829	0.779	0.705	0.643	0.590
<b>Feature 38</b>	<b>Feature 44</b>	<b>Feature 17</b>	<b>Feature 11</b>	<b>Feature 14</b>	<b>Feature 56</b>	<b>Feature 24</b>
0.550	0.381	0.361	0.360	0.297	0.292	0.208
<b>Feature 25</b>	<b>Feature 46</b>	<b>Feature 22</b>	<b>Feature 61</b>	<b>Feature 10</b>	<b>Feature 28</b>	<b>Feature 50</b>
0.173	0.173	0.171	0.170	0.168	0.109	0.109
<b>Feature 29</b>	<b>Feature 51</b>	<b>Feature 21</b>	<b>Feature 15</b>	<b>Feature 58</b>	<b>Feature 6</b>	<b>Feature 45</b>
0.109	0.109	0.081	0.081	0.056	0.051	0.040
<b>Feature 57</b>	<b>Feature 32</b>	<b>Feature 54</b>	<b>Feature 33</b>	<b>Feature 55</b>	<b>Feature 59</b>	<b>Feature 4</b>
0.035	0.031	0.031	0.027	0.027	0.023	0.021
<b>Feature 30</b>	<b>Feature 52</b>	<b>Feature 41</b>	<b>Feature 5</b>	<b>Feature 20</b>	<b>Feature 26</b>	<b>Feature 48</b>
0.017	0.017	0.012	0.012	0.012	0.010	0.010
<b>Feature 43</b>	<b>Feature 40</b>	<b>Feature 60</b>	<b>Feature 39</b>	<b>Feature 1</b>	<b>Feature 18</b>	<b>Feature 31</b>
0.009	0.009	0.008	0.007	0.004	0.004	0.003
<b>Feature 53</b>	<b>Feature 37</b>	<b>Feature 27</b>	<b>Feature 49</b>	<b>Feature 3</b>		
0.003	0.002	0.001	0.001	0.000		

**Table 3.A.4 Parsimonious feature set size screened by the proposed Fisher’s ratio and clustering overlap analysis method (from a total possible feature set size of 61)**

Number of features kept		Clustering analysis overlap tolerance						
		<b>0.6<math>\sigma</math></b> <b>(0.408)</b>	<b>0.7<math>\sigma</math></b> <b>(0.476)</b>	<b>0.8<math>\sigma</math></b> <b>(0.544)</b>	<b>0.9<math>\sigma</math></b> <b>(0.612)</b>	<b>1.0<math>\sigma</math></b> <b>(0.68)</b>	<b>1.1<math>\sigma</math></b> <b>(0.748)</b>	<b>1.2<math>\sigma</math></b> <b>(0.816)</b>
<b>Fisher’s ratio</b>	<b>2.0</b>	4	11	14	15	21	25	35
	<b>1.0</b>	8	12	15	16	22	26	36
	<b>0.5</b>	15	18	18	19	23	27	37
	<b>0.2</b>	21	24	24	25	29	30	38
	<b>0.1</b>	30	30	30	31	33	34	42
	<b>0.05</b>	34	34	34	34	36	36	42
	<b>0.02</b>	42	42	42	42	44	44	48
	<b>0.01</b>	49	49	49	49	49	49	53

**Table 3.A.5 The classification accuracy of parsimonious feature set size screened by the proposed Fisher’s ratio and clustering overlap analysis method (from a total possible feature set size of 61)**

Number of features kept		Clustering analysis overlap tolerance						
		<b>0.6<math>\sigma</math></b> <b>(40.8%)</b>	<b>0.7<math>\sigma</math></b> <b>(47.6%)</b>	<b>0.8<math>\sigma</math></b> <b>(54.4%)</b>	<b>0.9<math>\sigma</math></b> <b>(61.2%)</b>	<b>1.0<math>\sigma</math></b> <b>(68.0%)</b>	<b>1.1<math>\sigma</math></b> <b>(74.8%)</b>	<b>1.2<math>\sigma</math></b> <b>(81.6%)</b>
<b>Fisher’s ratio</b>	<b>2.0</b>	96.64%	99.17%	99.21%	99.22%	99.26%	98.99%	98.85%
	<b>1.0</b>	98.31%	99.21%	99.26%	99.31%	99.21%	99.16%	98.99%
	<b>0.5</b>	98.98%	99.21%	99.21%	99.31%	99.22%	99.03%	99.03%
	<b>0.2</b>	98.99%	99.35%	99.35%	99.53%	99.22%	99.17%	99.13%
	<b>0.1</b>	99.23%	99.23%	99.23%	99.27%	99.07%	98.81%	98.81%
	<b>0.05</b>	99.08%	99.08%	99.08%	99.08%	99.05%	99.05%	98.81%
	<b>0.02</b>	98.94%	98.94%	98.94%	98.94%	98.89%	98.89%	98.76%
	<b>0.01</b>	98.76%	98.76%	98.76%	98.76%	98.76%	98.76%	98.63%

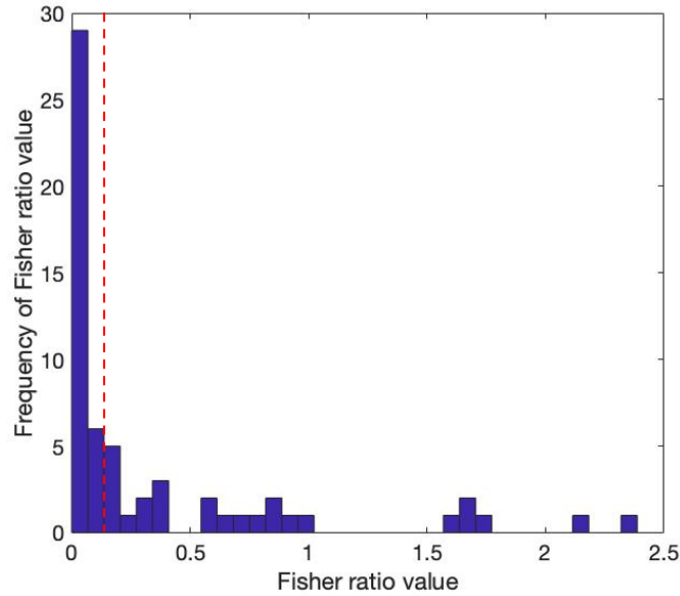


**Figure 3.A.1 The distribution of the Fisher’s ratio extracted from the ultrasonic composite welding process**

### Appendix 3.B

This Appendix 3.B section is a supplementary validation of BRNN methodology. Specifically, in order to verify the wide applicability of BRNN methodology, large amounts of UMW signals collected from the real manufacturing factories were used to conduct the weld quality classification research. The inputs of the algorithm were the features that are selected according to the above-mentioned Fisher’s ratio and clustering overlap analysis approach. The classification accuracy shows that BRNN method is also effective in classifying UMW based on features.

As the validation of the proposed BRNN classification method, two more classification case studies were conducted. One used data set ‘Features\_150R1\_Aug27toFeb07’, named dataset1, and the other used data set ‘Features\_130R2\_Oct18toFeb07’, named dataset2. The data came from UMW from Shao *et al.* [10]. Each data set consists of welds created on three product channels, indicated as a U channel, a W channel, and a J channel.

The feature selection and weld quality classification methods described above were applied to the UMW data. Twelve (from 52 possible features) and seventeen

features (from 61 possible features) were selected from dataset1 and dataset2, respectively. Therefore, the input size of each channel in dataset1 is 12. The corresponding sample size of each channel is 1811, 415 and 115. The input size in dataset2 is 17. And the sample size is 4592, 4624 and 919, respectively for each channel in dataset2. Since only good and suspect welds were reported for this data set, the size of the output layer is 2. The size of good and bad-welds of each dataset is listed in Table 3.B.1.

**Table 3.B.1 The size of good-welds and bad-welds of each channel in dataset1 and dataset2**

		Dataset1	Dataset2
<b>U channel</b>	Good-welds	1351	3600
	Bad-welds	460	992
<b>W channel</b>	Good-welds	363	4139
	Bad-welds	52	485
<b>J channel</b>	Good-welds	89	834
	Bad-welds	26	85
<b>Aggregated</b>	Good-welds	1803	8573
	Bad-welds	538	1562

Under the classification by BRNN training algorithm, the results for each channel from the two datasets are listed in Figure 3.B.1 and Figure 3.B.2. In Figure 3.B.1,  $\alpha$  error and  $\beta$  error of channel U, W and J of two datasets are both monotonically decreasing. Overall, the  $\alpha$  error and  $\beta$  error of dataset2 are higher than those of dataset1. When aggregating three channels together, the results classified with feature selection are slightly better than those classified without feature selection, except for the  $\alpha$  error in dataset1. In addition, the  $\alpha$  error and  $\beta$  error obtained for the data when aggregated without feature selection are the most unsatisfactory. While the results after feature selection processing by aggregating the data from three channels are approximately at the average level among the individual channels. In addition, the total accuracy shown in Figure 3.B.2 also validates the above statements. The total accuracy of each item in dataset1 is lower than the corresponding item in dataset2. It represents

that the data of channel J is the most distinguishable and channel U is the most indistinguishable among three channels. The results of two datasets both follow this trend. In addition, the total accuracy acquired after feature selection is slightly better than that without feature selection process.

Referring to the results of [10], the  $\alpha$  error,  $\beta$  error of training and testing is 12.04%, 0% and 10.66% and 0%, respectively. Compared to the results of the BRNN classification method, although the  $\beta$  error is slightly higher than the previous results, its value is still within an acceptable range according to industry requirements. Simultaneously, the  $\alpha$  error of BRNN classification method is much improved over that presented in paper [10]. Overall, the classification tasks by an BRNN method could reduce the calculation time while maintaining a relatively high classification accuracy in an UMW process.

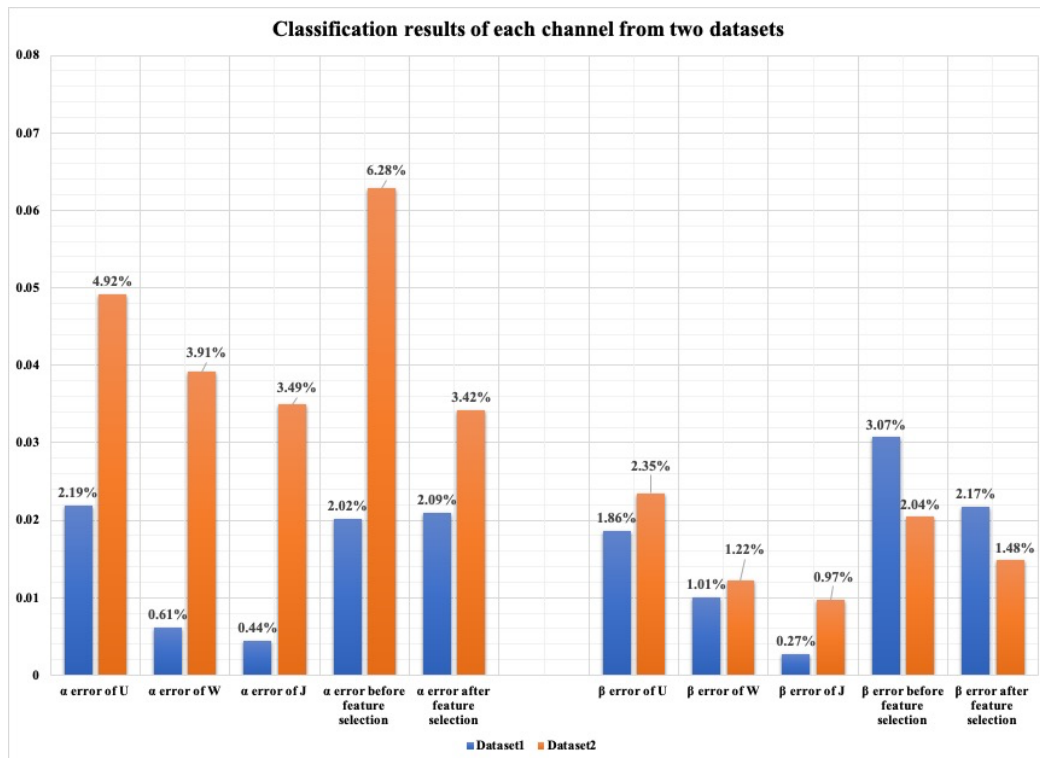


**Figure 3.B.1 Classification results of each channel from two datasets with and without feature selection**

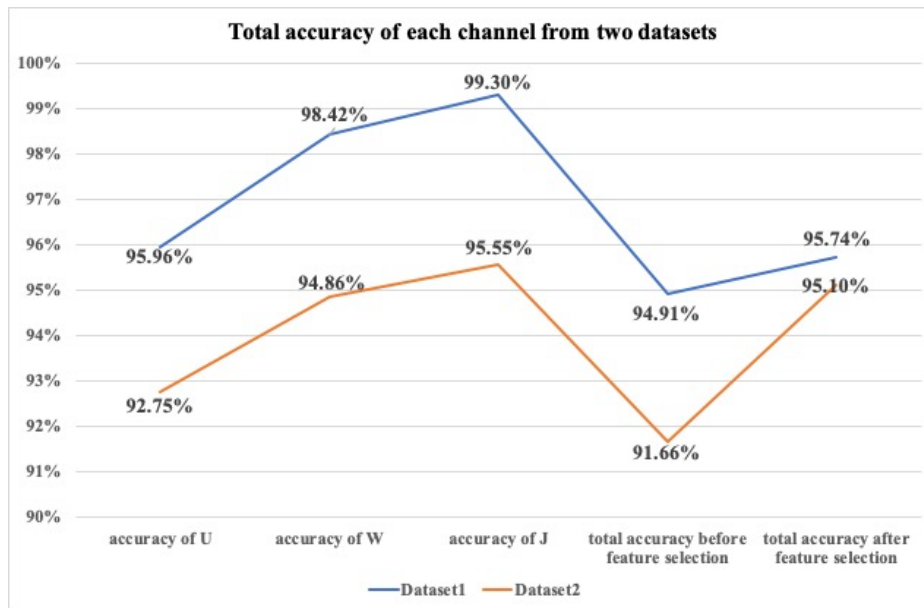


**Figure 3.B.2 Total accuracy of each channel from two datasets with and without feature selection**

In a conclusion, ANN methods, especially BRNN has a good effect on weld quality classification not only for UCW, but also for UMW when using feature-based data as the training input, when compared with the traditional machine learning techniques.

**CHAPTER 4**

**QUALITY DETECTION AND CLASSIFICATION FOR ULTRASONIC  
WELDING OF CARBON FIBER COMPOSITES USING TIME-SERIES  
DATA AND NEURAL NETWORK METHODS**

**4.1 Introduction**

Carbon fiber reinforced polymers (CFRP), also called carbon fiber composites, are increasingly applied in many industries due to their properties of lightweight, high temperature and corrosion resistance, and high stiffness and strength to weight ratios properties [1, 2]. These superior material properties are especially relevant for reducing vehicle weight and improving fuel efficiency in automotive and aerospace industry applications [3-6]. Important considerations for the adoption of CFRP is their joining processes and the effects of processing on their properties. Common techniques to join these composites are fusion-based joining, mechanical fastening, and adhesive bonding [7-9]. The fusion-based joining technique is a superior choice for CFRP in the automotive industry in order to realize product and manufacturing objectives such as lightweight, high strength, fuel economy, and fast processing time [9, 10]. Among the fusion-based joining techniques, ultrasonic welding is advantageous due to its joint strengths, better weld parameter control, less energy consumption, and good ability to join different shapes of CFRP materials [1, 11-13]. Therefore, ultrasonic welding is being increasingly utilized for joining CFRP material in the automotive industry [14, 15].

Although there are advantages to using CFRP, there is limited experience in the automotive industry in using ultrasonic composite welding (UCW), with concerns on the predictability of joint quality. Since poor joint quality can lead to higher costs and lower product durability and safety [16-18], quality prediction in ultrasonic welding has

been an active area of research recently. For example, Li *et al.* [16] combined artificial neural network and random forest techniques to perform online quality inspection of UCW based on welding process features such as weld duration and total acoustic energy. Their model's overall prediction accuracy of the joint failure load and weld quality classification was over 99%.

Examples of other welding techniques that have applied neural networks to weld quality include Wang *et al.* [19] and Martin *et al.* [20], who applied neural network models to control weld quality in laser welding and resistance spot welding, respectively. Wang *et al.*'s applied an artificial intelligence-based method to real-time monitoring during laser welding, while Martin *et al.* demonstrated a 100% success rate for distinguishing between *good spot-weld* and *stick spot-weld* classifications.

A review of the weld quality research literature finds that most non-neural network-based methods have a prediction accuracy that is higher than 90% [1, 21, 22], while neural network models have higher classification accuracy, usually nearly 100% [19, 20]. This indicates that the neural network-based models may be the best choice for weld quality classification in UCW. However, a limitation to the application of neural network-based models is that they need to be trained with experimental data that contains representative samples of the possible quality classifications with sufficient sample sizes for the various classifications [16, 18, 21, 23-26]. Since the current cost of CFRP material is high, it is expensive to run large sets of experiments, thus the quantity of experimental data may be insufficient to train deep neural network models prior to their implementation in production processes. Therefore, a method for augmenting experimental data for the preliminary training of neural networks is desirable.

The literature review also revealed that nearly all of the current classification or prediction models are based on features extracted and selected from weld process signals. Examples of such features are signal amplitude [27], weld duration time, and acoustic energy [16]. When using pre-defined features, there can be uncertainty in whether they were properly extracted from the weld process signals, even when there

is a large data set of these features to train a feature-based model. Uncertainties arise because there can be difficulty in defining the features either manually or automatically, and the signals need more preprocessing before extraction, potentially changing the feature [16, 20, 27, 28].

Feature-based methods only make use of limited information contained in the process signals. There is interest in making maximum use of the information in the entire signals, i.e., the time-series process signals. When the size of a training data set is small, e.g., tens of features, it is more straightforward to define these features based on an engineering understanding of the process, and then develop algorithms to extract the features automatically. However, as the size of the data set grows, non-feature-based methods, or methods based on automatic detection of significant features such as convolution neural networks, are needed. To make full use of the information contained in the data signal, this paper proposes replacing feature-based models with the direct input of the process signal as a time-series.

To address the challenge of limited experimental data, the simulation of process signals is proposed for the augmentation of training data. More data will facilitate the initial development of quality classification models before their deployment into real manufacturing processes. From small sets of experimental process signal training data, large sets of simulated process signals can be obtained for efficiently training neural network models. Monte Carlo simulation is proposed for enlarging data sets as it is a common method for generating time-series data from a given distribution. Papadrakakis *et al.* [29] used Monte Carlo simulation to resample input data and optimize the reliability-based structure of large-scale structural systems. Heslop and Dekkers [30] adopted Monte Carlo simulation for time-series paleoclimatic records, adding white and red noises to make their results more reliable, and demonstrated good consistency with their experimental data.

Neural networks have been applied to fault detection and diagnosis in a variety of manufacturing processes. As such, neural networks like a Bayesian regularized neural network (BRNN) using fully-connected layers and the convolutional neural network

(CNN) are promising techniques for classifying weld quality. For example, Lee *et al.* [31] and Hsu *et al.* [32] applied similar CNN models to detect faults in semiconductor manufacturing processes, where overall classification rates around 98% and 99.5%, respectively, were demonstrated with a much shorter training time. The theory behind CNN models is that they automatically emphasize significant signal features during the training process. Consequently, a CNN model will be demonstrated as providing superior accuracy when classifying weld quality in UCW when time-series process signals are used as inputs compared to non-neural network-based techniques such as support vector machines (SVM) and k-nearest neighbors (kNN).

This paper is organized as follows: Section 4.2 describes the collection of our experimental data and weld quality classification. Section 4.3 introduces the multi-layer BRNN and the CNN deep learning methods for quality classification in UCW. Section 4.4 proposes simulating time-series process data using Monte Carlo with copulas. Section 4.5 trains a large amount of simulated welding process signals in the classification task and compares the results to several machine learning techniques. Section 4.6 discusses the sensitivity of classification accuracy as the training data set sample size changes, and then demonstrates the robustness of a CNN model when increasing noise is imposed on the experimental data when the generating simulated data. Section 4.7 concludes the chapter.

## **4.2 Weld Experiments and Weld Quality Determination**

This section describes the design of the weld experiments and the collection of experimental data, as conducted in [18] and [23]. Additionally, pre-labeled CFRP weld quality criterion is also defined in this section.

### **4.2.1 Material Selection and Weld Machine**

The carbon fiber reinforced polymer weld coupons used in this research are a semi-crystalline material consisting of a 30% weight fraction short carbon fibers and an injection molded matrix of doped polyamide 6 polymer resin [18], which will be referred to hereafter as CFRP coupons. The mean diameter and length of the

reinforcement fibers were  $8\ \mu\text{m}$  and  $250\ \mu\text{m}$ , respectively [23]. The CFRP coupons have dimensions of  $138\ \text{mm}$  in length by  $38\ \text{mm}$  in width by  $3\ \text{mm}$  in thickness. In addition, the contact area of two CFRP coupons when positioned on the anvil of the weld machine is  $38\ \text{mm}$  length by  $38\ \text{mm}$  in width. More details of the material are described in paper [33]. The CRFP coupons and a schematic diagram of joining process is shown in Figure 4.1.

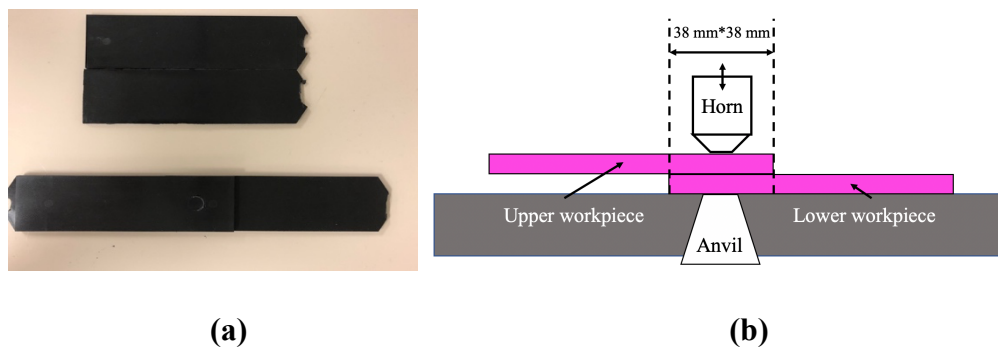


**Figure 4.1. (a) The CRFP coupons, and (b) schematic diagram of ultrasonic composite welding joining process**

The CFRP coupons were welded using an *iQ Servo Ultrasonic Welding Machine* [34], which generates a  $20\ \text{kHz}$  vibration. Other equipment used in the experiments include an oven [35] to remove the moisture in the CFRP sheet, a universal tensile testing system used for testing the maximum lap-shear strength of the workpiece [36], and a scanning electron microscope used to capture the microstructure of the weld zone [37]. Since the weld quality is sensitive to moisture in the material [38, 39], the CFRP sheet was baked at  $70^\circ\text{C}$  in the oven for at least 24 hours.

#### **4.2.2 Data Collection and Weld Quality Determination**

Five welding parameters are identified as having significant influences on weld attributes and the joint performance. They are weld energy, trigger force, plunge speed, holding time, and amplitude. Based on a two-level full factorial experimental design performed by Wang *et al.* [18], the weld energy was determined to be the most significant factor to the microstructure of the weld zone and the maximum lap-shear

strength of the weldment. A series of weld experiments was conducted to determine the optimal parameters, and 116 weldments were collected at different weld energy levels. A more detailed description of the weld experiments can be found in [33]. After removing four outliers, one hundred twelve weldments (112) with good process signals were obtained that are used for this data-driven classification research.

The weldments were assigned to one of three pre-determined weld quality classes according to their maximum lap-shear strength and the percentage of carbon fiber that mix within the weld zone [33]. Specifically, when weld energy was less than 800  $J$ , it was observed that little to no carbon fiber mixed within the weld zone [33]. Since carbon fiber reinforcement provides the strength of the composite material, insufficient carbon fiber in the weld is associated with lower lap-shear strength and is classified as an under-weld. When the weld energy is larger than 1200  $J$ , however, more pores are generated in the weld zone, which reduces the fatigue life of the weldment and is classified as an over-weld, even though it may have high lap-shear strength. Finally, when the weld energy is between 800  $J$  and 1200  $J$ , the weldments have no evidence of insufficient fiber flow or porosity and are classified as a good-weld. Among 112 weldments produced with good process signals, 15 coupons are identified as under-welds, 9 as over-welds, and 88 as good-welds. The maximum lap-shear strength to weld energy distribution is plotted in Figure 4.2. The centroid of the shear strengths of each weld class is calculated using  $k$ -means, which minimizes the distance within each category while maximizing the distance between categories as much as possible [40]. From the figure, the boundary between under- and good-welds is clear, but there is an overlap between good- and over-welds at a weld energy of 1300  $J$ . This is because of material microstructure variation [33].

Although weld energy is a significant factor, weld quality obtained by the UCW process is influenced by multiple process parameter. Thus, a weld quality classification model should be trained using a number of factors with pre-identified outcomes obtained by inspection. These 112 pre-labeled weldments are the experimental inputs

used to train the classification models or simulate additional data, as will be discussed in Sections 4.5 to 4.6.

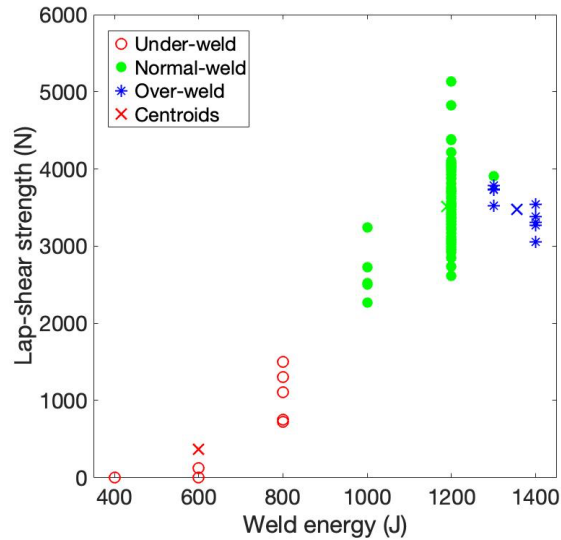


**Figure 4.2. Weld quality distribution of the relationship regarding with lap-shear strength and weld energy**

### 4.3 Deep Learning Classification Methodologies

Two neural network-based models useful for quality classification using time-series process signals are introduced in this section. The Bayesian regularized neural network (BRNN) and a deep convolutional neural network (CNN) are directly trained using the experimental welding process signals. The principle of these two models is introduced first, then their application and structure are described as applied in this research.

A Bayesian regularized neural network uses an algorithm that introduces Bayesian inference to the neural network training by setting a prior probability distribution, then using Bayes formula to update the prior probability distribution to a posterior probability distribution [41]. Regularization helps avoid overfitting during the training process. Sun *et al.* [1] demonstrated that this methodology works well on feature-based data extracted from experimental welding process signals, achieving a 99%

classification accuracy. Since the feature data is embedded in the time-series experimental process signals, it is therefore reasonable that the BRNN method can be used directly on time-series process signals. The details of the principles and the mathematical equation for a single-hidden-layer BRNN (SBRNN) are described in [1].

A convolutional neural network is a model that emphasizes features passively during a multi-layer training process [42]. The model uses a partially connected convolutional layer and a pooling layer before a fully connected layer to learn which aspects of the time-series signals to emphasize in its neural network weighing matrix [43-45]. A trained convolution layer has neuron weights that amplify distinguishing features within a time window of the process signals and reduces the dimension of the input to the fully connected layer, in effect filtering the input data through this window [43]. Pooling is a sample-based discretization process [44, 45]. Frequently, CNNs also contain batch normalization and dropout layers to reduce overfitting [46, 47]. A typical structure of a CNN is shown in Figure 4.3.

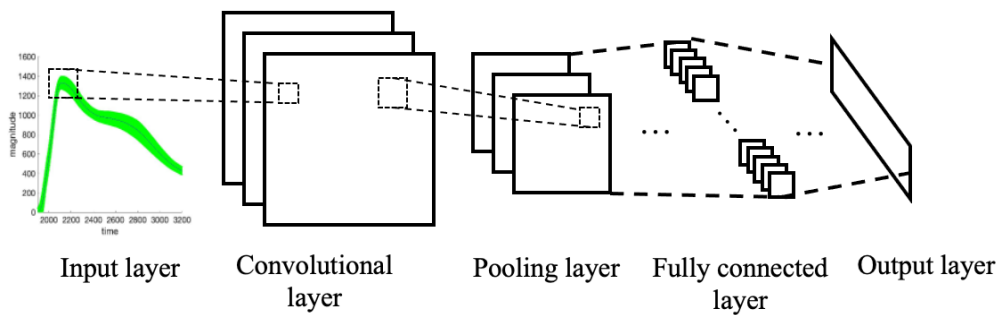


**Figure 4.3. Typical structure of CNN algorithm**

### 4.3.1 Neural Network Structure and Application

#### **Bayesian regularized neural network**

Since time-series process signals obtained directly from experiments are more complicated and potentially noisier compared to extracted feature data, a BRNN model including multiple hidden-layers was explored. Even though one hidden layer in BRNN

is sufficient to approximate any continuous function mapping from one space to another, a multi-hidden-layer BRNN model can solve more complex relationships between input data and output classifications. Using more hidden layers allows a BRNN to represent any decision boundary to any accuracy and can also approximate any mapping to any accuracy, as additional hidden layers can learn more complex representations of algorithms [48-51]. However, more hidden layers lead to longer training time and may have more issues with overfitting [51]. Therefore, considering both the complexity of input signals and training efficiency, both one- and two-hidden-layer BRNN (TBRNN) models are compared. A schematic diagram of the TBRNN structure is shown in Figure 4.4, where  $x_i$  is the size of input layer determined by the size of the input (time-series experimental process signals or feature-based signals),  $y_i$  is the output layer size (the number of pre-labeled weld quality classes to be predicted), and  $H_{1j}$  and  $H_{2k}$  are the number of neurons in the first and the second hidden layers. Each neuron used a *sigmoid* activation function, while the hidden layers used the *tansig* activation functions. Finally, a *softmax* transfer function connects to the output layer.

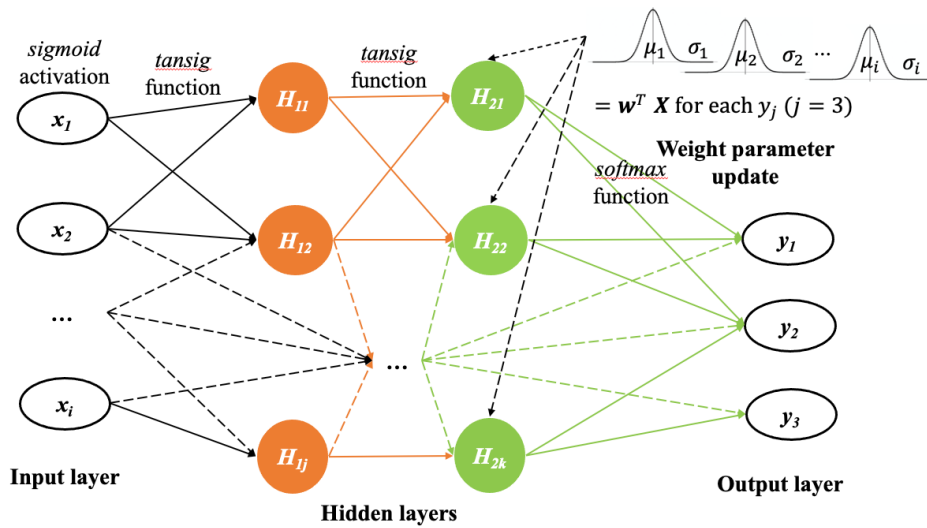


**Figure 4.4. A schematic diagram of the TBRNN model**

The number of neurons in each hidden layer is determined using two rule-of-the-thumbs: 1) the number of neurons in hidden layers should be between the size of the

input layer and the output layer; 2) the number of neurons in hidden layers should be approximately  $2/3$  of the sum of the input layer size and the output layer size [52, 53]. Therefore, in order to avoid overfitting and maintain high classification accuracy, the number of neurons in the two hidden layers is typically set between 10%-60% of the size of its previous layer. However, considering computational efficiency when training and when the input size is large, the number of neurons was adjusted downward accordingly. During training, 70% of the input process signals were selected for the training and validation set, while the rest were used for testing. Training was stopped when the performance gradient fell below  $10^{-7}$ , or the mean square error performance was less than 0.001.

### **Convolutional neural network**

In the CNN illustrated in Figure 4.5, the convolutional layer is separated from the pooling layer with a ReLu layer, that feeds into the fully connect layer, the *softmax* layer, and then to the output layer. A dropout layer was included during training in order to reduce overfitting [46, 47]. The size of the convolutional layer, pooling layer, and fully connected layer between the input ( $x_i$ ) and output layers ( $y_1$  to  $y_3$ ) are represented by  $C_c$ ,  $P_p$ , and  $F_f$ , respectively. A second convolutional and pooling layers are added before the fully connected layer. The model was trained by the stochastic gradient descent training algorithm using a  $10^{-3}$  learning rate. The training process was stopped when the number of epochs reached 100.

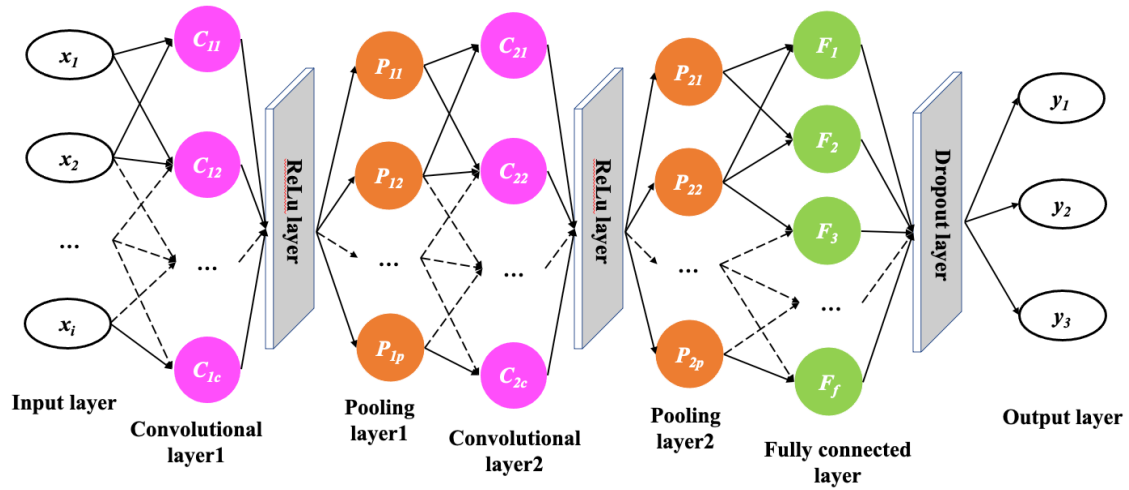


**Figure 4.5. The schematic diagram of transmission of CNN model**

Power, force, and distance signals were assembled into a matrix as the input for the CNN model. Each time-series signal has 402 data points over time defining its curve, giving an input size of  $402 \times 3$  signals. Experimentation and using rules-of-the-thumb [52, 53] found good classification accuracy with acceptable training time when the window size for the convolutional-ReLu-pooling layer was set to  $3 \times 2$  with a neuron size of 100. The second convolution layer window size was set to  $3 \times 1$  with a neuron size equals 50. A dropout probability in both dropout layers of 10% was found through experimentation to effectively reduce overfitting. The stochastic gradient descent algorithm and a learning rate of  $10^{-3}$  was used to train the simulated process signals.

#### **4.4 Simulation of Time-Series Signal Data with Multivariate Monte Carlo Simulation**

This section discusses the multivariate Monte Carlo simulation method for generating more time-series process signals from the experimental data. Several statistical methods and the SBRNN machine learning classification model are used to validate the consistency between the experimental and simulated process signals. As will be shown, the simulation data generated by this method matched the original experimental data very well.

##### **4.4.1 Multivariate Monte Carlo Simulation**

First published by Stanislaw Ulam, and used by Von Neumann in computer modelling in the late 1940s [54], multivariate Monte Carlo (MMC) simulation is a method for generating random samples using statistical distributions. Its basic principle is to create a probability model from experimental data with random parameters and to generate new samples [55].

A MMC simulation usually assumes the experimental data follows a Gaussian distribution [56]. Usually, there are three commonly types of MMC simulation for generating data: they are 1) normal approximation MMC simulation [54], 2) semi-empirical distribution MMC simulation [55], and 3) empirical distribution MMC simulation with copulas [56]. The detailed information of simulation approach selection is introduced of the Appendix 4.A. However, to make our MMC simulations more accurate, a copulas approach using an empirical distribution as well as the consideration of the dependency between the experimental data points was adopted in this research. By definition, a copula is a multivariate cumulative distribution function for which the marginal probability distribution of each variable is uniform on the interval  $[0, 1]$  [57]. Copulas use a coupling function to describe the dependency among multivariate random variables by first decomposing the joint probability distribution into a marginal distribution for each parameter. Then the marginal distribution is coupled into a new joint probability distribution that is simulated by the MMC through an inverse joint probability distribution. The strength of this approach is that it fully considers the marginal distributions of each parameter and the dependency among the original inputs.

#### **4.4.2 Process Signals Simulated by Multivariate Monte Carlo Simulation**

An MMC simulation with copulas was performed using the data from the 112 sets of process signals collected from the CFRP ultrasonic welding experiments by decomposing the time-series signal curves into several regions, simulating points within each region, and then connecting the regions to form a complete simulated process signal curve. This approach generated less variance than simulating the entire signal curve from its constituent data simultaneously. Further, to improve the simulation, the experimental data was separated into different weld energy levels before

the simulation. This approach captures nearly all of the signal inflection points that represent events that occur during the joining process. The detailed MMC process is described below using a power signal for illustration.

(1) *Reference point determination*: In order to segment the signal curve, a set of reference points describing the curve are determined as each curve varies even under nominally similar welding parameters. A set of time and corresponding magnitudes for the process signal's start point, inflection points, and the end point are extracted from the experimental time-series process signal curves at specific weld energies and weld classifications, and an empirical distribution is determined for each point. The criterion is to take the numerical gradient of process signal curve, then using a MATLAB function to find the paired time and magnitude vector  $[t_i \ y_i]$  at these points, Equation (4.1). This distribution of these inflection points over the set of experimental curves is illustrated as the red dots and their confidence intervals in Figure 4.6(a), while the green region represents the envelope of the experimental data curves. The MMC copula is then used to simulate a new set of reference points from these distributions, where a single set of reference points is illustrated by the blue dots in Figure 4.6(b). The position and the magnitude of the set of simulated reference points will vary with each simulation. A straight line is then drawn between both the experimental and simulated reference points to indicate their sequence and to allow the variance observed in the experimental data between the reference points to be imposed on the simulated curves (added in step 3). The slopes are given by Equation (4.2), where  $s_i$  and  $\hat{s}_i$  are the slopes of experimental and simulated process signal curves. The  $\hat{y}$  and  $\hat{t}$  variables are the reference points obtained from the MMC copulas simulation. The number of reference points is given by  $m$ .

$$f'(t) = 0 \quad (4.1)$$

$$s_i = \frac{y_{i+1} - y_i}{t_{i+1} - t_i}, i = 1, \dots, m - 1 \quad (4.2a)$$

$$\hat{s}_i = \frac{\hat{y}_{i+1} - \hat{y}_i}{\hat{t}_{i+1} - \hat{t}_i}, i = 1, \dots, m - 1 \quad (4.2b)$$

(2) *Scale match*: Since the simulated reference points occur at times different from the experimental reference points, the number of experimental data points between simulated reference points can vary. To resolve, the time between the reference points of experimental and simulated data is divided into  $j=1, \dots, n$  evenly spaced steps. An interpolated linear value for the corresponding signal is calculated at each of the  $n$  time steps, Equation (4.3), for each experimental time-series curve. The deviation between these points and its observed (interpolated) experimental value,  $f(t)$ , is calculated, Equation (4.4), which will be used in step 3 as the step-by-step empirical distribution for the MC copula. A schematic of the division between point2 and point3 is illustrated in Figure (4.7), with the evenly spaced points represented by the small black dots, and the deviation between an experimental signal curve and its interpolated linear reference point connector line represented by solid black lines.

$$y_{ij} = s_i \left( t_i + \frac{t_{i+1} - t_i}{n} j \right) + y_i, \quad i = 1, \dots, m - 1; j = 1, \dots, n \quad (4.3)$$

$$\Delta y_{ij} = f \left( t_i + \frac{t_{i+1} - t_i}{n} j \right) - y_{ij}, \quad i = 1, \dots, m - 1; j = 1, \dots, n \quad (4.4)$$

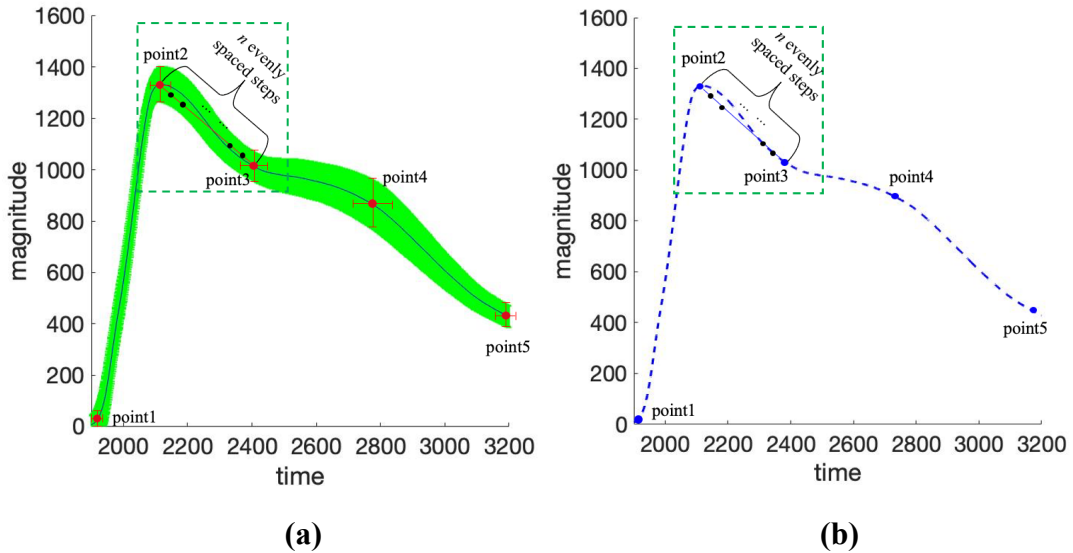


**Figure 4.6. A schematic diagram of MMC simulation with copulas on inflection points, (a) is the distribution of experimental process signals, (b) is the simulated process signals**

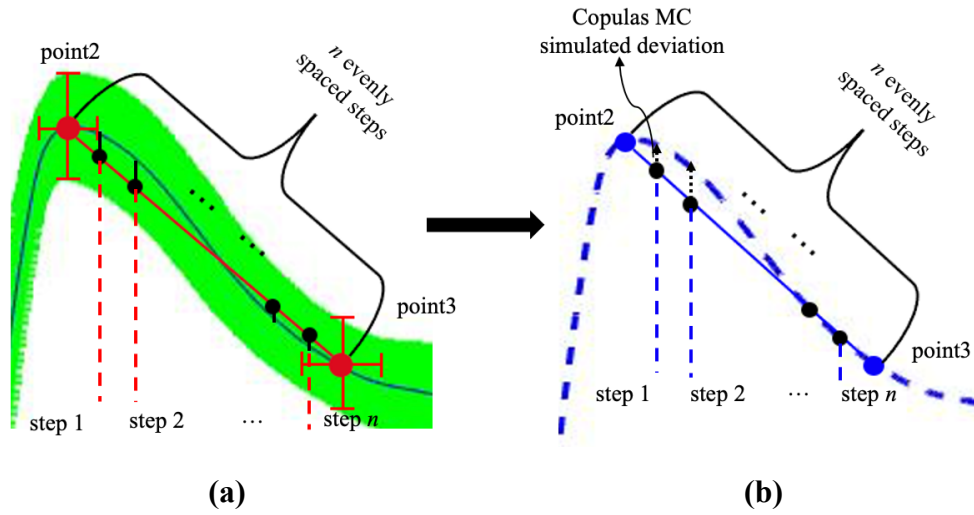


**Figure 4.7.** The enlarged region squared by green dashed line in Figure 4.6, (a) is the distribution of experimental process signals, (b) is the simulated process signals

- (3) *Data generation between reference points:* A MMC copula simulation is again used to generate the deviation at each evenly spaced data point between two adjacent simulated reference points. The simulated deviation, which can be either positive or negative, is added to the straight line between the simulated reference points at each of the  $n$  evenly spaced data points to form the final simulated process signal curve,  $\hat{f}(t)$ , in each region, Equation (4.5) and Equation (4.6). The simulated deviation,  $\Delta\hat{y}_{ij}$ , is generated using the MMC copula from the distribution of  $\Delta y_{ij}$  obtained in step 2. This is illustrated by the black dashed arrows on blue curves in Figure 4.7(b).

$$\hat{y}_{ij} = \hat{s}_i \left( \hat{t}_i + \frac{\hat{t}_{i+1} - \hat{t}_i}{n} j \right) + \hat{y}_i, \quad i = 1, \dots, m-1; j = 1, \dots, n \quad (4.5)$$

$$\hat{f}(t) = \hat{y}_{ij} + \Delta\hat{y}_{ij}, \quad i = 1, \dots, m-1; j = 1, \dots, n \quad (4.6)$$

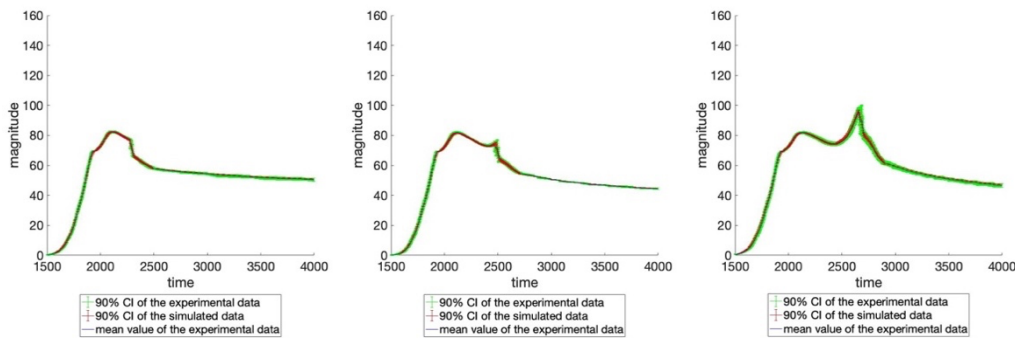
- (4) *Validation:* The simulated signal curves should be validated by comparing them to the experimental signal curves. In this work, validation is performed using a statistical comparison of the curves and a machine learning algorithm to check if the simulated curves predict their desired classes.

A statistical validation checks if the simulated curves fall within the 90% confidence interval of the experimental curve's variance under the assumption that the simulation samples are similar to the original experimental samples [58]. The standard error (SE) on the estimate of a mean is given by:

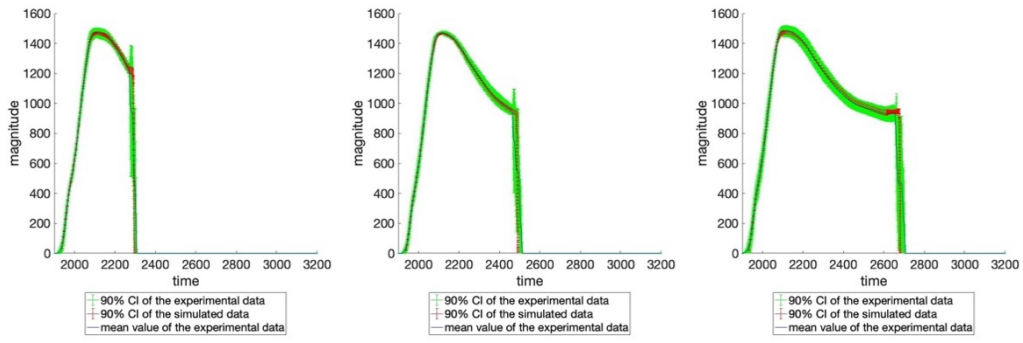
$$SE(\mu_w) = \frac{\sigma_w}{\sqrt{m_w}} \quad (4.7)$$

where  $\mu_w$ ,  $\sigma_w$  and  $m_w$  is the mean value, standard deviation, and the number of observations of the experimental or the simulated samples of weld energy with subscript  $w$ . For example,  $m_{400} = 100$  means there are 100 simulation observations at a weld energy of 400  $J$ .

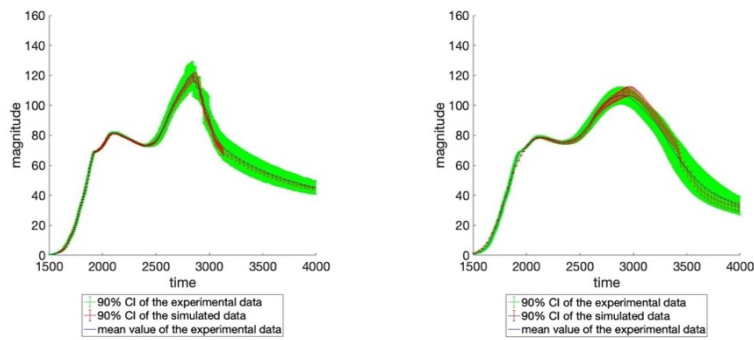
Since the weld quality classifications were partitioned into weld energy levels during the simulation, these are compared in Figure 4.8 to Figure 4.13 for force and power signals at 400  $J$ , 600  $J$ , and 800  $J$  for under-weld, 1000  $J$  and 1200-1300  $J$  for good-welds, and 1300  $J$  and 1400  $J$  for over-welds. In this figure, the green band is its 90% CI. The red error bars represent the 90% CI of the simulated process signals.



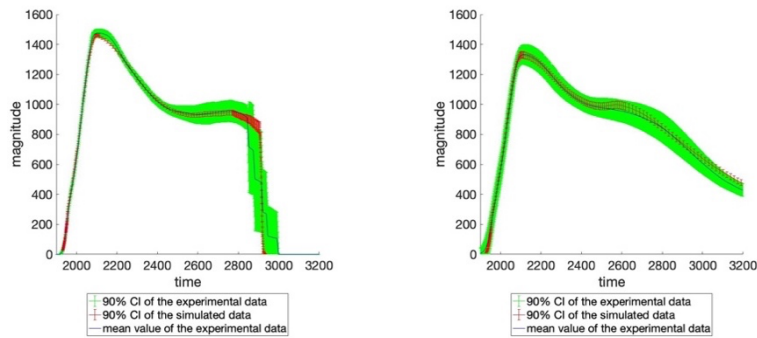
(a) (b) (c)  
**Figure 4.8. The comparison of 90% CI of the experimental and the simulated process signal curves of force signal for under-welds: (a) 400  $J$ , (b) 600  $J$ , and (c) 800  $J$**



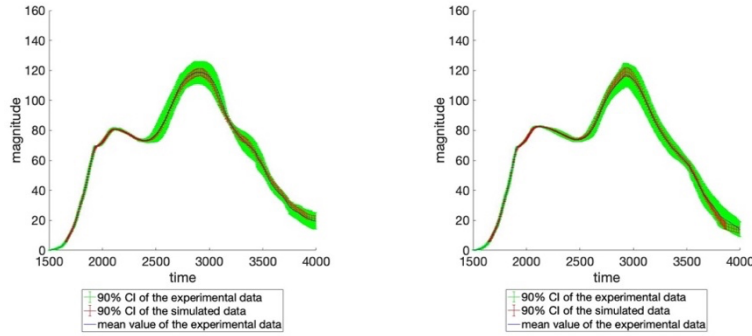
(a) (b) (c)  
**Figure 4.9.** The comparison of 90% CI of the experimental and the simulated process signal curves of power signal for under-welds: (a) 400 *J*, (b) 600 *J*, and (c) 800 *J*



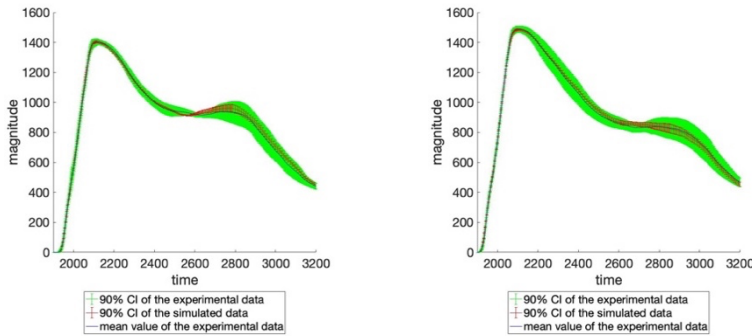
(a) (b)  
**Figure 4.10.** The comparison of 90% CI of the experimental and the simulated process signal curves of force signal for good-welds: (a) 1000 *J* and (b) 1200-1300 *J*



(a) (b)  
**Figure 4.11. The comparison of 90% CI of the experimental and the simulated process signal curves of power signal for good-welds: (a) 1000 J and (b) 1200-1300 J**



(a) (b)  
**Figure 4.12. The comparison of 90% CI of the experimental and the simulated process signal curves of force signal for of over-welds: (a) 1300 J and (b) 1400 J**



(a) (b)  
**Figure 4.13. The comparison of 90% CI of the experimental and the simulated process signal curves of power signal for of over-welds: (a) 1300 J and (b) 1400 J**

The simulated force signals for the under-welds and over-welds, the overlap with the experimental data was nearly 100%. The mean of the under-weld power signals, however, differ at some weld energy levels, e.g., 400 J and 600 J. This is due to a fast drop in weld power when the welding process ends. Although the 90%

CI for good-weld experimental curves are wider than that of the simulated curves, the simulated confidence interval is contained within the experimental confidence interval. In general, considering the amount of overlap between the confidence intervals, it can be concluded that the simulated sample curves are consistent with the experimental sample curves.

The second statistical validation looked at the difference between the experimental and simulated curves using a function comparison, where given two functions  $f(x)$  and  $g(x)$  over a closed interval  $[a, b]$ , the distance between the two functions can be measured as:

$$\|f(x) - g(x)\| = \sqrt{\int_a^b (f(x) - g(x))^2 dx} \quad (4.8)$$

$$\% \text{ error} = \frac{\text{magnitude of error}}{\text{original magnitude}} = \frac{\int \|f(t) - g(t)\| dt}{\int \|f(t)\| dt} \quad (4.9)$$

where  $f(t)$  and  $g(t)$  are the experimental and simulated process signal curves, respectively. The percentage error between the experimental and simulated curves is listed in the Table 4.1. The highest error found for the power and force signals was slightly larger than 5%, while the error for the distance signals was relatively small. We conclude that simulation using copula MMC produces reasonable process signals that are consistent with the experimental signals.

**Table 4.1 The percentage of error between the experimental and simulated process signal curves**

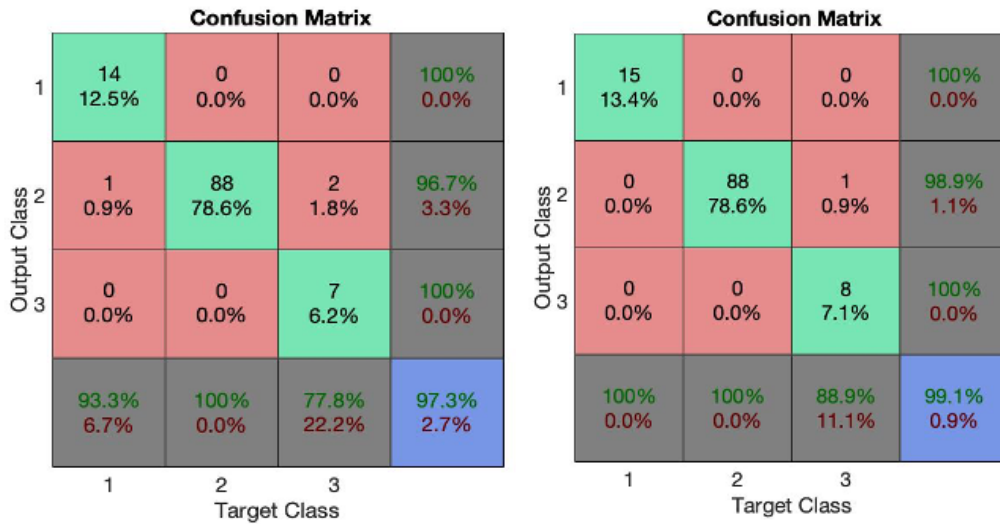
	Under-welds			Good-welds		Over-welds	
	400 J	600 J	800 J	1000 J	1200-1300 J	1300 J	1400 J
<b># of samples</b>	5	5	5	5	83	4	5
<b># of simulated samples</b>	50	50	50	50	830	40	50
<b>Power</b>	0.72%	1.41%	1.17%	3.29%	2.66%	1.07%	1.99%
<b>Force</b>	5.66%	4.25%	3.54%	1.96%	1.87%	1.23%	3.95%
<b>Distance</b>	0.03%	0.03%	0.03%	0.03%	0.03%	0.25%	0.25%

Additionally, an example of visualized comparison of experimental and simulated force, power, and distance process signals for under-welds, good-welds, and over-welds are plotted in Figure 4.B.1 and Figure 4.B.2 of the Appendix 4.B.

A machine learning validation of the simulated signals demonstrated that the classification accuracy of the simulated signals is similar to that of the experimental signals. The machine learning classification technique adopted for this validation was a single layer Bayesian regularized neural network (SBRNN), the method applied to feature-based classification using experimental data used in [1]. Using a feature-based SBRNN, an accuracy of 99.1% with an  $\alpha$  error of 0% and a  $\beta$  error of 0.9% was achieved for both the experimental and simulated data using the same size training set. Training an SBRNN with time-series signals using force, power and distance as inputs, the best models reached 95.5% and 97.3% total accuracy with 0%  $\alpha$  error, and 4.5% or 2.7%  $\beta$  error for the feature-based model and time-series-based model, respectively, as summarized in Table 4.2. An examination of the classification error at different weld energies found most error was concentrated at weld energies with the smallest training data set sizes, that of the under- and over-weld classes. A confusion matrix of the classification error is shown in Figure 4.14.

**Table 4.2 Classification accuracy comparison and validation of simulated data classified by SBRNN methodology with the same input dimension**

	Experimental data		Simulated data	
# of samples	112		112	
Experimental process signals	Total accuracy	95.5%	Total accuracy	97.3%
	$\alpha$ error	0%	$\alpha$ error	0%
	$\beta$ error	4.5%	$\beta$ error	2.7%
Feature-based signals	Total accuracy	99.1%	Total accuracy	99.1%
	$\alpha$ error	0%	$\alpha$ error	0%
	$\beta$ error	0.9%	$\beta$ error	0.9%



(a) time-series process signal

(b) feature-based signal

**Figure 4.14.** The confusion matrix of (a) simulated process signals, and (b) simulated features-based signals (Class 1 represents under-welds, Class 2 represents good-welds, and Class 3 represents over-welds)

We conclude from our validation tests that the overall accuracy of an SBRNN classifier trained using simulated data is as good or better than that using the experimental data. In summary, the statistical and machine learning validations lead us to conclude that the simulated process signals are consistent with the experimental process signals and thus lend confidence in their usefulness for supplementing experimental data when training classification models.

#### 4.5 Case Study

This section compares the classification accuracy of BRNN and CNN to SVM and kNN, two commonly used non-neural network classification methods, as trained with different size simulation data sets obtained from copula MMC. Six scenarios of simulation sample size, ranging from five to 50 times the 112 samples of the experimental data, were compared using both features extracted from the simulated signals as well as the full time-series process signals. Each scenario was repeated 20 times and an average classification accuracy is calculated.

##### 4.5.1 Feature-based Model

Twenty-five features were extracted from the time-series experimental signals as described in [1] and used as the smallest training data size set scenario. These features were also used in the copula MMC simulation as the reference points described in step one of the simulation procedure to generate five additional scenarios of training set sizes ranging from 560 to 5600 samples. For comparison, SVM and kNN classification techniques were also trained using the same simulated sample sets. The prediction outcomes were the three weld quality classes, under-, good-, and over-weld. A 10-fold cross validation was applied to validate the results of the training.

Two structures of BRNN were examined to classify the weld quality, one with a single hidden layer (SBRNN), and one with two hidden layers (TBRNN). The size of the hidden layers was 15 neurons for SBRNN model, and 15 and 9 neurons for the TBRNN model. Seventy percent of the input data was used for training and validation, while the remaining 30% was used for testing. Since the simulated data from copula MMC simulation process varied from scenario to scenario, in order to estimate the classification accuracy, each scenario was trained 20 times, recording both its mean and standard deviation. The classification accuracy and its binomial confidence interval versus simulation sample size is plotted in Figure 4.15. Detailed results are listed in the Table 4.C.1 of the Appendix 4.C.

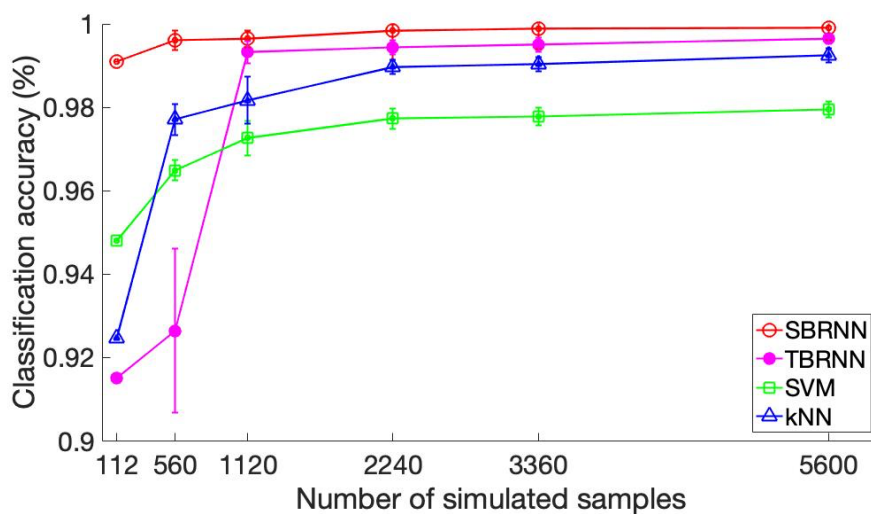


**Figure 4.15. The classification accuracy of SBRNN, TBRNN, SVM, and kNN under experimental and simulated feature-based signals**

Figure 4.15 shows that for feature-based models, as simulated sample size increases, the average classification prediction accuracy increases then stabilizes when the sample size is large. Moreover, the larger the simulated sample size, the smaller the variation in its accuracy. When the simulated sample size is larger than 2240, nearly all classification methodologies obtained >97% of accuracy, while the accuracy of the neural network models trained with a sample size of 5600 tended toward 99%. The accuracy of TBRNN model was observed to be slightly worse than for the SBRNN, but better than for SVM and kNN. Feature-based neural networks provide better models when the training set sample size is small, but as the training set sample size increases, both neural network and non-neural network-based methods have high and stable classification accuracy. A neural network-based SBRNN provided the best performance on feature-based signals in both small and large sized training sets.

#### **4.5.2 Time-series-based Model**

BRNN and CNN neural network models were next evaluated for their classification accuracy when using time-series signals of power, force, and displacement as input. Like the feature-based data, one scenario used the experimental process signals for training, while the other five scenarios used simulated process signals. For comparison, the SVM and kNN used an aggregation of the serially arranged experimental data used in the first scenario. A 10-fold cross validation was applied when training by SVM and kNN.

The input size of each BRNN model was 1206, from the 402\*3 data points from each power, force, and displacement signal generated by the MMC simulation process. Considering the computational limits of the computer used in this research, the neuron sizes for the SBRNN and TBRNN were limited to 100, and 100 and 50, respectively. The details of the CNN structure are described in section 3. Like the feature-based evaluation, 70% of the input data was randomly selected for training and validation, while 30% was reserved for testing. The simulation and training were repeated twenty times and the mean and binomial confidence interval of the classification accuracy are

plotted in Figure 4.16. Detailed results are listed in the Table 4.C.2 of the Appendix 4.C.

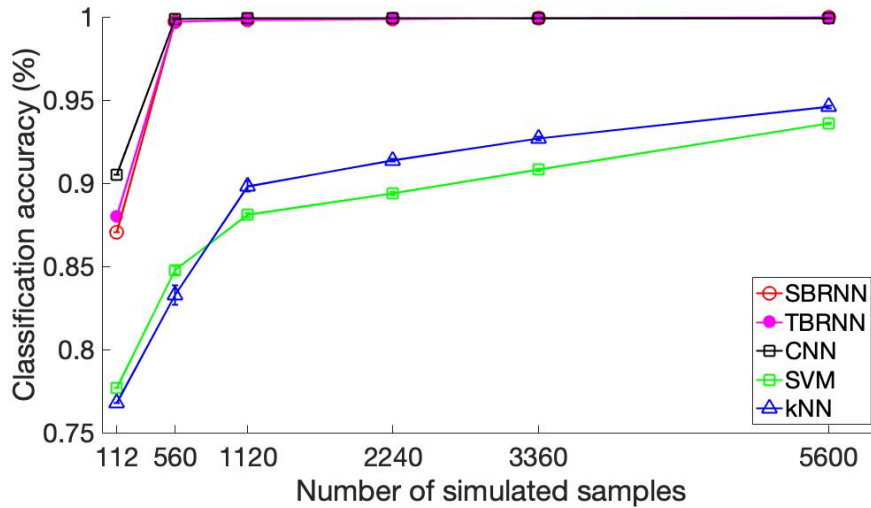


**Figure 4.16. The classification accuracy of SBRNN, TBRNN, CNN, SVM, and kNN under original and simulated process signals**

Similar to Figure 4.15, Figure 4.16 shows that the classification accuracy increases with the increase of number of simulated samples for all models. Moreover, the neural network models perform 5-10% better than the SVM and kNN models when using time-series process signals as their input. When the simulated sample size is greater than 560 for BRNN and CNN, the accuracy is nearly 100%, which may indicate the models are over-fit. However, this high accuracy may be reasonable as the copula MMC simulation is based on constructing signals from reference points that had been previously identified as the most significant features for classifying weld quality in UCW [1]. Moreover, the operating principle behind the CNN structure is to automatically identify and emphasize features in an input signal through convolution and pooling. Therefore, the dual effect of the copula MMC simulation and a CNN, combined with the addition of dropout layers introduced to avoid overfitting, is to reach a very high classification accuracy. While the overall classification accuracy obtained from training with the simulation data set does not necessary mean 100% accuracy will be observed for real

UCW process signals, it was observed to be not less than 90% as shown in Table 4.C.2 of the Appendix 4.C.

In summary, CNN and BRNN models are can produce high accuracy classification predictions when using time-series process signals as input when trained with both small and large size data sets when compared to SVM and kNN classification methods.

## 4.6 Discussion

The relationship between classification accuracy and the size of the simulated time-series process signal training set is important to the computational efficiency and training time of neural network-based models, as time-series process signals have a much larger input data size and thus require the determination of more model parameters than required of feature-based neural network models. As our top performing algorithm, a CNN model trained solely with simulated process signals will be tested to determine if it accurately predicts weld classifications using experimental signals. Finally, the robustness of CNN models trained using that simulated data that has variation in the data used to simulate time-series process signals will be examined for its effect on their accuracy.

### 4.6.1 Sensitivity of the Size of Simulated Process Signals

While the feature- and time-series process signal-based models explored earlier demonstrated the classification accuracy and variance increased as the number of simulated training samples increased, the efficiency of the training process decreased. Consequently, the best tradeoff between simulated sample size and accuracy should be determined. A comparison of sample size versus classification accuracy is plotted in Figure 4.17, where the x-axis is the size of simulated sample training set, and the y-axis represents the change classification accuracy percent given by Equation (4.10):

$$y = \frac{A_{i+1} - A_i}{A_i}, i = 1, \dots, 5 \quad (4.10)$$

in Equation (4.10),  $A_i$  is the classification accuracy of the  $i$ th scenario, corresponding to a training set size of 112, 560, 1120, 2240, 3360, 5600. The general trend is the rate

of increase in accuracy gradually decreases as the number of simulated samples increases. In most cases, when the number of simulated samples reaches 1120 to 2240, the accuracy improvement is at its lowest or is thereafter stable. At this size training set, the classification accuracy is at its best balance between computational efficiency and accuracy.

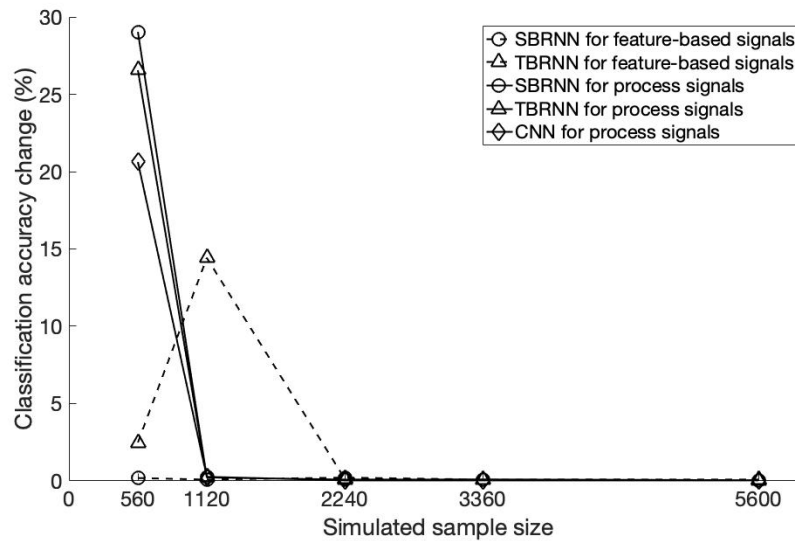


**Figure 4.17. The sensitivity of classification accuracy with the number of simulated samples under the condition of feature-based signals and process signals**

The training time of the neural network-based models is expected to increase exponentially as the training set size increases. Table 4.3 shows the training time recorded using single GPU hardware and 32-gigabytes of memory. It was found that training a CNN is significantly shorter than both the SBRNN and TBRNN, although all models reached high classification accuracy as shown in Figure 4.16. It is expected that as the number of simulated samples increases, the difference of computation time between CNN and BRNN models will further increase. Therefore, with a large training data set, CNN is the favored algorithm. Moreover, when the simulated sample size changes from 1120 to 2240 for CNN, the training time increases five folds, from ~1.5 minutes to ~7.5 minutes. In conclusion, considering the classification accuracy and

training time, the best model for classifying weld quality based on time-series process signals is a CNN trained using a simulated sample size is ~1000.

**Table 4.3 Training time comparison of SBRNN, TBRNN, and CNN under 560, 1120, 2240, and 3360 simulated sample size**

Sample size		Training time (second)			
		560	1120	2240	3360
Models	SBRNN	~450	~1200	~3000	>7200
	TBRNN	~600	~1150	~3150	>7200
	CNN	~50	~100	~450	~1250

#### 4.6.2 Classification Accuracy of CNN Model Trained with Simulated Data on Experimental Signals

Since the time-series CNN models described in section 5 show high accuracy when trained with both experimental and simulated process signals, a CNN model that was trained using only simulated process signals was used to determine if it is a good predictor of experimental process signal classifications. In this verification, CNN models are trained using different simulated training set sizes, then tested against the same 112 experimental data samples.

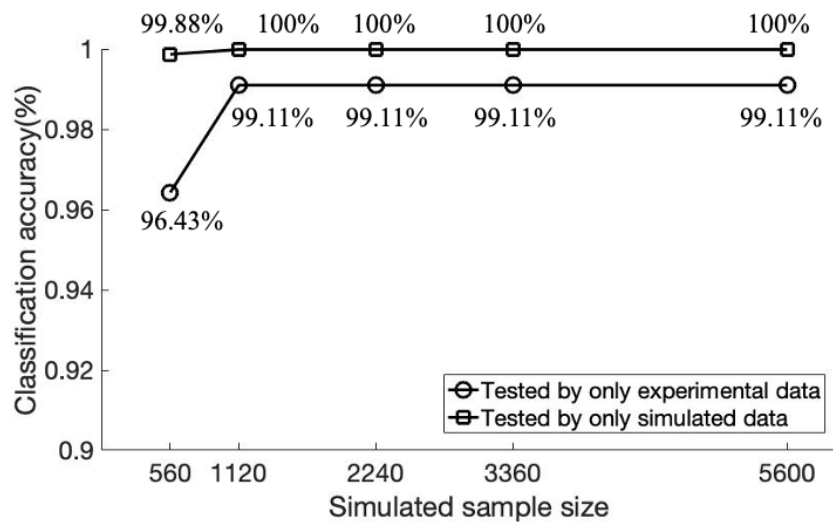


**Figure 4.18. Classification accuracy of a CNN model trained under different sizes of simulated process signals and tested by only experimental process signals or only simulated process signals**

The accuracy of this CNN model is shown in Figure 4.18. When the training data size is 560, the testing accuracy of CNN model is ~96%. Training data set sizes 1120 and larger reached a stable testing accuracy of 99%. This indicates that a high classification accuracy can be obtained for experimental process signals from a model trained using simulated data. Additionally, the testing accuracy using simulated data can obtain ~100% when training set size is larger than 560. Consequently, we predict that a CNN model trained with simulated process signals should work well for predicting the outcomes of a real ultrasonic composite welding process.

**4.6.3 Robustness of CNN Models Trained with Simulated Data**

The robustness of the CNN algorithm to variation in the input data used to simulate time-series process signals was explored using a training set size of 1120 as the baseline. First, noise was added to the 112 experimental process signals by imposing different multiplies to its standard error,  $\sigma_j$ , at each of the 3000-time steps of the original 112 experimental samples, Equation (4.11a):

$$\sigma_j = \sqrt{\frac{1}{N} \sum_{i=1}^N (x_{ij} - \mu_j)^2}, i = 1, 2, \dots, 112, j = 1, 2, \dots, 3000 \quad (4.11a)$$

$$x'_{ij} = x_{ij} + nz\sigma_j \quad (4.11b)$$

where  $x_{ij}$  is the  $j$ th node of  $i$ th sample,  $\mu_j$  is the mean value of the  $j$ th node for all samples, and  $N$  equals to 112, and  $z$  is a random scalar drawn from the standard normal distribution. This standard error was multiplied by an amplification factor  $n$  ranging from 0.5 to 10.0, and added as Gaussian noise to the process signal curves, as shown in Equation (4.11b). MMC simulations were generated based on the 112 experimental samples with their different levels of imposed noise to obtain 112 or 1120 noisy simulated time-series process signal curves. A CNN classification model was then trained with both the noisy experimental and simulated data in order to determine its

loss in accuracy as noise increases. Note that since there were only 402-time steps for each process signal curve simulated by the copula MMC simulation, the simulated curves were increased to 3000-time steps by interpolation in order to ensure the comparison to the experimental process signal curves was consistent. The classification accuracy of the CNN models trained using the original 112 experimental signals, 112 simulated signals with added noise, and 1120 simulated signals with added noise are plotted in Figure 4.19.

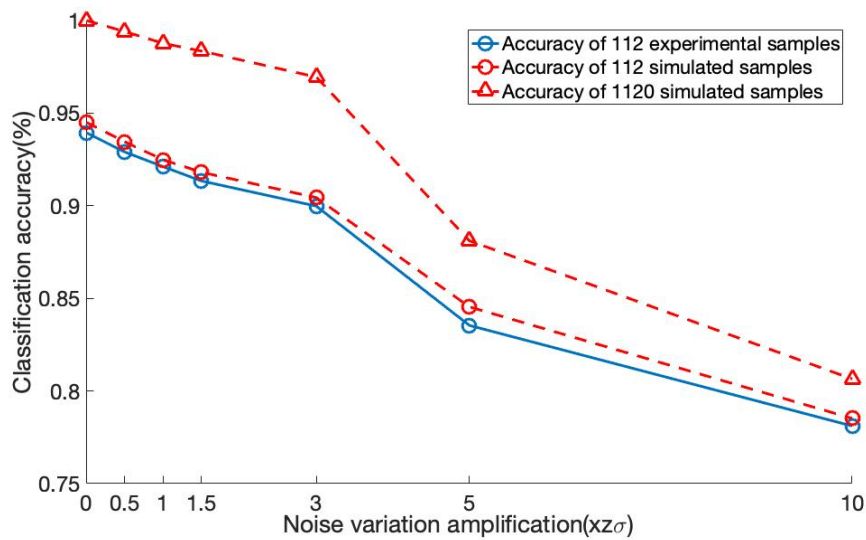


**Figure 4.19. Classification accuracy variation with noise variation added on the experimental 112 process signal curves, simulated 112 process signal curves, and simulated 1120 process signal curves**

In Figure 4.19, the x-axis represents the degree of noise amplification in the process signal curves, while the y-axis represents the predicted classification accuracy with a model trained with this additional noise. The solid and dashed lines are the classification accuracy of experimental and simulated process signals, respectively. As expected, increased training noise decreases the model accuracy. Moreover, the classification accuracy drops significantly when the amplification factor is greater than  $n=3$ . Note that when the imposed noise is amplified by around 3~4, the accuracy of simulated process signals approximately equals that of experimental data without

adding noise. Considering only the original experimental samples, when noise is less than  $\sim 3\sigma$ , the classification accuracy is still higher than 90%. Although added noise decreases accuracy, the noise in experimental manufacturing process data is expected to be smaller than the artificially added noise, as shown in Figure 4.20. In fact, even an amplification factor greater than 1 changes the simulated process signals significantly from the original experimental process signals. Therefore, we conclude a CNN model can efficiently classify weld quality in UCW using time-series process signals even when noise is present in the experimentally collected training data.

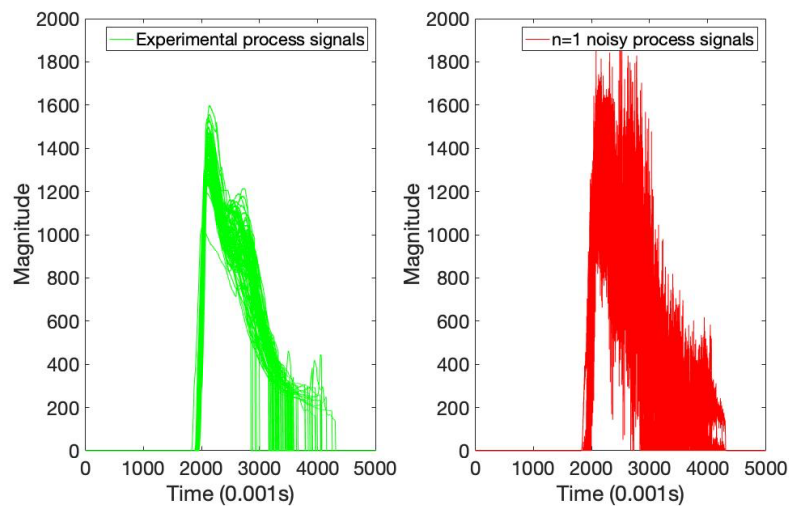


**Figure 4.20. The comparison of experimental process signals and the noisy process signals when amplification factor  $n = 1$**

#### 4.7 Conclusion

A multivariate Monte Carlo simulation with copulas was proposed for generating a large data set of time-series process signals to train neural network quality classifier models. A copula MMC takes the dependency between data points into consideration and was demonstrated for simulating signals from ultrasonic welding of CFRP. The simulated data was compared in several classification methods, including feature-based signals and time-series process signals. Neural network-based BRNN and CNN models were shown to have superior performance for classifying weld quality in UCW

compared with non-neural network-based models. We concluded a training set sample size can be determined that is the best balance between classification accuracy, sample size, and computational efficiency.

The following summarizes our conclusions for the proposed MMC simulation with copulas, generating time-series manufacturing process signals, and training SBRNN, TBRNN, and CNN neural networks to classify the weld quality of UCW of CFRP materials:

- (1) A piecewise multivariate Monte Carlo copula approach was shown to produce simulated signals consistent with the experimental UCW process signals. These simulated signals support the development of deep neural network models when there is insufficient input data.
- (2) A neural network-based CNN is an accurate, efficient, and robust classification method for predicting UCW quality classes when both small and large size data sets are available as input for training. This method was demonstrated to reach at least 90% classification accuracy when the input data size was small.
- (3) Neural network-based BRNN have better quality prediction classification accuracy for UCW feature-based models when compared with to SVM and kNN classification methods when both the training set size is small or large. Additionally, the BRNN model was demonstrated to achieve high classification accuracy on time-series process signals, but this method does not handle the data as efficiently compared with the CNN model.
- (4) There is a tradeoff between classification accuracy and the training sample set size. We found that in UCW a training sample set size of around 1000 was the best balance between computational efficiency and model classification accuracy.

To further support the findings of this research, future verification work should be conducted in the areas:

- (1) *Verification on Monte Carlo simulation:* Use the time-series process signals extracted in real manufacturing process should further verify whether the copulas Monte Carlo simulation approach is reasonable and effective.
- (2) *Verification on CNN model:* Use a large amount of UCW process signals in real welding process should further verify the efficiency of CNN model.

## References

- [1] L. Sun, S.J. Hu, T. Freiheit, Feature-based quality classification for ultrasonic welding of carbon fiber reinforced polymer through Bayesian regularized neural network, *Journal of Manufacturing Systems* 58 (2021) 335-347.
- [2] M. Sauer, M. Kuhnel, *Composites Market Report 2019*, Carbon Composite e.V., Ed, 2019.
- [3] K. Salonitis, J. Pandremenos, J. Paralikas, G. Chryssolouris, Multifunctional materials: engineering applications and processing challenges, *Journal of Advanced Manufacturing Technology* 49 (2010) 803-826.
- [4] Y. Lu, Y. Li, N. Li, X. Wu, Reduction of composite deformation based on tool-part thermal expansion matching and stress-free temperature theory, *Journal of Advanced Manufacturing Technology* 88 (2017) 1703-1710.
- [5] M. Golzar, M. Poorzeinolabedin, Prototype fabrication of a composite automobile body based on intergraded structure, *Journal of Advanced Manufacturing Technology* 49 (2010) 1037-1045.
- [6] A.v. Grootel, J. Chang, B.L. Wardle, E. Olivetti, Manufacturing variability drives significant environmental and economic impact: The case of carbon fiber reinforced polymer composites in the aerospace industry, *Journal of Cleaner Production* 261 (2020) 121087.
- [7] What techniques can I use to weld Nylon? TWI. <https://www.twi-global.com/technical-knowledge/faqs/faq-what-techniques-can-i-use-to-weld-nylon>. (Accessed May 20, 2021).
- [8] J. Leone, Plastic joining methods. Science. <https://sciencing.com/plastic-joining-methods-6924074.html>. (Accessed May 20, 2021).
- [9] A. Pramanik, A.K. Basak, Y. Dong, P.K. Sarker, M. Uddin, G. Littlefair, A.R. Dixit, S. Chattopadhyaya, Joining of carbon fibre reinforced polymer (CFRP) composites and aluminium alloys-A review, *Composites Part A: Applied Science and Manufacturing* 101 (2017) 1-29.
- [10] T. Ishikawa, K. Amaoka, Y. Masubuchi, T. Yamamoto, A. Yamanaka, M. Arai, J. Takahashi, Overview of automotive structural composites technology developments in Japan, *Composites Science and Technology* 155 (2018) 221-246.
- [11] Y.P. Korkolis, J. Li, B. Carlson, E. Chu, Special issue: Forming and joining of lightweight and multimaterial systems, *Journal of Manufacturing Science and Engineering* 137(5) (2015) 050201.
- [12] S.S. Lee, T.H. Kim, S.J. Hu, W.W. Cai, J.A. Abell, J. Li, Analysis of weld formation in multilayer ultrasonic metal welding using high-speed images, *Journal of Manufacturing Science and Engineering* 137(3) (2015) 031016.
- [13] B. Kang, W. Cai, C.-A. Tan, Dynamic response of battery tabs under ultrasonic welding, *Journal of Manufacturing Science and Engineering* 135(5) (2013) 051013.

- [14] H.P.C. Daniels, Ultrasonic welding, *Ultrasonics* 3(4) (1965) 190-196.
- [15] F. Lionetto, C. Mele, P. Leo, S. D'Ostuni, F. Balle, A. Maffezzoli, Ultrasonic spot welding of carbon fiber reinforced epoxy composites to aluminum: mechanical and electrochemical characterization, *Composites Part B: Engineering* 144 (2018) 134-142.
- [16] Y. Li, B. Yu, B. Wang, T.H. Lee, M. Banu, Online quality inspection of ultrasonic composite welding by combining artificial intelligence technologies with welding process signatures, *Materials & Design* 194 (2020).
- [17] T. Zhao, C. Broek, G. Palardy, I.F. Villegas, R. Benedictus, Towards robust sequential ultrasonic spot welding of thermoplastic composites: Welding process control strategy for consistent weld quality, *Composites Part A: Applied Science and Manufacturing* 109 (2018) 335-367.
- [18] K. Wang, D. Shriver, Y. Li, M. Banu, S.J. Hu, G. Xiao, J. Arinez, H.-T. Fan, Characterization of weld attributes in ultrasonic welding of short carbon fiber reinforced thermoplastic composites, *Journal of Manufacturing Processes* 29 (2017) 124-132.
- [19] W. Cai, J. Wang, P. Jiang, L. Cao, G. Mi, Q. Zhou, Application of sensing techniques and artificial intelligence-based methods to laser welding real-time monitoring: A critical review of recent literature, *Journal of Manufacturing Systems* 57 (2020) 1-18.
- [20] Ó. Martín, M. López, F. Martín, Artificial neural networks for quality control by ultrasonic testing in resistance spot welding, *Journal of Materials Processing Technology* 183(2-3) (2007) 226-233.
- [21] Y. Li, Z. Liu, J. Shen, T.H. Lee, M. Banu, S.J. Hu, Weld quality prediction in ultrasonic welding of carbon fiber composite based on an ultrasonic wave transmission model, *Journal of Manufacturing Science and Engineering* 141(8) (2019) 081010.
- [22] Q. Nazir, C. Shao, Online tool condition monitoring for ultrasonic metal welding via sensor fusion and machine learning, *Journal of Manufacturing Processes* 62 (2021) 806-816.
- [23] Y. Li, J. Arinez, Z. Liu, T.H. Lee, H.-T. Fan, G. Xiao, M. Banu, S.J. Hu, Ultrasonic welding of carbon fiber reinforced composite with variable blank holding force, *Journal of Manufacturing Science and Engineering* 140(9) (2018) 091011.
- [24] Y. Li, T.H. Lee, C. Wang, K. Wang, C. Tan, M. Banu, S.J. Hu, An artificial neural network model for predicting joint performance in ultrasonic welding of composites, 7th CIRP Conference on Assembly Technologies and Systems, Elsevier BV, 2018, pp. 85-88.
- [25] K. Wang, Y. Li, M. Banu, J. Li, W. Guo, H. Khan, Effect of interfacial preheating on welded joints during ultrasonic composite welding, *Journal of Materials Processing Technology* 246 (2017) 116-122.

- [26] W.G. Guo, J.J. Jin, S.J. Hu, Profile monitoring and fault diagnosis via sensor fusion for ultrasonic welding, *Journal of Manufacturing Science and Engineering* 141(8) (2019) 081001.
- [27] Y. Chen, H.-W. Ma, G.-M. Zhang, A support vector machine approach for classification of welding defects from ultrasonic signals, *Nondestructive Testing and Evaluation* 29(3) (2014).
- [28] B. Wang, S.J. Hu, L. Sun, T. Freiheit, Intelligent welding system technologies: State-of-the-art review and perspectives, *Journal of Manufacturing Systems* 56 (2020) 373-391.
- [29] M. Papadrakakis, N.D. Lagaros, Reliability-based structural optimization using neural networks and Monte Carlo simulation, *Computer Methods in Applied Mechanics and Engineering* 191(32) (2002) 3491-3507.
- [30] D. Heslop, M.J. Dekkers, Spectral analysis of unevenly spaced climatic time series using CLEAN: signal recovery and derivation of significance levels using a Monte Carlo simulation, *Physics of the Earth and Planetary Interiors* 130(1-2) (2002) 103-116.
- [31] K.B. Lee, S. Cheon, C.O. Kim, A convolutional neural network for fault classification and diagnosis in semiconductor manufacturing processes, *IEEE Transactions on Semiconductor Manufacturing* 30(2) (2017) 135-142.
- [32] C.-Y. Hsu, W.-C. Liu, Multiple time-series convolutional neural network for fault detection and diagnosis and empirical study in semiconductor manufacturing, *Journal of Intelligent Manufacturing* (2020).
- [33] K. Wang, D. Shriver, M. Banu, S.J. Hu, G. Xiao, J. Arinez, H.-T. Fan, Performance prediction for ultrasonic spot welds of short carbon fiber-reinforced composites under shear loading, *Journal of Manufacturing Science and Engineering* 139(11) (2017) 111001.
- [34] iQ Servo Ultrasonic Welding. Dukane. <https://www.dukane.com/plastic-welding-products/iq-servo-ultrasonic-welding-2/>. (Accessed May 20, 2021).
- [35] Lindberg/Blue M™ Moldatherm™ Box Furnaces. ThermoFisher Scientific. <https://www.thermofisher.com/order/catalog/product/BF51794C#/BF51794C>. (Accessed May 20, 2021).
- [36] Universal testing systems. Instron. <https://www.instron.us/en-us/products/testing-systems/universal-testing-systems/electromechanical/3300/3340-single-column>. (Accessed May 20, 2021).
- [37] ImageJ. ImageJ. <https://imagej.nih.gov/ij/>. (Accessed May 20, 2021).
- [38] R. Selzer, K. Friedrich, Mechanical properties and failure behaviour of carbon fibre-reinforced polymer composites under the influence of moisture, *Composites Part A: Applied Science and Manufacturing* 28(6) (1997) 595-604.

- [39] B. Yu, Z. Jiang, J. Yang, Long-term moisture effects on the interfacial shear strength between surface treated carbon fiber and epoxy matrix, *Composites Part A: Applied Science and Manufacturing* 78 (2015) 311-317.
- [40] J.B. MacQueen, Some methods for classification and analysis of multivariate observations, L.M.L. Cam, J. Neyman (Eds.) ed., University of California Press, Berkeley, USA, 1967.
- [41] D. MacKay, Bayesian interpolation, *Neural Computation* 4(3) (1992) 415-447.
- [42] I. Goodfellow, Y. Bengio, A. Courville, *Deep Learning*, MIT Press 2016.
- [43] H.H. Aghdam, E.J. Heravi, *Guide to convolutional neural networks: A practical application to traffic-sign detection and classification*, Switzerland, 2017.
- [44] D. Ciresan, U. Meier, J. Masci, L.M. Gambardella, J. Schmidhuber, Flexible, high performance convolutional neural networks for image classification, *Proceedings of the Twenty-Second International Joint Conference on Artificial Intelligence*, 2011, pp. 1237-1242.
- [45] A. Krizhevsky, I. Sutskever, G. Hinton, ImageNet classification with deep convolutional neural networks, In *Advances in Neural Information Processing Systems* 25, 2012.
- [46] N. Srivastava, G. Hinton, A. Krizhevsky, I. Sutskever, R. Salakhutdinov, Dropout: A simple way to prevent neural networks from overfitting, *Journal of Machine Learning Research* 15(1) (2014) 1929-1958.
- [47] L. Wan, M. Zeiler, S. Zhang, Y.L. Cun, R. Fergus, Regularization of neural networks using DropConnect, *Proceedings of the 30th International Conference on Machine Learning*, 2013, pp. 1058-1066.
- [48] G. Cybenko, Approximations by superpositions of sigmoidal functions, *Mathematics of Control, Signals and Systems* 2 (1989) 303-314.
- [49] K. Hornik, Approximation capabilities of multilayer feedforward networks, *Neural Networks* 4(2) (1991) 251-257.
- [50] G.E. Hinton, S. Osindero, Y.-W. Teh, A Fast Learning Algorithm for Deep Belief Nets, *Neural Computation* 18(7) (2006) 1527-1554.
- [51] R.M.I. Choldun, J. Santoso, K. Surendro, *Determining the Number of Hidden Layers in Neural Network by Using Principal Component Analysis*, Springer, Cham 2020.
- [52] J. Heaton, *Optimal size of the hidden layer*, Heaton Research, Inc.2008.
- [53] S.W. Smith, *The scientist and engineer's guide to digital signal processing*, second edition ed., California Technical Publishing, United States of America, 1999.
- [54] N. Metropolis, The beginning of the Monte Carlo method, *Los Alamos Science* (1987) 125-130.
- [55] C.Z. Mooney, *Monte Carlo simulation*, Sage, Newbury Park, CA, 1997.

[56] R.M. Neal, Monte Carlo implementation of Gaussian process models for Bayesian regression and classification, Department of Statistics, University of Toronto, Department of Statistics, University of Toronto, 1997.

[57] R.B. Nelsen, An Introduction to Copulas, Springer, New York, 1999.

[58] J.H. Zar, Biostatistical Analysis, 4th ed., Prentice Hall., Upper Saddle River, N.J., 1998.

## Appendix

### Appendix 4.A

For three commonly types of MMC simulation: 1) normal approximation MMC simulation [54], 2) semi-empirical distribution MMC simulation [55], and 3) empirical distribution MMC simulation with copulas [56]. For the 1<sup>st</sup> approach, it assumes that the original input follows the normal distribution. For the 2<sup>nd</sup> approach, it is a semi-empirical distribution MMC simulation. The only difference between the 1<sup>st</sup> and 2<sup>nd</sup> method is the former generates the data based on normal distribution, while the latter is based on empirical distribution. However, for the 3<sup>rd</sup> simulation approach, it uses the empirical distribution with copulas. A copula is defined as a multivariate cumulative distribution function for which the marginal probability distribution of each variable is uniform on the interval [0,1] [57]. Copulas are used to describe the dependency among multivariate random variables with a coupling function. It allows the simulation to first decompose joint the probability distribution into a marginal distribution for each parameter. Then couples the new marginal distribution of the parameters into a new joint probability distribution that is simulated by MMC. The strength of this approach is that it fully considers the marginal distributions of each parameter and the dependency among the original inputs. The steps of a MMC simulation with copulas are listed as follows:

- (1) Calculate the joint probability distribution of the input;
- (2) Decompose joint probability distribution into the marginal distribution and generate new marginal distribution;
- (3) Couple new marginal distribution into joint probability distribution and finally inverse joint probability distribution into new input.

In order to validate the simulation approach, we iterated for 10 times than original input for each inflection points by three MMC simulation approaches. Recall that there are 112 experimental observations. With MMC simulation, there are 1120 samples for

validating (880 are good-welds, 150 are under-welds and 90 are over-welds). The simulation distribution comparison of three approaches is plotted in Figure 4.A.1.

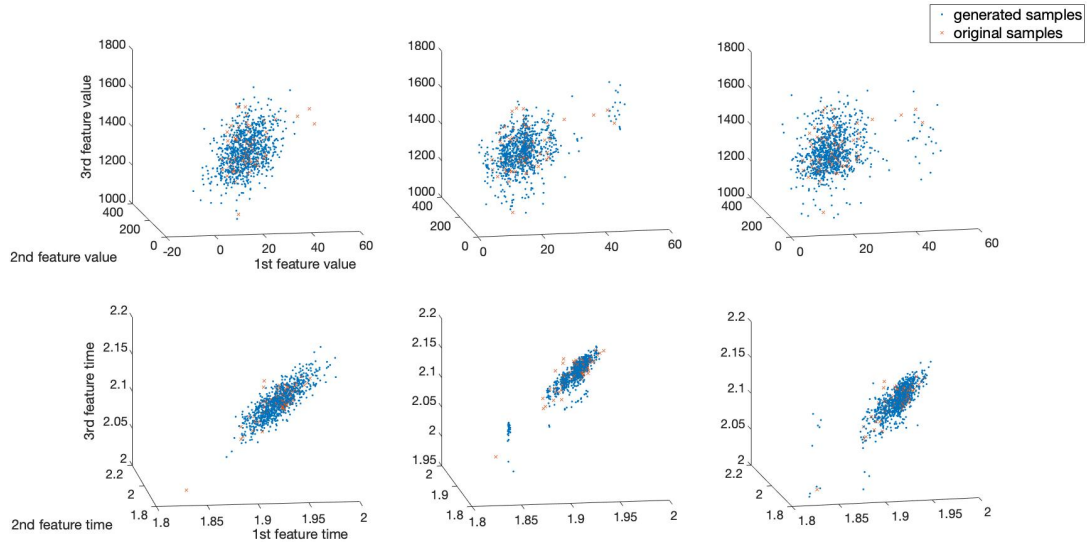
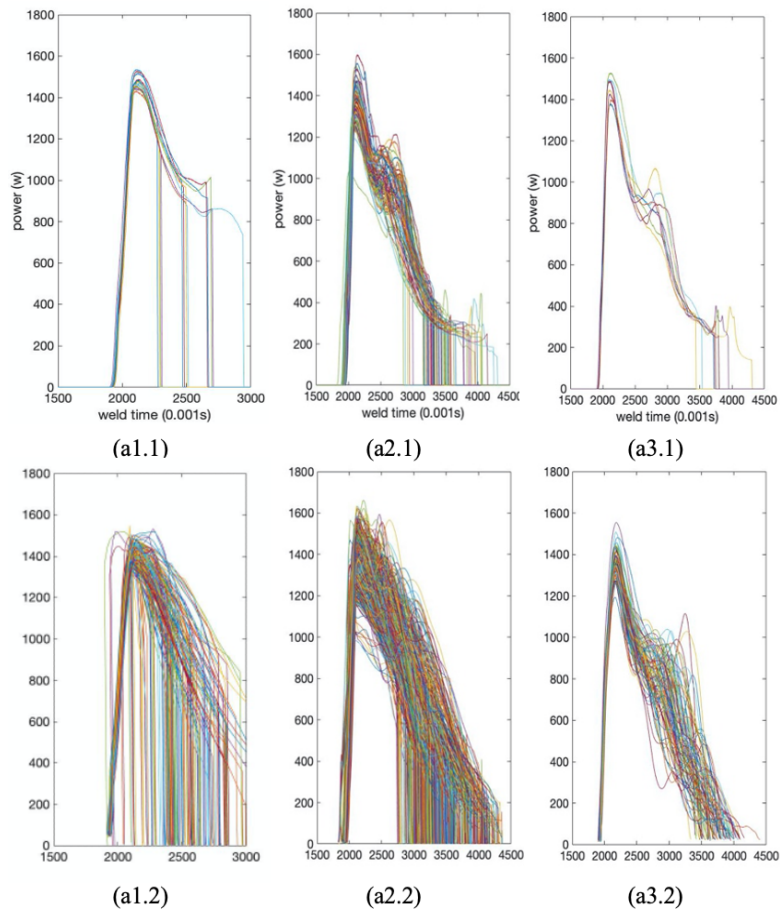


**Figure 4.A.1 The simulation distribution comparison of three MMC simulation approaches**

In the figure, we select three inflection points' value and the corresponding time from power signal as an example, there are start point, midpoint1, and the peak point. All of the inflection points could be found in paper [1]. The first row represents the joint distribution of start point, midpoint1, and the peak point, and the second row represents the corresponding time of them. Each column shows the results that are generated by 1) normal approximation MMC simulation, 2) semi-empirical distribution MMC simulation, and 3) empirical distribution MMC simulation with copulas approach, respectively. As in the figure, the data distribution generated by normal approximation MMC simulation has the most concentrated simulated distribution. However, the approach ignores the data points which are far from the centroid, there are almost no simulated points around these points. Although, these original data points are far from the center, we could not assume them the outliers, in contrast, we need to consider them and simulate some points around them. Under these circumstances, the

third column gives the best consideration of simulated points. The simulated points are relatively normalized generated both around the left centroid, but also the right centroid which is far from the left one. In addition, not only the inflection point values, but also the corresponding times which are generated by the 3<sup>rd</sup> approach has proved the above statement. Both bottom left and bottom middle figures show that the 1<sup>st</sup> and the 2<sup>nd</sup> approach did not take too much consideration of the points that are away from the center. While, the bottom right shows the more reasonable results. In conclusion, the empirical distribution MMC simulation with copulas is the best suitable approach for generating large number of process signals.

#### Appendix 4.B



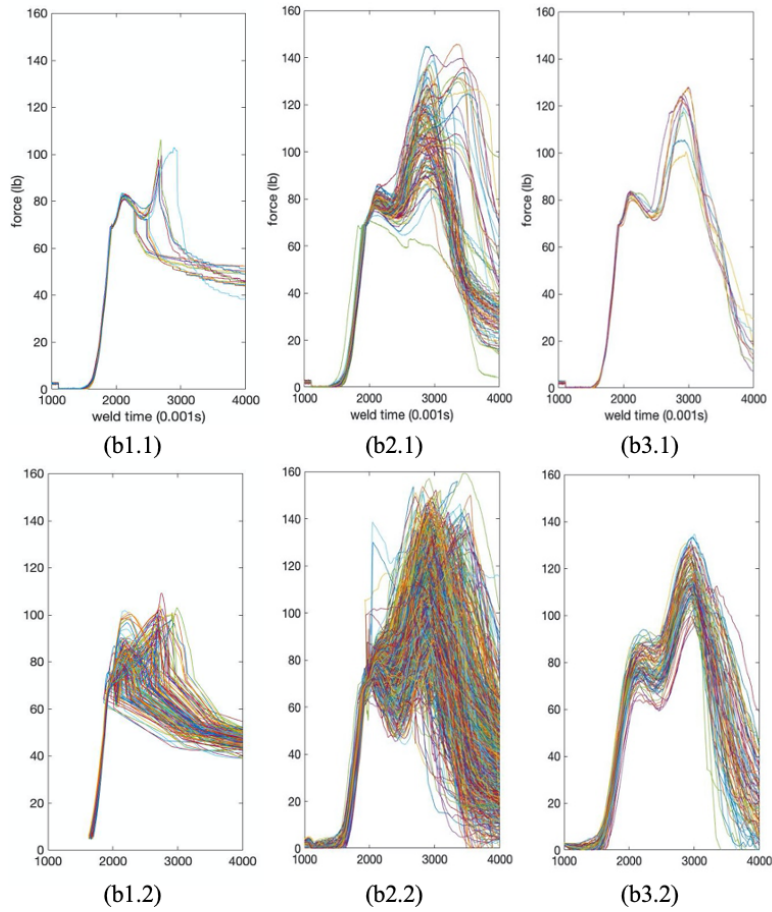


**Figure 4.B.1 Power and force signals comparison of the experimental and the simulated process signal curves listed by under-welds, good-welds, and over-welds (the size of the simulation is 10 times than the size of the experimental signals, (a) represents power signals, (b) represents force signals)**

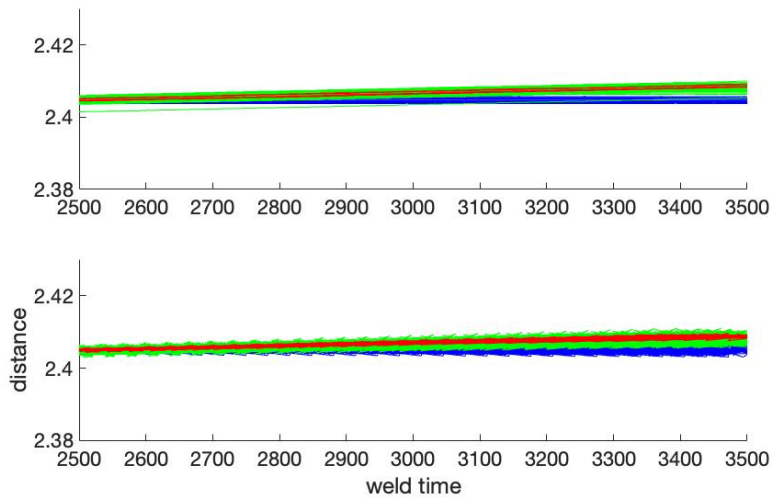


**Figure 4.B.2 Distance signals comparisons of the experimental and the simulated process signal curves (the size of the simulation is 10 times than the size of the experimental signals)**

**Appendix 4.C**

**Table 4.C.1 The classification accuracy of feature-based signals obtained by different machine learning and deep learning methodologies**

Sample size	Sample size (features)					
	The experimental signals (112)	560	1120	2240	3360	5600
Single-hidden-layer BRNN	99.53%	99.61%± 0.23%	99.64%± 0.21%	99.83%± 0.09%	99.89%± 0.05%	99.91%± 0.03%
Two-hidden-layers BRNN	91.51%	92.64%± 1.97%	99.32%± 0.26%	99.44%± 0.17%	99.51%± 0.17%	99.64%± 0.11%
CNN	N/A					
SVM	94.80%	96.49%± 0.24%	97.26%± 0.42%	97.73%± 0.24%	97.78%± 0.22%	97.95%± 0.20%
kNN	92.50%	97.71%± 0.37%	98.17%± 0.56%	98.96%± 0.17%	99.04%± 0.17%	99.25%± 0.17%

**Table 4.C.2 The classification accuracy of experimental and simulated process signals obtained by different machine learning and deep learning methodologies**

Sample size	Sample size (features)					
	The experimental signals (112)	560	1120	2240	3360	5600
Single-hidden-layer BRNN	87.06%	99.71%± 0.09%	99.81%± 0.09%	99.86%± 0.06%	99.93%± 0.05%	99.96%± 0.05%
Two-hidden-layers BRNN	88.00%	99.70%± 0.08%	99.80%± 0.08%	99.86%± 0.05%	99.93%± 0.04%	99.97%± 0.04%
CNN	90.52%	99.88%± 0.02%	100.00%± 0.00%	100.00%± 0.00%	100.00%± 0.00%	100.00%± 0.00%
SVM	77.70%	84.80%± 0.22%	88.10%± 0.12%	89.39%± 0.10%	90.81%± 0.09%	93.59%± 0.07%
kNN	76.80%	83.29%± 0.60%	89.80%± 0.32%	91.39%± 0.10%	92.69%± 0.09%	94.59%± 0.09%

## CHAPTER 5

### CONCLUSION AND FUTURE WORK

#### 5.1 Summary and Conclusion

Ultrasonic welding is considered a low-cost, energy efficient, controllable, safe, and environmentally friendly technique for joining thermoplastic materials in the automotive industry. However, compared to the traditional joining processes, this technique is relatively new. Consequently, weld quality is of most concern in ultrasonic composite welding (UCW). Therefore, this dissertation was devoted to exploring machine learning models for monitoring weld quality in UCW under different input data formats and input data size to meet the increasing demand for high product quality and reliability in UCW as applied in the automotive industry. Specifically, considering feature-based data, this dissertation demonstrates a neural network-based BRNN model that can acquire better weld quality monitoring results than previous non-neural network-based techniques. The BRNN model has been validated to be also suitable for ultrasonic metal welding (UMW) under a large amount of feature-based data.

A CNN neural network model was developed for monitoring weld quality under different data set sizes of time-series process signals. Consequently, the model was shown to be accurate, computationally efficient, and robust when conducting quality monitoring in UCW. Additionally, a Monte Carlo simulation approach is adopted to generate large amounts of time-series-based data that helps provide sufficient training data for a deep CNN model. In general, the major findings of this dissertation can be summarized below:

- (1) *Weld quality determination*: Weld quality in UCW for this research is determined by the maximum lap-shear strength and the presence of carbon fiber flowing into

the weld zone. Since acquiring these characteristics is destructive to the weldment, the corresponding weld energy is selected as an indicator that approximately pre-defines three weld quality classes, under-welds (weld energy  $< 800 J$ ), good-welds ( $800 J < \text{weld energy} < 1200 J$ ), and over-welds ( $1200 J < \text{weld energy}$ ). The weld quality determination is the output criteria for all classification algorithms in this research.

(2) *Feature-based weld quality classification for ultrasonic welding of carbon fiber reinforced polymer through Bayesian Regularized Neural Network*: A new feature selection method that combines Fisher's ratio and a clustering overlap analysis can go beyond distinguishing between normal and abnormal classifications to differentiate between multiple weld quality classes. This proposed method provides a weld quality classification prediction accuracy of at least equivalent or better than models developed from other commonly used feature selection methods. In addition, the BRNN model is found superior with higher classification accuracy and more robust than SVM and kNN machine learning methods on both UCW and UMW. Features such as the start and peak points and the trough-crest pattern in the power signals, inflection point features from the force signals, and the relative slopes of these points are found to be the most significant features for weld quality classification in UCW.

(3) *Quality detection and classification for ultrasonic welding of carbon fiber composites using time-series data and neural network methods*: A neural network-based CNN trained with sufficient input data was found to be more accurate, computationally efficient, and robust classification method for predicting UCW quality classes when both small and large size time-series-based data sets are available as input for training. When input data sets are small, simulation of time-series process signals using piecewise copulas Monte Carlo simulation can provide sufficient data set size for training deep CNN algorithm. The simulation approach can reasonably generate large amounts of time-series-based data and was shown to be consistent with the experimental welding process signals. The CNN model

was also demonstrated to reach at least 90% accuracy even when the input data size is small. Moreover, given large amounts of feature-based data simulated by a multivariate Monte Carlo simulation approach, the BRNN model showed better weld quality classification accuracy for feature-based data when compared with SVM and kNN machine learning methods on both small and large training set sizes. Additionally, the BRNN model was demonstrated to achieve high accuracy on time-series-based data, but the method does not handle the data as efficiently when compared with the CNN model.

## **5.2 Applicability of the Work**

There are some applicability for this research, they are:

- (1) Insufficient experimental UCW data to train and validate deep learning algorithms. In the research, there are only 112 valid samples collected from ultrasonic welding experiments to conduct classification tasks. However, insufficient samples cannot provide sufficient and effective training input for deep learning networks, which may cause the results and models to be less reliable. The model could be further validated if a large amount of experimental welding process signals was collected.
- (2) The Monte Carlo simulation approach was not validated for accuracy against a large amount of experimental welding process signals. The simulation data was only validated by statistical and machine learning techniques. The simulation approach should be further validated with a sufficiently experimental welding process signals data set.
- (3) The neural network models proposed in the dissertation are only applicable to weld quality monitoring in ultrasonic welding. There is lack of verification of other welding techniques.

## **5.3 Contributions**

The intellectual merits and the broader impacts of this research can be summarized as follows:

- (1) An understanding of the relationship between how weld parameters affect weld attributes and joint performance and the weld quality determination extracted among weld attributes and performance will make weld quality monitoring models more accurate and help manufacturers develop processes that are more robust.
- (2) A new feature selection method for considering multiple weld quality classes in ultrasonic welding process. The method is simple but efficient to screen the most significant features especially for multiple weld quality classes.
- (3) A neural network-based BRNN model that is developed for monitoring weld quality in UCW using feature-based data. The model can accurately and stably classify weld quality classes based on feature signals, whether it is a small amount of experimental data, a large amount of simulated data, or a large amount of real welding data.
- (4) A simulation approach that can generate large amounts of data similar to the real welding process signals. This simulation approach can effectively solve the issues where a large amount of real or experimental data cannot be obtained due to experimental or practical limitations. In addition, the simulated data can provide a sufficiently sized training data set for deep learning models. Typically, the simulation process can directly simulate all data points or first select special inflection points as reference points, and then simulate data by segments.
- (5) A neural network-based CNN model that is developed for monitoring weld quality in UCW using time-series experimental welding process signals. This method can eliminate the requirement for complicated feature definition, extraction, and selection. With sufficient training data, the model is accurate, computationally efficient, and robust on monitoring weld quality when the input is time-series based welding process signals. Moreover, the model can also withstand a large degree of noise when it is trained.

#### **5.4 Recommendations for Future Work**

It has been shown that in weld quality monitoring in UCW that a neural network based BRNN model when using feature-based data as input is superior and robust when compared to SVM and kNN machine learning classification methods, whether the data set size is small or large. In addition, the neural network-based CNN model was shown to be more accurate and computationally efficient when using time-series-based process signals for weld quality monitoring in UCW. A CNN model can also withstand a large degree of noise when being trained. These neural network models and methodologies researched in this dissertation could be further improved and extended in the following directions:

- (1) *Further sensitivity analysis of the CNN model:* Use a time-series prediction method and different sampling frequencies for signal processing of original experimental time-series process signals. Then use the processed data as the input to further verify the sensitivity of the CNN model to sampling frequencies and signal prediction accuracy.
- (2) *Further verification of Multivariate Monte Carlo simulation and the CNN model:* Use a large amount of UCW process signals from a real manufacturing process to verify whether the Multivariate Monte Carlo simulation approach is reasonable and effective. Simultaneously, use the same real UCW process signals to verify the efficiency of the CNN model.
- (3) *Research the applicability of CNN model for ultrasonic metal welding:* In Chapter 3, the BRNN model was shown to be effective not only for UCW, but also UMW, when using feature-based data to train the algorithm. Therefore, the CNN model should be explored for use on weld quality monitoring in UMW.
- (4) *Research on self-diagnosis, self-feedback, and self-control systems for ultrasonic welding:* Given weld quality is pre-defined from weld attributes and joint performance, weld parameters and weld quality should be connected to form a feedback system by constructing a mapping relationship among welding parameters, weld attributes, and joint performance. Then, implement self-feedback and self-control for weld parameters through the subsequent weld quality

monitoring to make welding process more automated and intelligent. A schematic of this system is shown in Figure 5.1.

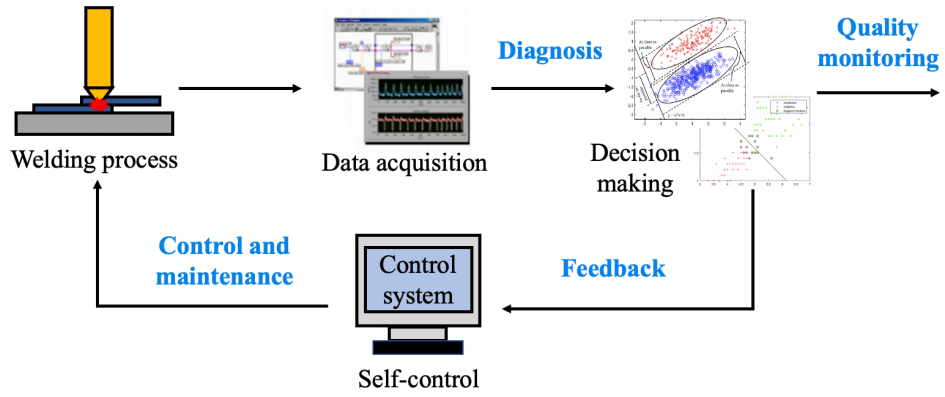


**Figure 5.1. The structure of self-diagnosis, self-feedback, and self-control system**